EFFICIENT SENSITIVITY ANALYSIS AND OPTIMIZATION WITH FULL-WAVE EM SOLVERS

By

SHIROOK M. ALI, M.SC.

A Thesis

Submitted to the School of Graduate Studies

in Partial Fulfillment of the Requirements

for the Degree

Doctor of Philosophy

McMaster University

Your file Votre référence
ISBN: 0-494-04212-5
Our file Notre référence
ISBN: 0-494-04212-5

EFFICIENT SENSITIVITY ANALYSIS AND OPTIMIZATION WITH FULL-WAVE EM SOLVERS

DOCTOR OF PHILOSOPHY (2004) McMASTER UNIVERSITY
(Electrical and Computer Engineering) Hamilton, Ontario

TITLE: **EFFICIENT SENSITIVITY ANALYSIS AND OPTIMIZATION WITH FULL-WAVE EM SOLVERS**

AUTHOR: Shirook M. Ali
M.Sc.
Department of Electrical and Computer Engineering
(Jordan University for Science and Technology)
B.Sc.
Department of Electrical and Computer Engineering
(University of Baghdad)

SUPERVISOR: N.K. Nikolova, Associate Professor
Department of Electrical and Computer Engineering
Dipl. Eng. (Technical University of Varna)
Ph. D. (University of Electro-Communications)
P. Eng. (Ontario)

CO-SUPERVISOR M.H. Bakr, Assistant Professor
Department of Electrical and Computer Engineering
B. Sc. (Cairo University)
M. Sc. (Cairo University)
Ph. D. (McMaster University)
P. Eng. (Ontario)

NUMBER OF PAGES: XX, 141

ABSTRACT

The thesis presents a breakthrough in the sensitivity analysis of high-frequency structures with structured-grid solvers. The proposed techniques are adjoint-based and aim at efficient and accurate sensitivity estimates. They surpass the traditional finite-difference techniques and the original adjoint variable methods with respect to required computational resources, versatility and feasibility in practical implementations.

Sensitivity information is crucial in many engineering applications such as gradient-based optimization, tolerance, and yield analyses. Current commercial full-wave electromagnetic simulators provide only responses but not sensitivities. Therefore, sensitivities are typically obtained by repeated analysis of the structures, which are a slightly perturbed version of the design in each of the design parameters, i.e., response-level finite difference approximations. Such procedure can be prohibitively expensive especially with computationally large problems with many design parameters.

The adjoint variable method, on the other hand, is a well-known efficient technique for sensitivity analysis. The method requires at most two system analyses to compute the response and all its derivatives. This is independent of the

size of the problem and the number of involved design parameters.

Adjoint-based techniques have been applied in many fields such as control theory and circuits. Their implementation in the field of electromagnetics, however, is only recent. Furthermore, its implementation has been limited to full-wave solvers that are based on unstructured grids such as the Method of Moments, the Finite Element Method, etc. To our knowledge, prior to this work, the method has never been implemented with structured-grid solvers. A main reason for this is the lack of analytically differentiable system matrix derivatives needed in the sensitivity expression. These derivatives are a key feature of the method's computational efficiency.

For the first time, the implementation of the adjoint variable method has been possible with frequency-domain structured-grid solvers through the techniques presented in this thesis. The thesis presents a family of discrete adjoint-based techniques for sensitivity analysis with structured-grid solvers. The implementation of the techniques is as simple as that of response-level finite-difference approaches. Their computational efficiency is, however, comparable to the original adjoint variable method, i.e., two system analyses are sufficient to compute the response and all its sensitivities.

The work in this thesis is concluded by gradient-based optimization which uses the discrete sensitivities computed with our techniques. We consider practical optimization of a number of microwave problems. These span a variety of structures such as waveguides, printed circuits, and antennas.

ACKNOWLEDGEMENTS

The fruitful outcome of this thesis is not just a result of my own work. But it is also a result of the love, knowledge, experience and support of the people surrounding me. I would like to acknowledge their efforts and thank them.

I wish to express my appreciation and gratitude to my supervisor, Dr. Natalia Nikolova, for her supervision and guidance during the course of my studies. I have greatly benefited from her expert advice, her knowledge and ideas on important research topics. Her patience, encouragement and understanding during the years of study will always be remembered.

My gratitude goes also to my co-supervisor, Dr. Mohamed Bakr, for the expert and valuable advice. His insight and encouragement during the research development is sincerely appreciated.

I would like also to thank the administrative staff at the Department of Electrical and Computer Engineering, McMaster University, for the friendly atmosphere they try to keep. They would truly go out of their way trying to help and encourage students.

Last but not least, I would like to thank with all my heart to my parents for always loving me regardless of the outcome and for supporting me all my life.

ACKNOWLEDGEMENTS

Special thanks go to my husband, Ali, for his understanding, encouragement and support every day during the course of this work. Tania and Adam, my lovely children, I love you.

CONTENTS

CONTENTS

CONTENTS

CONTENTS

LIST OF FIGURES

LIST OF TABLES

LIST OF SYMBOLS

K	Number of design parameters
N	Total number of TLM cells in the computational domain
N_d	Number of cells along the height of the substrate
M	Number of links in the whole computational domain
P	Number of optimization iterations
δ_c	Size of the TLM cell
δ	Uniform TLM cell size
l	Index of the lth cell
i, j, k	Indices
f_0	Operating frequency
γ_l	Propagation constant of the lth cell
β_l	Phase constant of the lth TLM cell
ω	Angular frequency
ε	Permittivity
σ	Conductivity
μ	Permeability
v^r	Reflected voltage waves of the TLM cell
v^i	Incident voltage waves of the TLM cell
S	Scattering matrix
A	Complex system matrix
v	Complex vector of incident voltages (solution vector)
V_s	Complex excitation vector
A_R	Real system matrix

v_R	Real solution vector
$V_{R,s}$	Real excitation vector
λ	Complex Adjoint solution vector
E_x	The electric field in the x-direction
E_y	The electric field in the y-direction
E_z	The electric field in the z-direction
H_y	The magnetic field in the y-direction
H_x	The magnetic field in the x-direction
H_z	The magnetic field in the z-direction
Z	Medium intrinsic impedance
Z_1	Intrinsic impedance of medium 1
Z_2	Intrinsic impedance of medium 2
Z_{wg}	Wave impedance
Z_c	Characteristic impedance
Z_{in}	Input impedance
R_{in}	Input resistance
X_{in}	Input reactance
Γ_e	Reflection coefficient from a perfect conductor boundary
Γ_{12}	Reflection coefficient for transmission from medium 1 to medium 2
Γ_{21}	Reflection coefficient for transmission from medium 2 to medium 1
D	Distance from the absorbing boundary
λ_0	Wavelength for propagation in free space
C	Constant
k_w	Wave number
k_c	Dominant mode cut-off wave number
L	Length of the design parameter
p_{out}	Output observation point
p_{in}	Input observation point
S_{21}	Transmission coefficient

S_{11}	Reflection coefficient
S_x, S_y, S_z	Variables
v^{inc}	Incident wave
v^{trans}	Transmitted wave
v^{ref}	Reflected wave
f	Response function
F	Objective function
$\boldsymbol{x}^*$	Optimum vector of design parameters
$\boldsymbol{x}^0$	Initial vector of design parameters
$\boldsymbol{x}$	Vector of design parameters
∇_x	Gradient with respect to $\boldsymbol{x}$
x_k	The kth design parameter
$\partial/\partial x_k$	Partial derivative with respect x_k
Δ_k	Difference due to perturbation in the kth design parameter
$\Re$	Real part of a vector or matrix
$\Im$	Imaginary part of the vector or matrix
^{H}	Hermetian
$^+$	Forward perturbed
$^-$	Backward perturbed
h	Substrate height
W	Design parameter width
a	Waveguide width
L_t	Length of the quarter wavelength transformer for the printed Yagi antenna
S	Separation from the driven element for the printed Yagi antenna
L_d	Length of the director element for the printed Yagi antenna

LIST OF ABBREVIATIONS

RF	Radio Frequency
EM	Electromagnetic
FDA	Finite Difference Approximation
AVM	Adjoint Variable Method
FDTLM	Frequency-Domain Transmission Line Method
DAVM-I	Discrete adjoint-variable method I
CAVM-I	Central Discrete adjoint-variable method I
TLM	Transmission Line Modeling
DAVM-II	Discrete Adjoint-perturbed expression II
CAVM-II	Central Adjoint-perturbed expression II
TDTLM	Time-Domain Transmission Line Method
ZRT	Zero Reflection Termination
DRF	Double Resonator Filter
FDTD	Finite-Difference Time Domain
LPF	Low Pass Filter
FEM	Finite Element Method
MoM	Method of Moments
EM-FAST	Electromagnetic Feasible Adjoint Sensitivity Technique
FDTD-DSI	Finite-Difference Time-Domain Discrete Surface Integral method
FFD	Forward Finite Difference
BFD	Backward Finite Difference
CFD	Central Finite Difference
1-D	One dimensional problem

3-D	Three dimensional problem
TE_{01}	Dominant Transverse Electric mode
PC	Personal Computer
dB	decibel

Chapter 1

INTRODUCTION

1.1 MOTIVATION

The past century has witnessed a rapid growth in telecommunications technology. Advances in different fields of this technology – such as satellite communications, integrated microwave circuits, etc. – have created strong markets for new products. Competition between commercial companies for a bigger market share demanded efficient and accurate design within the shortest possible time.

Because of the short design cycle and in order for a microwave engineer to build a good design, rapid information on a number of factors is always an advantage. These factors may include the desired design specifications, the limitations and the constraints associated with the manufacturing technology, the environmental factors affecting the operation of the device, etc. To evaluate the performance of the design with respect to these factors, response analysis and response sensitivity analysis is performed.

Sensitivity analysis measures the rate of change of a given/chosen device response function with respect to changes in a set of design parameters. Mathematically,

it is the evaluation of the gradient (derivatives vector) of the response function with respect to changes in a set (vector) of design parameters.

Changes – or, equivalently, perturbations – in design parameters may occur due to a number of different reasons: (i) during the design stage, the optimization modules recommend changes of the structure in order to enhance its performance, (ii) during the manufacturing stage, deviations from the exact design occur within certain tolerance range, or (iii) environmental factors inevitably affect the shape and material properties. Knowing the sensitivity of the device response to changes in certain material or shape parameters helps in predicting the corresponding variations in its response. Sensitivity information is crucial in many engineering applications such as gradient-based optimization, yield and tolerance analyses.

Commercial software for high-frequency structure analysis and design treat the full-wave electromagnetic (EM) simulator as a black box. It utilizes simple approaches for sensitivity analysis, such as the finite-difference approximations (FDA) at the level of the response. The EM simulator is invoked to analyze the EM structure resulting from a finite change in one of the design parameters while keeping the other parameters unchanged. Hence, if the vector of design parameters has K components, then, K full-wave simulations are required for a first-order sensitivity estimate, and $2K$ simulations are needed for a more accurate second-order estimate. Obviously, these approaches are computationally inefficient especially when simulating time intensive large problems with many design parameters. Their advantage is in the simple and straightforward implementation with the existing EM numerical codes.

The adjoint-variable method (AVM), on the other hand, is a known efficient technique for response sensitivity analysis. It provides the sensitivity information only through the solution of the original problem and what is called the adjoint problem. Thus, the response and its sensitivities are obtained through two system analyses regardless of the number of design parameters K.

Traditionally, the AVM assumes the existence of the analytical derivatives of the system matrix with respect to the shape and material perturbations. With such derivatives, the response sensitivity computations are exact. While such derivatives may be possible (although rather difficult) to obtain with unstructured grid solvers, they are simply not available when the solver utilizes a discrete structured grid. These difficulties have prevented the use of adjoint-based sensitivity analysis with full-wave EM solvers based on structured grids. There is a need in full-wave sensitivity analysis for numerical approaches, which are feasible, simple to implement, and do not require modification of the existing numerical codes regardless of whether they use structured grids or unstructured grids.

This thesis addresses these limitations. A family of discrete adjoint-based approaches for sensitivity analysis with structured-grid solvers is developed. These approaches feature both computational efficiency and simplicity in implementation with existing numerical codes.

1.2 CONTRIBUTIONS

A number of contributions have been achieved by the author. These are as follows:

1.2.1 Theoretical contributions

The main theoretical accomplishment of this work is in the successful implementation of the AVM with discrete full-wave simulators. The limitations due to the lack of analytical system matrix derivatives are overcome. We propose a family of approximate discrete AVM approaches for sensitivity analysis with structured-grid solvers. Our techniques combine the simplicity of response-level FDA and the computational efficiency of the exact AVM.

The proposed approaches feature the computational efficiency of the exact AVM in the sense that they require at most two system analyses in order to obtain the response and its sensitivity. In fact, they have a number of advantages over the exact AVM. Firstly, they do not require analytical derivatives of the system matrix. Thus, cumbersome and often case specific analytical pre-processing is avoided. Secondly, there is no need for the computation of K system matrix derivatives, which is the major overhead with exact sensitivity analysis. Thirdly, the techniques are versatile – they accommodate all possible shape and material changes, as long as they conform to the discretization grid. And last but not least, the implementation of the proposed techniques in existing numerical codes is straightforward.

We have tested our discrete adjoint techniques through sensitivity analysis of a variety of realistic numerical examples: waveguide structures, antennas, open boundary

printed structures, etc. Reliable and accurate sensitivity estimates have been obtained in all cases.

1.2.2 Publications

The work presented in this thesis has resulted in the publication/acceptance of four papers in refereed journals and three refereed conference papers. These are cited throughout the thesis and are explicitly listed at the end of Chapter 7.

1.2.3 Other contributions

The full-wave EM simulator used in the course of this work – the frequency-domain transmission line method (FDTLM) solver – is an in-house simulator developed by the author. The simulator has been used to simulate a variety of different EM problems.

1.3 OUTLINE OF THE THESIS

The thesis presents a framework of techniques developed for sensitivity analysis with structured-grid solvers.

We first start in Chapter 2 with a detailed discussion of the FDTLM as a full-wave solver. The discussion involves numerical and computational aspects of the method as a numerical EM simulator. The chapter presents a number of practical problems simulated using the FDTLM.

Chapter 3 first introduces a background of classical sensitivity analysis techniques. These include response-level finite differences and the original AVM. Later, the chapter introduces our first discrete adjoint-based technique, the DAVM-I. Through a

variety of examples, we show that the presented technique is computationally efficient, accurate, robust, and versatile.

Our first improved discrete adjoint-based technique, the central adjoint-variable method (CAVM-I), is introduced in Chapter 4. The technique targets cases where the response of interest is a highly nonlinear function of its design parameters and/or cases where the TLM grid is coarse. The implementation of the technique is discussed in detail. In addition, a number of examples are also given.

The research into approaches to further improve the accuracy of the computed derivatives continues into Chapter 5. There, two new discrete adjoint-based approaches are introduced; the second discrete adjoint-variable method (DAVM-II) and its central formulation, the CAVM-II. The implementation of both techniques is discussed in detail in this chapter. The developed sensitivity expressions are tested through a number of examples. The chapter is concluded with a convergence analysis, which tests the performance of all four proposed techniques as the grid size of the TLM simulator becomes finer.

As an application where sensitivity information is crucial, the proposed techniques are integrated in a gradient-based optimization loop in Chapter 6. Optimization of a number of practical problems is performed using gradients supplied by our techniques.

The thesis concludes in Chapter 7. Suggestions for future work are also given in this chapter.

Chapter 2

THE FREQUENCY-DOMAIN TRANSMISSION LINE METHOD

This chapter describes practical computational issues in the full-wave simulation of electromagnetic (EM) problems using the frequency-domain transmission line method (FDTLM). The algorithm is a relatively recent development in the field of numerical electromagnetics. It was developed in the early 1990's. The FDTLM simulator used in the course of this work is an in-house simulator developed by the author. It has been verified and tested through robust and thorough comparisons with alternative numerical and analytical approaches.

The implementation of the TLM algorithm is discussed with closed waveguide problems as well as with open boundary and antenna problems. We emphasize the computational aspects of the algorithm that relate to the implementation of our discrete adjoint techniques in later chapters.

2.1 INTRODUCTION

There is a variety of numerical algorithms (solvers) for full-wave EM analysis. These algorithms may be classified according to the domain that they operate in as time-domain solvers or as frequency-domain solvers. An alternative way to classify them is according to their discretization grid, i.e., whether they are based on structured grids or on unstructured grids. The latter classification is used during the course of this work for the purpose of sensitivity analysis.

The FDTLM is a structured-grid solver, which is used to model time-harmonic electromagnetic waves in the frequency domain. The solver is, essentially, a discretized form of the Huygens principle (Huygens 1690).

2.2 THE FDTLM COMPUTATIONAL DOMAIN

The FDTLM discretizes the computational domain into rectangular cells based on the symmetrical condensed node (Johns *et al.* 1994) shown in Fig. 2.1. The cell is assembled from twelve transmission lines (links). Incident voltage waves propagate along these links to scatter and couple to other links from the neighboring cells. The reflected voltage waves $\boldsymbol{v}^{l,r}$ for the lth link are related to the incident voltage waves $\boldsymbol{v}^{l,i}$ by[1]

$$\boldsymbol{v}^{l,r} = \boldsymbol{S} \cdot \boldsymbol{v}^{l,i} \tag{2.1}$$

where $\boldsymbol{S} \in \mathbb{R}^{12\times12}$ is the scattering matrix.

[1] Throughout the thesis, matrices and vectors are denoted with bold italic characters while variables are denoted with italic characters.

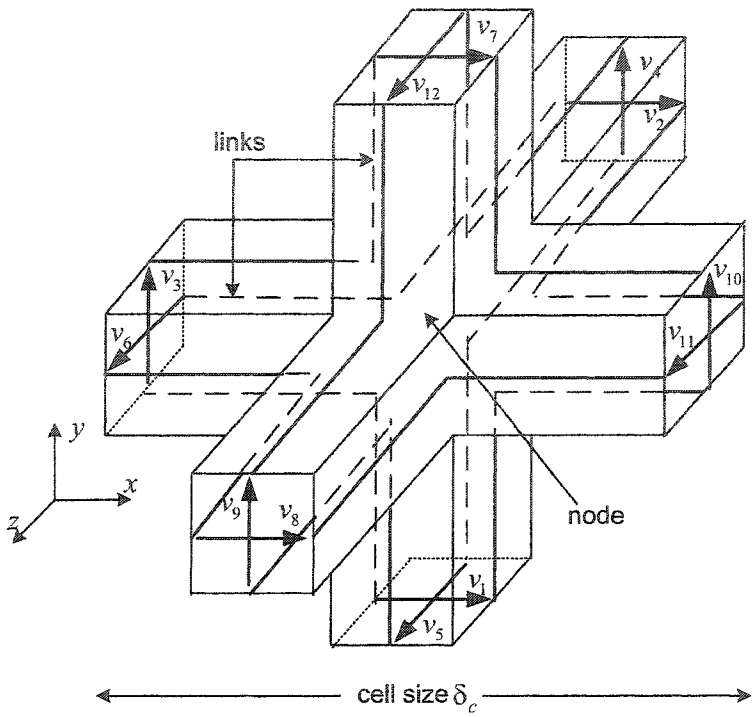

Fig. 2.1 The symmetrical condensed TLM node.

The scattering and coupling processes are similar to those of the time-domain transmission line method (TDTLM) (Christopoulos 1995). An equation is written for each link at each cell in relation with the corresponding incident voltages from the neighboring cells and the reflected voltages from the cell itself. These voltages are delayed through propagation factors of the type:

$$e^{-\gamma_l \frac{\delta_c}{2}} \tag{2.2}$$

where γ_l is the propagation constant of the lth link and δ_c is the corresponding cell size along the lth link. The factor of $(1/2)$ reflects the fact that the length of the link is one-half the cell size. The propagation factor in (2.2) is a function of the operating frequency f_0, the local material constitutive parameters, and the cell size. For the particular case of a lossless medium modeled by a uniform mesh of size δ, $\gamma_l = j\beta_l$, where the phase constant β_l is (Johns *et al.* 1994)

$$\beta_l = \omega\sqrt{\varepsilon\mu}. \tag{2.3}$$

Here, $\omega = 2\pi f_0$; $\varepsilon = \varepsilon_l\varepsilon_0$ and $\mu = \mu_l\mu_0$ are the medium permittivity and permeability for the respective l th link. A more general case when modeling a lossy medium or when the grid discretization is nonuniform is discussed in Appendix A.

When the equations for all the links in all the cells are put together, a complex linear system of equations is obtained:

$$A \cdot v = V_s. \tag{2.4}$$

In (2.4), $A \in \mathbb{C}^{M\times M}$ is the system matrix, where $M = 12\times N$ (N is the total number of cells in the computational domain); $v \in \mathbb{C}^{M\times 1}$ is the vector of incident voltages, and $V_s \in \mathbb{C}^{M\times 1}$ is the source vector. The matrix A is related to the parameters of the medium and to the boundary conditions of the problem.

The system of equations in (2.4) is usually very large and sparse. Therefore, (2.4) is solved using iterative methods (Sadiku 2001). Using the solution v, the electric and

magnetic fields can be computed. They are calculated at the center of the cell, i.e., at the node [see Fig. 2.1] as

$$
\begin{aligned}
E_x &= -\frac{v_1^i + v_{12}^i + v_2^i + v_9^i}{2\delta} \\
E_y &= -\frac{v_3^i + v_{11}^i + v_4^i + v_8^i}{2\delta} \\
E_z &= -\frac{v_6^i + v_{10}^i + v_5^i + v_7^i}{2\delta} \\
H_x &= \frac{v_4^i - v_8^i + v_7^i - v_5^i}{2Z\delta} \\
H_y &= \frac{v_9^i - v_2^i + v_6^i - v_{10}^i}{2Z\delta} \\
H_z &= \frac{v_{11}^i - v_3^i + v_1^i - v_{12}^i}{2Z\delta}
\end{aligned}
\tag{2.5}
$$

where $Z = \sqrt{\mu_l \mu_0 / \varepsilon_l \varepsilon_0}$ is the medium impedance for the respective link with μ_l and ε_l being its corresponding permeability and permittivity.

A final note about the FDTLM as a computational simulator is that the choice of discretization, i.e., cell size δ does not cause numerical instability of the algorithm. It may, however, cause detritions in the accuracy of the results as δ becomes coarser. The research into the best choice of δ for a given operating frequency is beyond the scope of this thesis.

2.3 IMPLEMENTATION OF THE FDTLM WITH OPEN AND CLOSED BOUNDARY PROBLEMS

Full-wave analysis of waveguides, antennas and printed circuits using the FDTLM is possible as long as the appropriate boundary conditions are set throughout the problem. Fig. 2.2(a) is an illustration of a printed structure. The substrate is modeled by TLM cells with constitutive parameters ε_2 and μ_2, which are incorporated in the propagation factor γ of each link inside the substrate region (2.3). Similarly, in the air, $\varepsilon_1 = \varepsilon_0$ and $\mu_1 = \mu_0$. The printed metallizations of the structure are modeled as infinitesimally thin metallic plates. They have zero thickness and are located between the nodes, i.e., the incident voltages on the links in the normal y-direction are reflected back to the center of the same cell with a reflection coefficient $\Gamma_e = -1$. This applies to the links of the cells above (in the air) and below (in the dielectric) the metallic plate(s). The voltage-waves of the air cells at the air-dielectric interface have a reflection coefficient $\Gamma_{12} = (Z_1 - Z_2)/(Z_1 + Z_2)$, where $Z_2 = \sqrt{\mu_2/\varepsilon_2}$ is the intrinsic impedance of the substrate, and $Z_1 = Z_0 = \sqrt{\mu_0/\varepsilon_0}$ is that of air. Likewise, the voltage-waves of the cells in the substrate at the air-dielectric interface are reflected back with a reflection coefficient $\Gamma_{21} = (Z_1 - Z_2)/(Z_1 + Z_2)$.

The absorbing boundary conditions used to terminate the open computational domain are the zero reflection termination (ZRT) boundaries proposed by Pasalic *et al.* (1999). The recommended distance D of the ZRT boundaries from the metal plates, i.e., the printed structure, is (Pasalic *et al.* 2001)

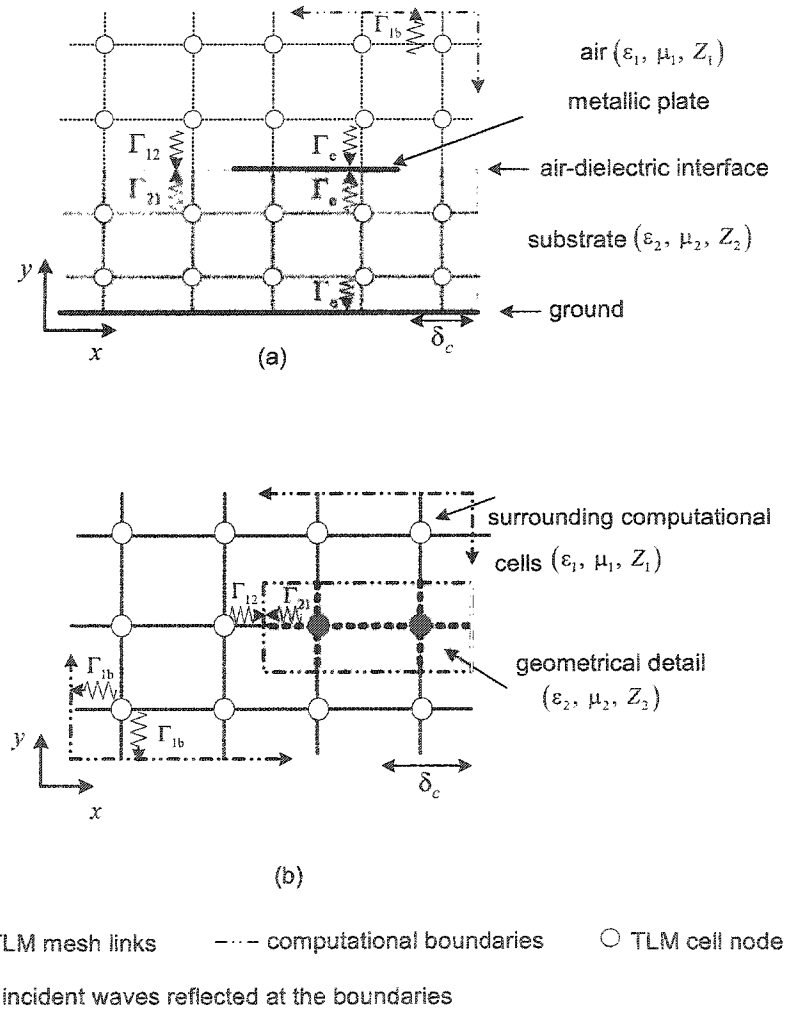

Fig. 2.2 Discretization mesh of a TLM problem: (a) open boundary (printed structure) model, (b) closed boundary model.

$$D \approx \frac{\lambda_0}{C \cdot \sqrt{\varepsilon_2}} \tag{2.6}$$

where λ_0 is the free-space wavelength, and C is a frequency dependent constant:

$$C = \begin{cases} 15, & \text{for } 0 < f_0 < 5 \text{ GHz} \\ 7, & \text{for } 5 < f_0 < 10 \text{ GHz} \\ 4, & \text{for } 10 < f_0 < 20 \text{ GHz.} \end{cases} \tag{2.7}$$

These boundaries terminate the computational domain from all sides except from the bottom side, where a ground plane is placed. The ground plane is modeled as a perfect conductor with a reflection coefficient $\Gamma_c = -1$.

The same principles are applied when modeling closed waveguide structures such as the one shown in Fig. 2.2(b). The figure illustrates the FDTLM computational domain for a dielectric-magnetic detail. The detail is modeled with constitutive parameters ε_2 and μ_2. The surrounding computational domain is modeled by TLM cells with constitutive parameters ε_1 and μ_1. The computational boundaries between the different domains including those that terminate the problem are defined $\delta/2$ away from the center of the corresponding boundary cells. If a boundary is defined as an electric wall, then $\Gamma_{1b} = -1$. In the case of magnetic wall, $\Gamma_{1b} = +1$. In the case of a reflection-free wall, $\Gamma_{1b} = 0$ (Palasic *et al.* 2001).

2.4 NUMERICAL EXAMPLES

We discuss some of the EM problems simulated with our in-house FDTLM simulator.

2.4.1 Hollow waveguide

Fig. 2.3 shows a uniform hollow waveguide simulated for its dominant mode with the FDTLM solver. The guide is discretized into uniform TLM cells of size $\Delta x = \Delta y = \Delta z = \delta = 1$ mm. The computational domain is of size $N = 50 \times 1 \times 60$ nodes. The input and output ports are matched to air. The structure is excited with the dominant mode uniform half sine-wave excitation at 4 GHz applied along the width a of the input port.

The E_y field component is shown in Fig. 2.4. The wave impedance of the guide is computed for a range of frequencies as the ratio between the electric and the orthogonal magnetic field components,

$$Z_{wg} = -\frac{E_y}{H_x}. \tag{2.8}$$

The results are compared to the analytically calculated ones using the well-known impedance expression (Pozar 1993)

$$Z_{wg} = \frac{k_w Z}{\beta} \tag{2.9}$$

where $k_w = \omega\sqrt{\mu_0 \varepsilon_0}$ is the wave number, $\beta = \sqrt{k_w^2 - k_c^2}$ is the propagation constant, $k_c = \pi/a$ is the dominant mode cut-off wave number, and $Z = \sqrt{\mu/\varepsilon}$ is the intrinsic

impedance of the material filling the waveguide. An excellent match is obtained between the two results as shown in Fig. 2.5.

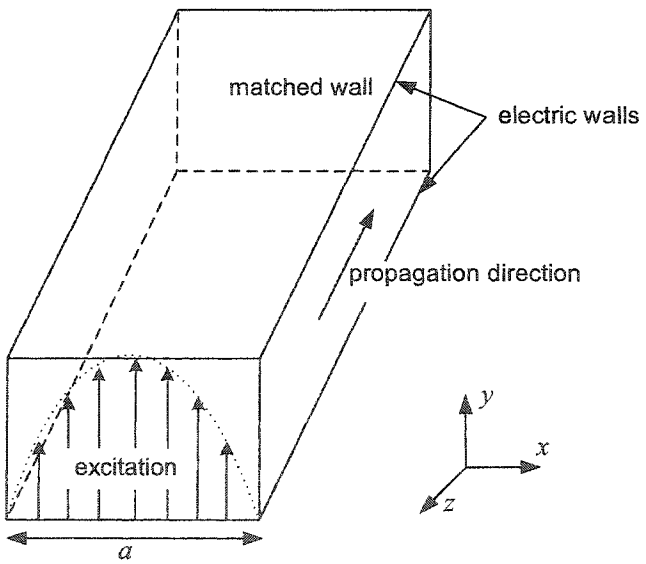

Fig. 2.3 Hollow waveguide.

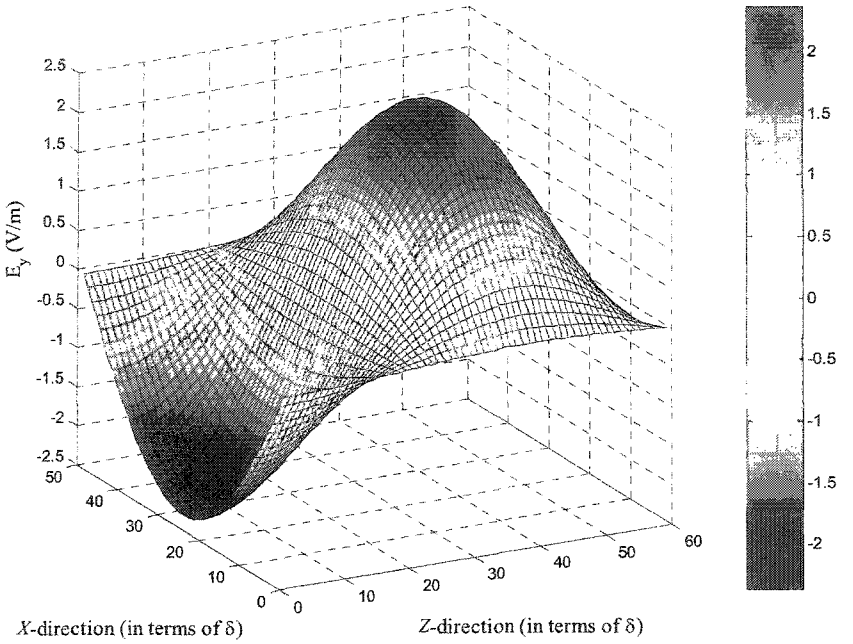

Fig. 2.4 The real part of the propagating electric field in the waveguide.

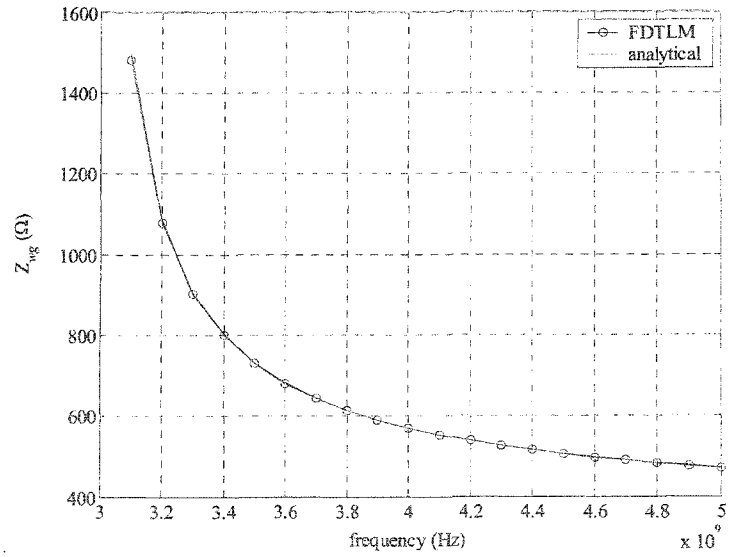

Fig. 2.5 The wave impedance of the dominant mode in the hollow waveguide for a range of frequencies.

2.4.2 Double-resonator filter (DRF)

We simulate next the double-resonator filter shown in Fig. 2.6. The filter is discretized with a uniform TLM mesh with size $\delta = 1$ mm. It is excited with a 4.6 GHz uniform half sine-wave at the input port set at $z = 0$. The size of the computational domain is $N = 30 \times 1 \times 120$ nodes. The septa are perfectly conducting discontinuities. They are one cell thick (in the z-direction), and their lengths are $L_1 = 17\delta$ and $L_2 = 18\delta$. The structure is symmetrical both in its geometry and with respect to the applied excitation. Therefore, only half of the computational domain needs to be simulated when employing a magnetic-wall boundary. Figs. 2.7 and 2.8 show the amplitude of the field components

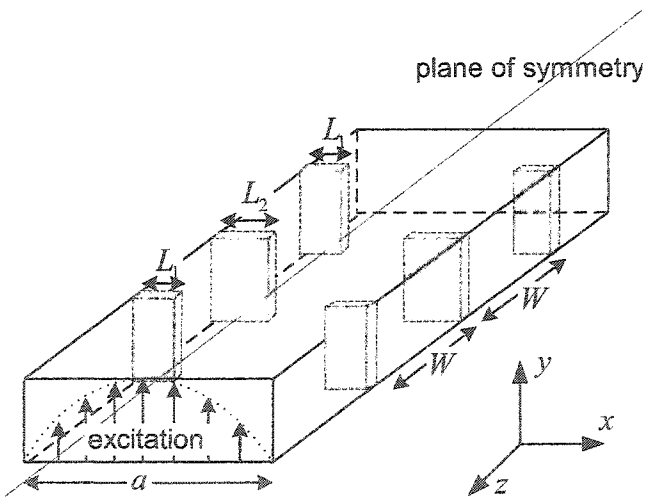

Fig. 2.6 Double resonator filter.

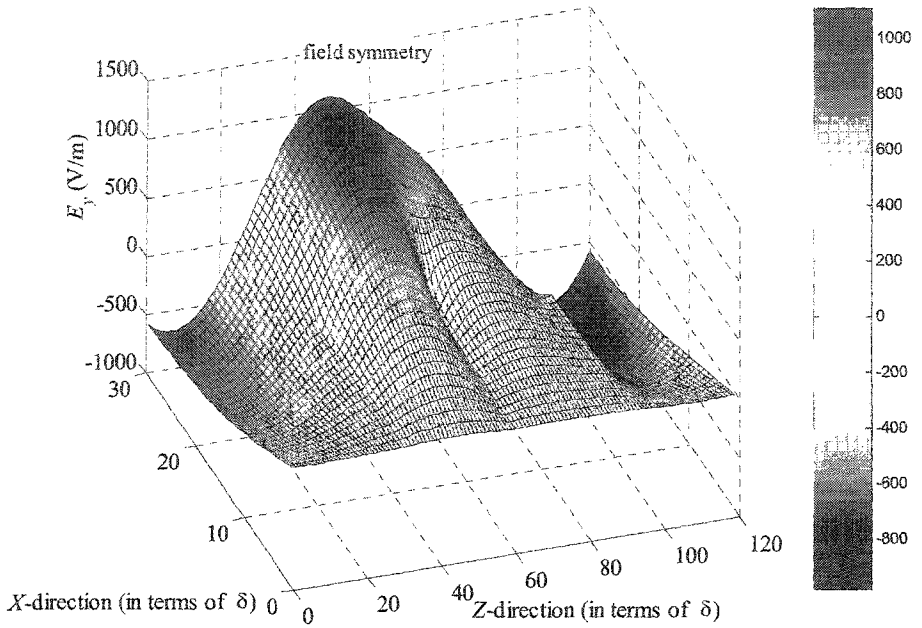

Fig. 2.7 The amplitude of the electric field in half of the double resonator filter.

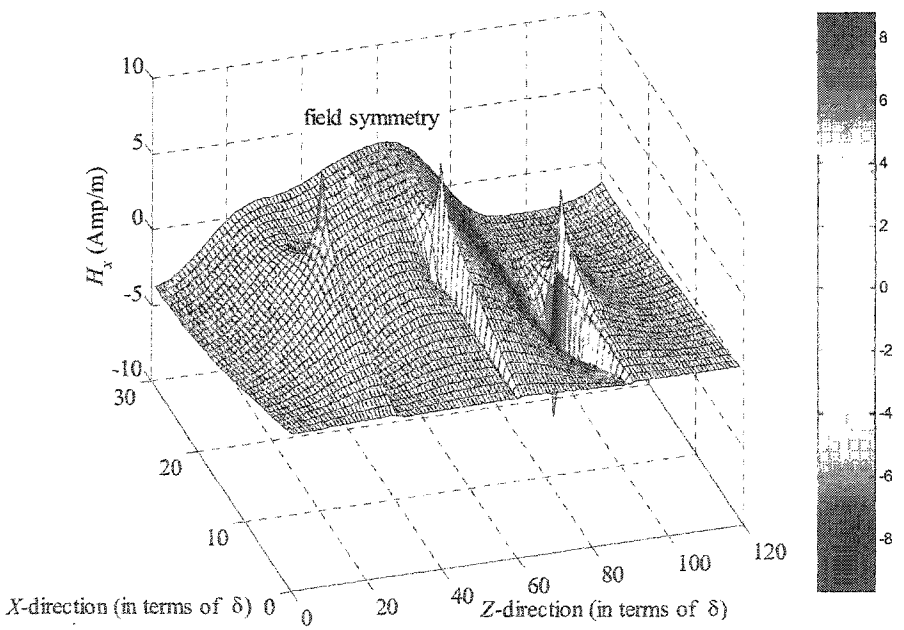

Fig. 2.8 The amplitude of the magnetic field in half of the double resonator filter.

E_y and H_z.

The transmission *S*-coefficient of the filter is computed as the ratio between the transmitted voltage at an observation point p_{out} located at the output port and the incident voltage at a point located in the input port p_{in}, i.e.,

$$S_{21} = \frac{v^{trans}(p_{out})}{v^{inc}(p_{in})}. \tag{2.10}$$

The observation points are set away from the matching boundaries terminating the filter and from any discontinuities, i.e., the septa. In this example, they are set at $p_{in}(15,1,10)$ and $p_{out}(15,1,110)$. The *S*-parameters of this filter are given in Fig. 2.9 where they are compared to those computed using Ansoft HFSS (2001) simulator.

The incident voltage v^{inc} in (2.10) is derived by simulating a uniform waveguide with the same dimensions and excited at the same frequency points where S_{21} is to be computed. The transmitted voltage v^{trans} is obtained by simulating the actual filter at the respective frequency points. The reflection coefficient S_{11} is computed as

$$S_{11} = \frac{v^{ref}(p_{in})}{v^{inc}(p_{in})} \tag{2.11}$$

where $v^{ref}(p_{in}) = v^{tot}(p_{in}) - v^{inc}(p_{in})$. Here, $v^{tot}(p_{in})$ is obtained as the total voltage at p_{in} when the actual filter is simulated.

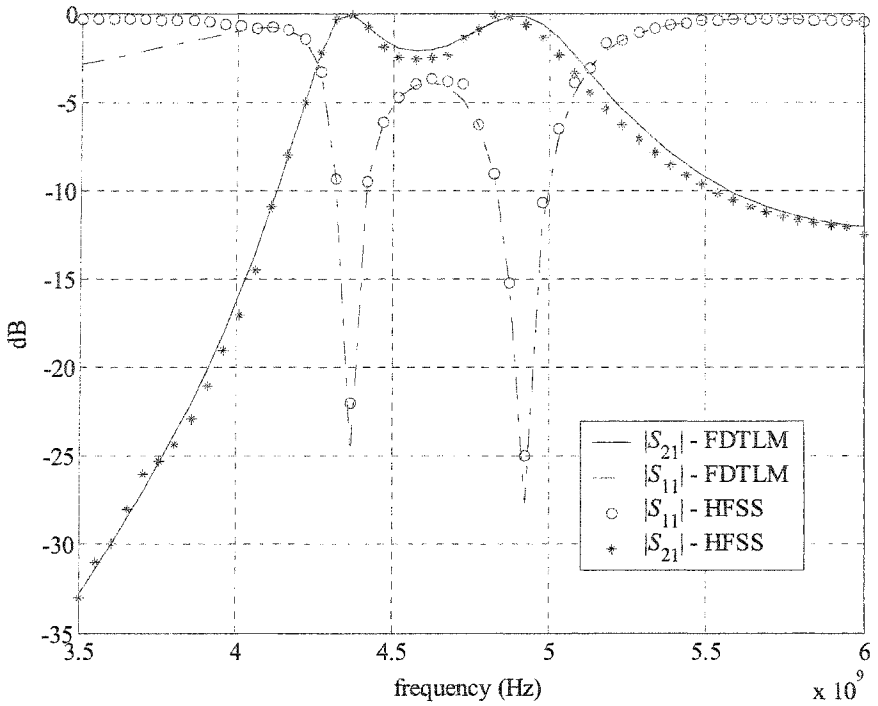

Fig. 2.9 *S*-parameters for the double-resonator filter.

Since we are interested in the magnitude of the *S*-parameters only, and the input and output feed guides are lossless, we do not perform de-embedding with respect to the actual junctions between the feed guides and the device.

2.4.3 Probe-fed patch antenna

Our first printed structure is a probe-fed patch antenna as the one shown in Fig. 2.10. The dielectric material of the substrate supporting the patch has relative permittivity $\varepsilon_r = 2.2$ and its height is $h = \Delta y = \delta = 1.524$ mm. The length of the patch is $L = 19.812$ mm and

its width is $W = 28.956$ mm. To achieve approximately a $50\,\Omega$ input impedance at resonance, the probe feed is set at about $L/4$ in the x-direction and at about $W/2$ in the y-direction (Lee 1997).

According to (2.6)-(2.7), eight layers of air are set on top of the patch where the ZRT boundaries are imposed. The ZRT boundaries, although simple to implement, provide excellent absorption of the propagating field. Fig. 2.11 shows a comparison between the electric field on the patch and the fading field just before the ZRT boundary.

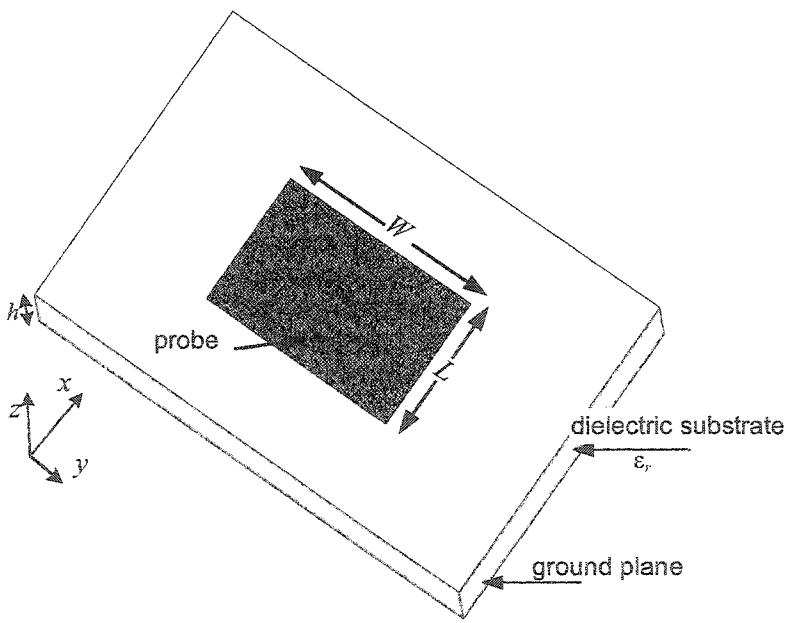

Fig. 2.10 Probe-fed patch antenna.

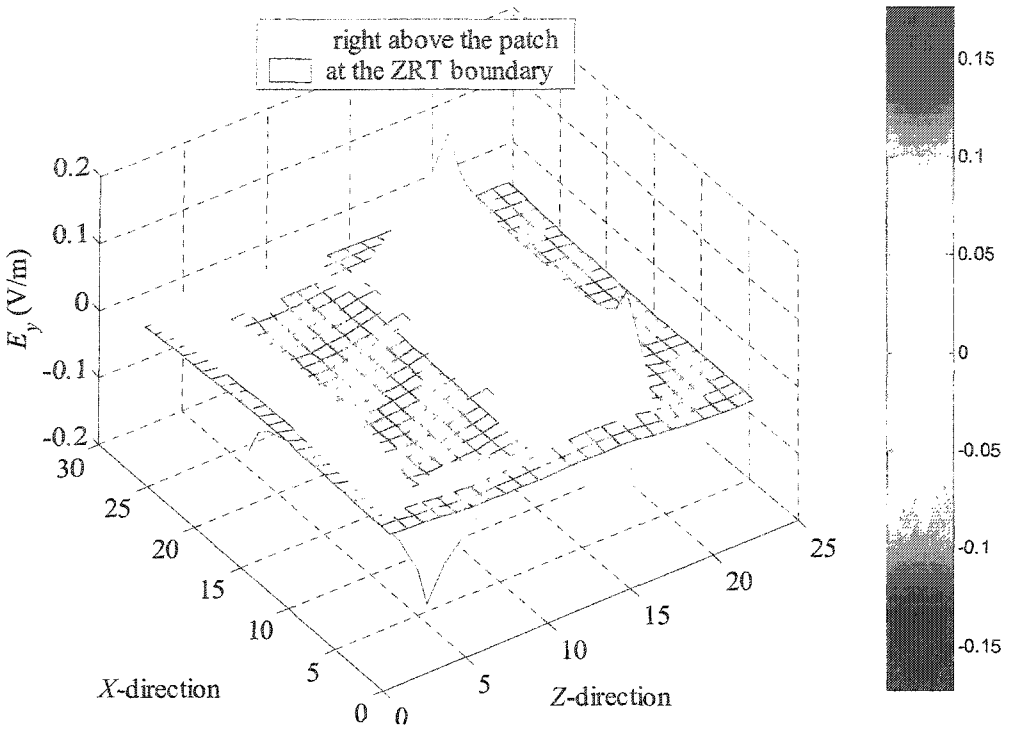

Fig. 2.11 A comparison between the field on the patch and that at the ZRT boundary.

The probe excitation of the antenna is at the (i, j, k) th location [see Fig. 2.12(a)].

It is computed as

$$V_z = \sum_{n=1}^{N_d} E_z(i, j, k_n) \cdot \Delta z \tag{2.12}$$

where N_d is the number of cells along the height of the dielectric layer, and $E_z(i, j, k_n)$ is the electric field at the points along the vertical z-axis in the substrate. Its coordinates in the xy-plane are $i\Delta x$ and $j\Delta y$.

According to Ampere's law, the current I_s flowing into the antenna at the (i, j, k) th location is obtained by performing the line integral of the magnetic fields around the base of the probe [see Fig. 2.12(b)] as

$$I_s = \left[H_x(i, j-1, k_{Nd}) - H_x(i, j, k_{Nd})\right]\Delta x + \left[H_y(i, j, k_{Nd}) - H_y(i-1, j, k_{Nd})\right]\Delta y \,. \quad (2.13)$$

The response function of interest for the patch antenna is its input impedance $Z_{in} = R_{in} + jX_{in}$. It is computed as the ratio between the input voltage V_z (2.12) to the current I_s (2.13), i.e.,

$$Z_{in} = \frac{V_z}{I_s}. \quad (2.14)$$

Using (2.12)-(2.14), the input impedance is computed with the FDTLM simulator for a range of frequencies, see Fig. 2.13. The figure also shows a comparison with results taken from (Lee *et al.* 1997).

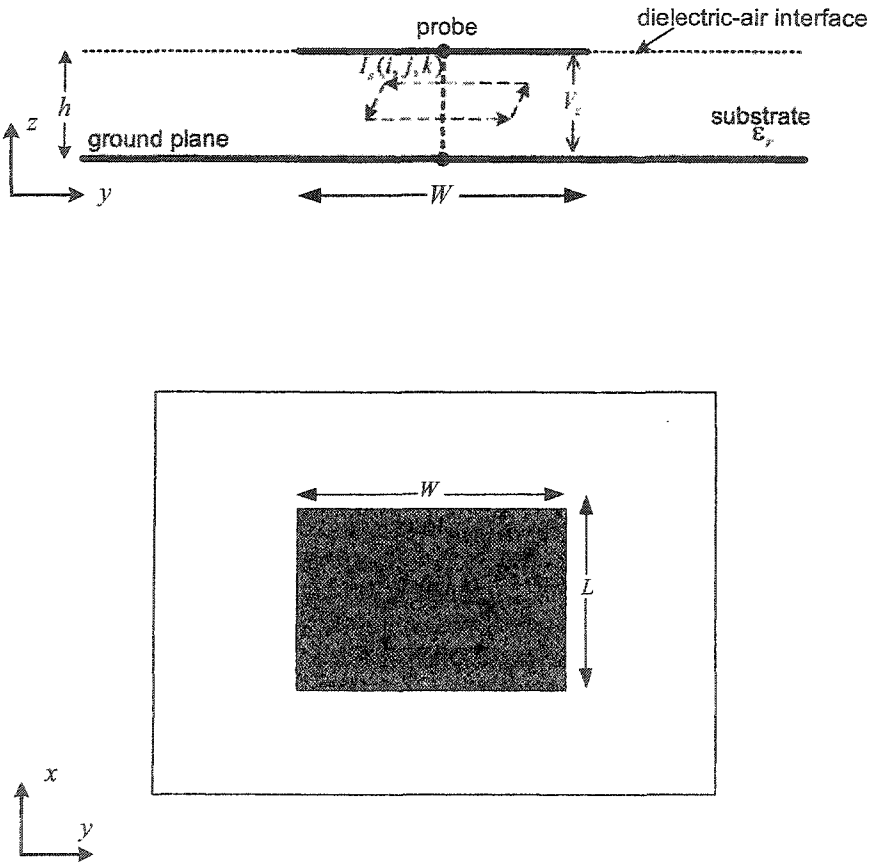

Fig. 2.12 2D view of the probe-fed patch: (a) in the *yz*-plane, (b) in the *xy*-plane.

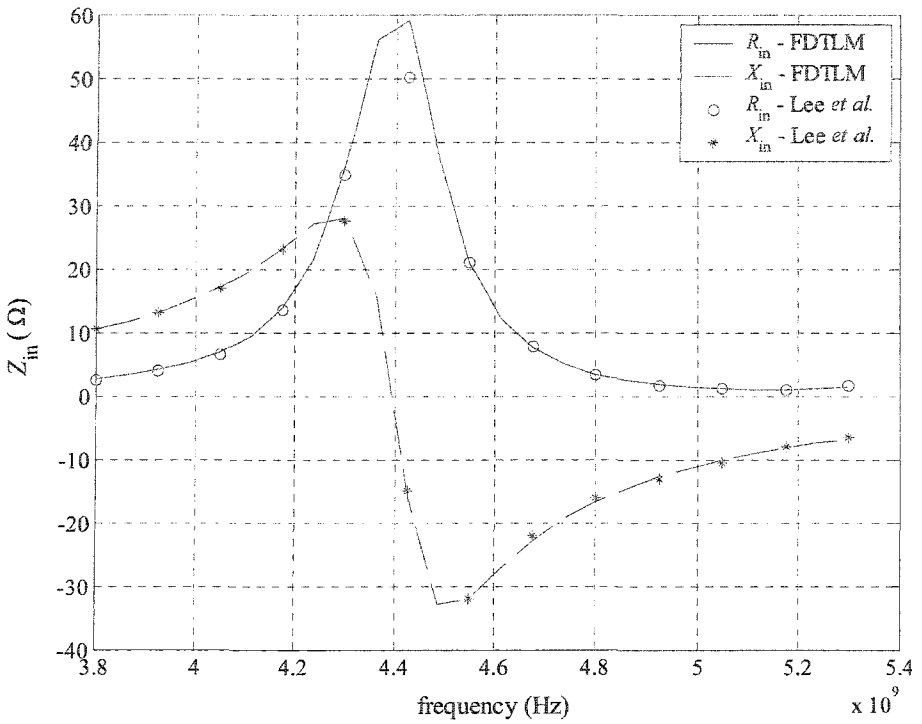

Fig. 2.13 Input impedance of the patch for a range of frequencies.

2.4.4 Printed low-pass filter (LPF)

In this example, we simulate the printed low-pass filter shown in Fig. 2.14. The relative permittivity of the substrate is $\varepsilon_r = 2.2$. The total size of the simulated problem is $N = 43 \times 37 \times 7$. We excite the structure with a voltage source applied uniformly underneath the strip-line at port 1 in the y-direction.

The transmission and reflection coefficients of the filter are computed using the same principles as with the DRF example in Section 2.4.2, i.e., the incident field is

obtained at an observation point in port 1 by simulating first the feed structure as a microstrip line. The transmitted field at an observation point in port 2 is obtained by simulating the actual filter. The responses, i.e., the *S*-parameters, are computed using (2.10) and (2.11). They are plotted in Fig. 2.15. The figure also shows a comparison with results obtained by a finite-difference time domain (FDTD) simulator.

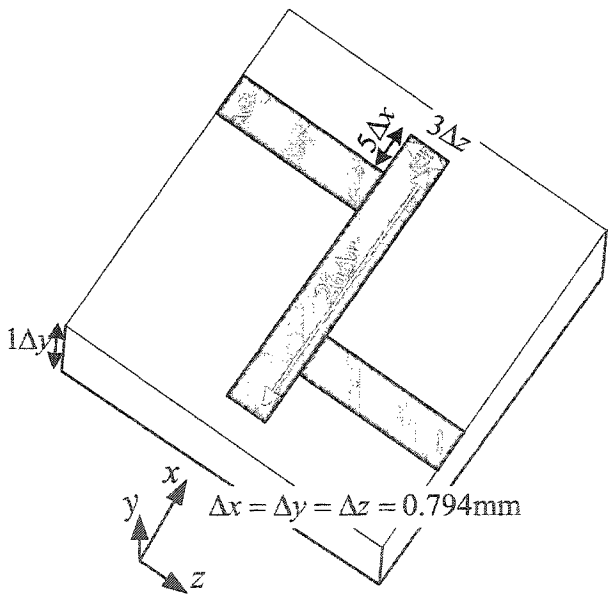

Fig. 2.14 Printed low-pass filer.

Figs. 2.16(a) and (b) plot the electric field profile underneath the microstrip circuit in the LPF at two different frequencies, in the passband at 2 GHz and in the stopband at 7 GHz.

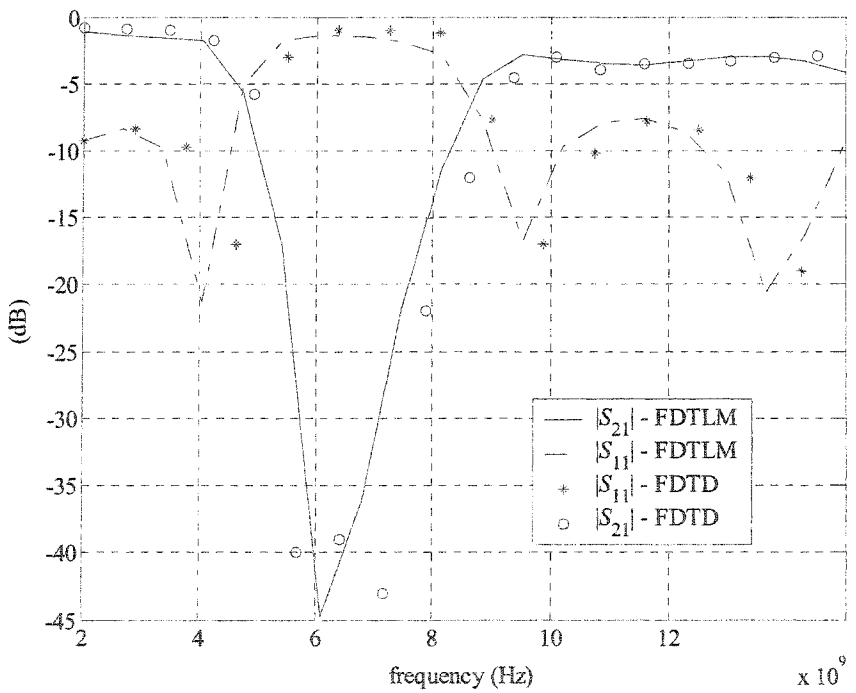

Fig. 2.15 The transmission and reflection coefficients for the printed LPF.

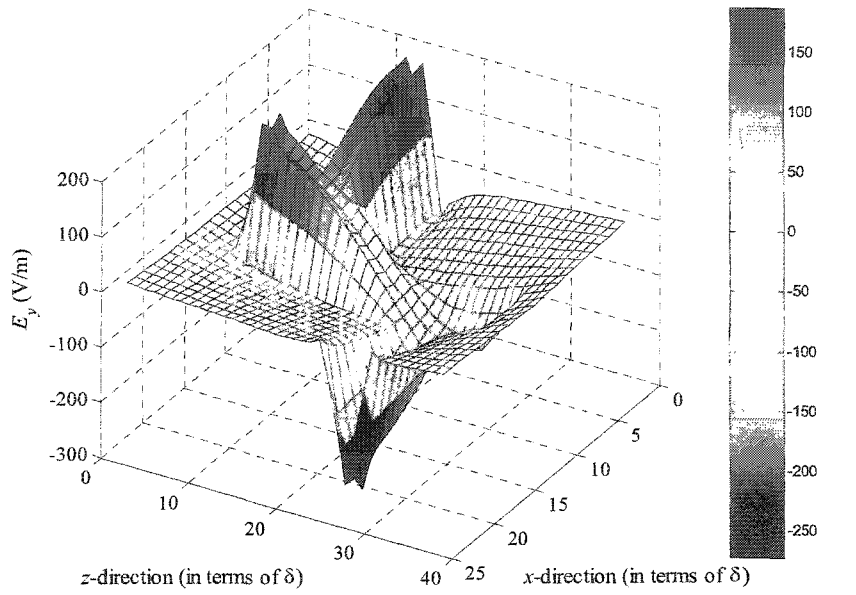

(a)

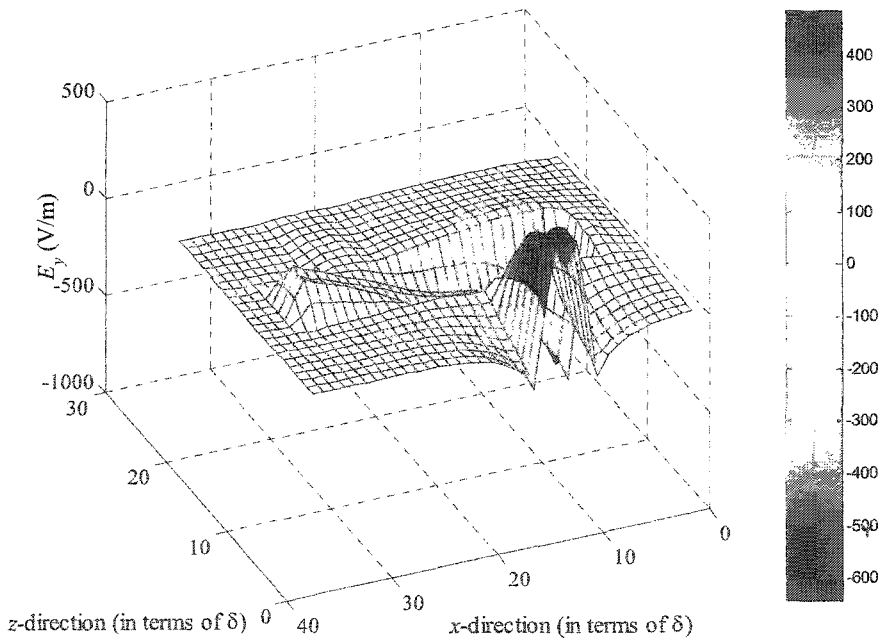

(b)

Fig. 2.16 The electric field profile in the lowpass filter: (a) at 2 GHz, (b) at 7 GHz.

2.5 SUMMARY

In this Chapter, we reviewed the FDTLM as a frequency-domain full-wave EM computational algorithm. Important computational aspects of the algorithm are discussed such as its discretization scheme, the assembly of its system of equations and their solution, the boundary conditions that terminate open problems, etc. A number of practical EM problems simulated with our in-house FDTLM solver were presented. The simulated problems discuss issues such as pre- and post-processing of the EM solution and some possible responses of interest.

The results obtained with our FDTLM simulator were tested and verified through comparisons with alternative numerical and analytical results. Our simulator showed excellent agreement and accuracy in all cases.

BIBLIOGRAPHY

Ansoft HFSS (2001), Version 3.0.25, Ansoft Corporation, Four Station Square, Suite 200, Pittsburgh, PA 15219.

Christopoulos, C., 1995. *The Transmission-line Modeling Method TLM.* IEEE Press, New York.

Johns, D. and C. Christopoulos, 1994. New frequency-domain TLM method for numerical solution of steady-state electromagnetic problems. *IEE Proc. Sci. Means Technol.*, vol. 141, pp 310-316.

Huygens, C., 1690. *Traite de la Lumiere.* Paris: Leiden.

Pasalic D., R. Vahldieck and J. Hesselbarth, 1999. The frequency-domain TLM method with absorbing boundary conditions. *IEEE MTT-S Int. Microwave Symp. Dig.*, pp. 1669-1672.

Pozar, D.M., 1993. *Microwave Engineering.* New York: Addison-Wesley Publishing Company, Inc.

Taflove, A., 1995. *Computational Electromagnetics: The Finite-Difference Time-Domain Method*, Norwood: Artech House, Inc.

Sadiku, M.N., 2001. *Numerical Techniques in Electromagnetics.* Boca Raton, FL: CRC Press LLC.

Lee, H.F. and Wei Chen, 1997. *Advances in Microstrip and Printed Antennas.* New

York: John Wiley & Sons, Inc.

Chapter 3

SENSITIVITY ANALYSIS AND STRUCTURED-GRID FULL-WAVE EM SOLVERS

In Chapter 1, we discussed the importance of robust sensitivity analysis in engineering design. We also discussed the need for computationally efficient approaches, which can significantly outperform the finite-difference approximations (FDAs) typically used for sensitivity analysis. In this chapter, we review an efficient technique for design sensitivity analysis, the adjoint variable method (AVM). We give a brief background of the method and discuss possible implementations with numerical EM solvers. We emphasize the limitations encountered with the implementation of the method when the EM solver is based on a structured grid such as the grid of the FDTLM.

As an answer to these limitations, we propose our first approximate discrete adjoint-variable technique (DAVM-I) as a possible implementation of the AVM with structured-grid solvers. The computed approximate sensitivity results are compared with FDAs, exact AVM sensitivities and analytical derivatives whenever available.

3.1 INTRODUCTION

Gradient-based optimization needs not only the objective (or response) function of the system but also its gradient in the design parameter space. The gradient may also be used for tolerance and yield analysis. With the AVM, the response and its gradient are computed with at most two system analyses regardless of the number of design parameters.

Adjoint-based sensitivity analysis has been used in control theory (Lions 1971), structural design (Haug *et al.* 1986), circuit theory (Director *et al.* 1969), etc. The implementation of the adjoint approach with EM solvers for high-frequency problems is only recent (Akel *et al.* 2000)-(Webb 2001). Exact sensitivities with the finite element method (FEM) are considered in (Webb 2001) and (Lee 1995), where analytical derivatives of the FEM system matrix with respect to the Cartesian coordinates of the mesh vertices are available. With method of moments (MoM) solvers, exact sensitivities are often not practical due to the complexity of the utilized Green's functions, expansion and weighting functions. A feasible technique for adjoint-based sensitivity analysis (EM-FAST) with the MoM is suggested in (Georgieva *et al.* 2002) where regeneration of the mesh discretizing a slightly perturbed structure is used to compute the system matrix derivatives with finite differences. In (Chung *et al.* 2000) and (Chung *et al.* 2001), unstructured grids are used to obtain exact sensitivities with the finite-difference time-domain discrete surface integral (FDTD-DSI) method. In practice, the technique requires finite-element meshing procedure. All these approaches are either impractical or inapplicable with solvers on structured grids such as the FDTD method, the TDTLM, and

the FDTLM.

In the course of this work, we formulate a family of techniques through which the AVM can be easily implemented in practical sensitivity analysis with structured-grid EM computational algorithms.

We first discuss the exact sensitivity expression with the FDTLM. In this case, analytical derivatives of the system matrix are utilized. These are available when global design parameters – such as the constitutive parameters of the material filling the whole computational domain or shape parameters stretching across the structure – are perturbed. We show that the application of the exact adjoint technique with EM solvers on structured grids is limited. This is because local shape perturbations result in system matrices that are not analytical functions of the coordinates of the mesh nodes. The local shape perturbations are restricted to multiples of the grid cell size in the respective direction. When perfect conducting boundaries are perturbed, the size of the system matrix changes, and, therefore, a meaningful definition of a derivative is not possible. When dielectric-magnetic interface boundaries are perturbed, the size of the system matrix is preserved but its coefficients, affected by the stepwise change, assume values from a predefined discrete set. The lack of continuity of the allowed matrix coefficient values forbids reliable approximations of the system matrix derivatives, and thus makes the exact adjoint-based analysis inapplicable.

Subsequently, we propose our first approximate adjoint technique for sensitivity analysis, which does not require analytical system matrix derivatives (Ali[1] *et al.* 2005), (Ali[2] *et al.* 2004), (Bakr *et al.* 2003), (Nikolova *et al.* 2004). The change in the matrix

coefficients, corresponding to a perturbation, is a "binary" switch between two known values related to the original and the perturbed boundary/interface. Our technique, unlike the finite-difference EM-FAST technique (Georgieva *et al.* 2002) puts no restrictions on the magnitude of the coefficients of these difference matrices. They can be as large as the original coefficients themselves.

3.2 SENSITIVITY ANALYSIS AND NUMERICAL EM SOLVERS

Sensitivity is a measure of the rate of change of a response function f with respect to changes in a set of design parameters $\boldsymbol{x} = [x_1, \ldots, x_K]^T$. Mathematically, it is given by the gradient of f with respect to $\boldsymbol{x}$, i.e., $\nabla_x f$.

Assume that f is a general scalar function that represents a response of interest for the linear system in (2.4). This function may have an explicit dependence on $\boldsymbol{x}$, and an implicit dependence through the state variable $\boldsymbol{v}$, i.e., $f(\boldsymbol{x}, \boldsymbol{v}(\boldsymbol{x}))$. Our objective is to determine the sensitivity of the response f with respect to $\boldsymbol{x}$, i.e.,

$$\nabla_x f, \text{ subject to } \boldsymbol{A}_R(\boldsymbol{x}) \cdot \boldsymbol{v}_R = \boldsymbol{V}_{R,s} \tag{3.1}$$

where ∇_x is defined as a row operator (Haug *et al.* 1986)

$$\nabla_x = \left[\frac{\partial}{\partial x_1} \quad \frac{\partial}{\partial x_2} \quad \cdots \quad \frac{\partial}{\partial x_K} \right], \tag{3.2}$$

and the system of equations in (3.1) illustrates a real system that corresponds to (2.4)[1] where[2]

$$A_R = \begin{bmatrix} \Re A & -\Im A \\ \Im A & \Re A \end{bmatrix},\ v_R = \begin{bmatrix} \Re v \\ \Im v \end{bmatrix},\ \text{and}\ V_{R,s} = \begin{bmatrix} \Re V_s \\ \Im V_s \end{bmatrix}. \tag{3.3}$$

Two common approaches to the solution of (3.1) are the FDA at the level of the response and the AVM.

3.2.1 Finite-difference approximations (FDA)

The forward finite-difference (FFD) approximation of the response gradient (3.1) utilizes

$$\frac{df(x_k)}{dx_k} \simeq \frac{f(x_k + \Delta x_k) - f(x_k)}{\Delta x_k},\quad k = 1,\ \ldots,\ K \tag{3.4}$$

where x_k is the value of the kth design parameter in the original problem (3.1), and Δx_k is the corresponding perturbation. Equation (3.4) is a first-order accurate approximation which requires $K+1$ full wave analyses in order to generate the response function and its sensitivity. An equivalent possibility is the backward finite-difference (BFD) approximation. Second-order accuracy can be achieved using central finite differences (CFD), which leads to $2K+1$ system analyses. Obviously, these techniques are computationally inefficient for large problems with multiple design parameters. Their advantage is in their straightforward implementation.

[1] See Appendix B for details on the transformation of complex-to-real systems of equations.
[2] Hereafter, the operators $\Re$ and $\Im$ result in the real and imaginary parts of the respective element, matrix or vector. The subscript R shows that the element, vector or matrix is real-valued.

3.2.2 Exact Adjoint-Variable Method (AVM)

On the other hand, the exact AVM obtains an estimate of the response gradient of the form (Georgieva *et al.* 2002)

$$\frac{df}{dx_k} = \frac{\partial f}{\partial x_k} + \lambda_R^T \cdot \left[\frac{\partial V_{R,s}}{\partial x_k} - \frac{\partial A_R}{\partial x_k} v_R \right], \quad k = 1, \ldots, K. \tag{3.5}$$

The partial derivative $\partial/\partial x_k$ represents an explicit dependence on x_k; A_R and $V_{R,s}$ are defined in (3.1)-(3.3); v_R represents the solution of (3.1) at the current design; and λ_R is the adjoint variable, which is the solution of the real adjoint system

$$\begin{bmatrix} \Re A & \Im A \\ -\Im A & \Re A \end{bmatrix}^T \begin{bmatrix} \Re \lambda \\ \Im \lambda \end{bmatrix} = \begin{bmatrix} \nabla_{\Re v} f & \nabla_{\Im v} f \end{bmatrix}^T. \tag{3.6}$$

In (3.6), the matrix, which is in fact A_R^T, is called adjoint to A_R in analogy with adjoint operators in functional space analysis. The right-hand term is referred to as the adjoint excitation vector. Its elements are the derivatives of the response function f with respect to the state variables v_R.

Note that the derivatives in (3.5) are computed for all K design parameters in one step, once v_R and λ_R are found. Thus, there is no need for K or $2K$ additional system analyses as in the case of response-level FDA. Only one additional analysis is needed in order to solve (3.6). In fact, if the system matrix is not very large and is LU-decomposed during the original system analysis, the same LU-factors are used to solve the adjoint problem (3.6). Thus, the additional system analysis is avoided and the gradient with

respect to all design parameters is computed with a minor computational overhead. The superior efficiency of the AVM over FDA techniques becomes more pronounced as the number of design parameters increases.

3.3 EXACT SENSITIVITY ANALYSIS LIMITATIONS WITH STRUCTURED-GRID SOLVERS

The exact AVM assumes that the analytical derivatives $\partial f/\partial x_k$, $\partial f/\partial v_R$, $\partial V_{R,s}/\partial x_k$ and $\partial A_R/\partial x_k$, $k = 1, ..., K$ exist. Usually, the first three derivatives are analytically available. On the other hand, the computation of the derivatives of the system matrix is a major problem when the solver utilizes a structured grid. Analytical system matrix derivatives are only available if the elements of the matrix are differentiable functions of the grid node coordinates. Local grid node perturbations, however, lead to unstructured grids such as the one illustrated in Fig. 3.1(b). Even if the solver permits a graded mesh, a perturbation of the geometrical detail would always require a shift of the whole grid plane as shown in Fig. 3.1(c). This is unacceptable as such perturbations may affect unrelated details of the structure, see for example, obstacle B in Fig. 3.1.

We propose to consider design parameters which are restricted to integer multiples of the TLM grid cell size δ. We then assume that their perturbations are equal to one cell size in the respective direction [see Fig. 3.2]. As we show with an example later, with such perturbations, the exact formula (3.5) is inapplicable as the accuracy of the computed sensitivities is low. A new approximate sensitivity expression is needed which can accommodate large discrete changes of the A-matrix coefficients due to the

stepwise shape parameter changes.

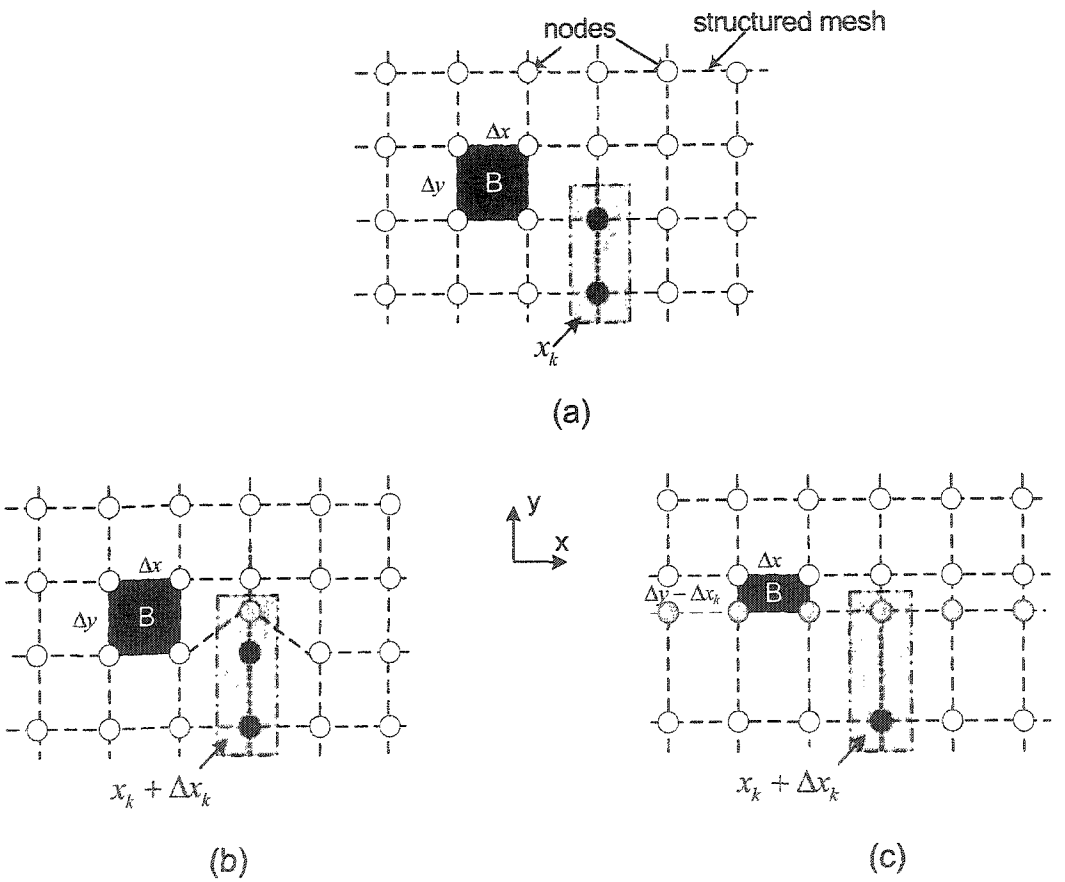

Fig. 3.1 Grid changes due to a perturbation in the design parameter x_k : (a) the original structure, (b) deformed (unstructured) grid, (c) graded structured grid due to a perturbation causing an unwanted change in the size and location of obstacle B.

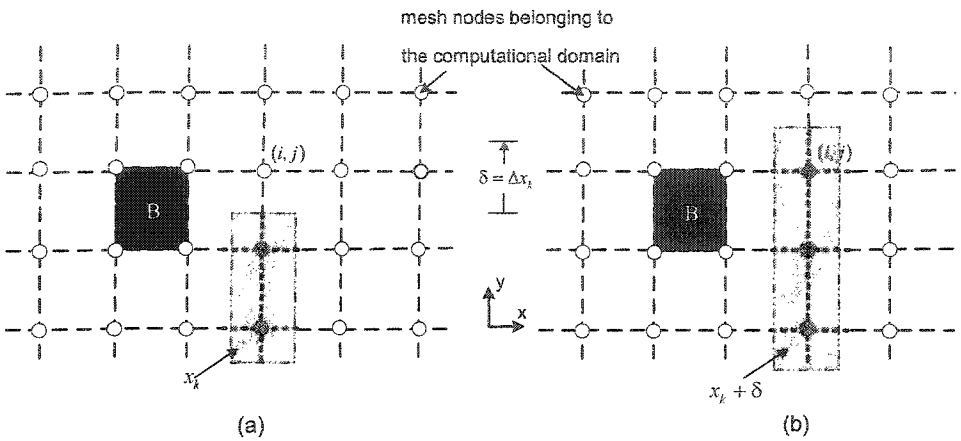

Fig. 3.2 Discrete on-grid local perturbations of δ in the design parameter x_k : (a) the original structure with the design parameter x_k; (b) the perturbed structure with the design parameter changed to $x_k + \delta$.

3.4 THE DISCRETE AVM FOR SENSITIVITY ANALYSIS WITH STRUCTURED-GRID SOLVERS (DAVM-I)

In this section, we present our first approximate adjoint-based sensitivity formula as an answer to the limitations encountered with the implementation of the AVM with structured-grid solvers. We consider the general complex-variable case, and propose a sensitivity expression that produces sensitivity estimates for a response function f subject to the complex system of equations (2.4).

Let $A_k(x + e_k) = A(x) + \Delta_k A$ be the complex perturbed system matrix due to a stepwise perturbation of $\Delta x_k = \delta$ in x_k, where $e_k \triangleq [0, ..., \underbrace{\Delta x_k}_{k\text{th-element}}, 0, ...]^T$. The respective

perturbed system of equations is

$$\left[A(x)+\Delta_k A\right]\cdot\left[v(x)+\Delta_k v\right]=V_s+\Delta_k V_s. \tag{3.7}$$

Here, $\Delta_k v$ is the change in the solution vector due to the perturbation in x_k. Simplifying (3.7), we arrive at

$$A\cdot\Delta_k v+\Delta_k A\cdot v+\Delta_k A\cdot\Delta_k v=\Delta_k V_s. \tag{3.8}$$

A possible expression for the variation of the state variables is

$$\Delta_k v=A^{-1}\left[\Delta_k V_s-\Delta_k A\cdot\left(v+\Delta_k v\right)\right] \tag{3.9}$$

assuming that A^{-1} exists.

This variation is needed to find the derivative of the response function df/dx_k, where f can be a complex quantity, $f = f_{\Re} + jf_{\Im}$. We assume that f is an analytic function of the state variables $v = v_{\Re} + jv_{\Im}$. In expanded form

$$\begin{aligned}\frac{df}{dx_k}=\frac{\partial f_{\Re}}{\partial x_k}+\left(\frac{\partial f_{\Re}}{\partial v_{1\Re}}\frac{dv_{1\Re}}{dx_k}+\frac{\partial f_{\Re}}{\partial v_{1\Im}}\frac{dv_{1\Im}}{dx_k}+\cdots+\frac{\partial f_{\Re}}{\partial v_{M\Re}}\frac{dv_{M\Re}}{dx_k}+\frac{\partial f_{\Re}}{\partial v_{M\Im}}\frac{dv_{M\Im}}{dx_k}\right)+\\ j\frac{\partial f_{\Im}}{\partial x_k}+j\left(\frac{\partial f_{\Im}}{\partial v_{1\Re}}\frac{dv_{1\Re}}{dx_k}+\frac{\partial f_{\Im}}{\partial v_{1\Im}}\frac{dv_{1\Im}}{dx_k}+\cdots+\frac{\partial f_{\Im}}{\partial v_{M\Re}}\frac{dv_{M\Re}}{dx_k}+\frac{\partial f_{\Im}}{\partial v_{M\Im}}\frac{dv_{M\Im}}{dx_k}\right).\end{aligned} \tag{3.10}$$

Due to the analyticity of f, the Cauchy-Riemann relations

$$\frac{\partial f_{\Re}}{\partial v_{m\Re}}=\frac{\partial f_{\Im}}{\partial v_{m\Im}},\quad \frac{\partial f_{\Re}}{\partial v_{m\Im}}=-\frac{\partial f_{\Im}}{\partial v_{m\Re}},\qquad m=1,\ \ldots,\ M \tag{3.11}$$

hold. Using (3.11), we write (3.10) as

$$\frac{df}{dx_k} = \frac{\partial f}{\partial x_k} + \nabla_v f \cdot \frac{dv}{dx_k}, \tag{3.12}$$

where

$$\nabla_v f = \nabla_{v\Re} f_\Re - j\nabla_{v\Im} f_\Re = \nabla_{v\Re} f_\Re + j\nabla_{v\Re} f_\Im, \text{ etc.,} \tag{3.13}$$

and

$$\frac{dv}{dx_k} = \frac{dv_\Re}{dx_k} + j\frac{dv_\Im}{dx_k}. \tag{3.14}$$

We approximate (3.12) as

$$\frac{df}{dx_k} \approx \frac{\partial f}{\partial x_k} + \nabla_v f \cdot \frac{\Delta_k v}{\Delta x_k} \tag{3.15}$$

and substitute (3.9). The result is our complex sensitivity expression-I, which we refer to as DAVM-I (Ali[1] *et al.* 2005)[3]:

$$\left(\frac{df}{dx_k}\right)_{DAVM\text{-}I} \approx \frac{\partial f}{\partial x_k} + \lambda^H \cdot \left[\frac{\Delta_k V_s}{\Delta x_k} - \frac{\Delta_k A}{\Delta x_k}\left(v + \Delta_k v\right)\right], \quad k = 1, \ldots, K. \tag{3.16}$$

In (3.16), λ is the solution of the complex adjoint system,

$$A^H \cdot \lambda = [\nabla_v f]^H. \tag{3.17}$$

Here, A^H is the Hermitian of the system matrix A in (2.4), obtained by transposition and conjugation of A. As per (3.13), the complex adjoint excitation is defined as

[3] The derivation of the sensitivity expression subject to a real system (3.3) can be found in Appendix C (Ali[2] *et al.* 2004).

$$[\nabla_v f]^H = \left[\left(\frac{\partial f_{\Re}}{\partial v_{1\Re}} + j\frac{\partial f_{\Re}}{\partial v_{1\Im}}\right)\cdots\left(\frac{\partial f_{\Re}}{\partial v_{M\Re}} + j\frac{\partial f_{\Re}}{\partial v_{M\Im}}\right)\right]^T . \tag{3.18}$$

If f is a real function, then

$$\left(\frac{df}{dx_k}\right)_{DAVM-I} \approx \frac{\partial f}{\partial x_k} + \Re\left\{\lambda^H \cdot \left[\frac{\Delta_k V_s}{\Delta x_k} - \frac{\Delta_k A}{\Delta x_k}\left(v + \Delta_k v\right)\right]\right\}, \quad k = 1, \ldots, K \tag{3.19}$$

where λ is the solution of the adjoint problem (3.17)-(3.18) with $f = f_{\Re}$. The computational effort involved in the sensitivity calculations of a complex analytic response function is equivalent to that of a real-valued response function. If f is complex but not analytic, then its real and imaginary parts, $f_{\Re}$ and $f_{\Im}$, have to be treated as two separate real-valued response functions, and two separate adjoint systems of the form (3.17)-(3.18) must be solved. In (3.18), $f_{\Re}$ is replaced by $f_{\Im}$, when solving for the sensitivity of $f_{\Im}$.

Below we summarize the features of the sensitivity formulas (3.16),(3.19):

- The adjoint vector λ requires one additional system analysis (3.17); unless LU decomposition is used to solve (2.4), in which case this analysis is reduced to forward-backward substitutions. The adjoint problem (3.17) is perturbation independent.
- The perturbed original system solutions, $v_k = v + \Delta_k v$, is perturbation dependent, and thus requires K additional system analyses, i.e., K linear systems of the form (3.7) must be solved. This drawback is overcome with

suitable approximations as discussed in detail in Section 3.5.2.

- No assumptions are made for the magnitudes of the system matrix perturbations $\Delta_k A$, $k = 1, \ldots, K$; the ratio $\Delta_k A / \Delta x_k$ does not need to represent the respective system matrix derivative with high fidelity, and, in general, it *should not* be considered its FDA.
- If, however, $\Delta_k A$, $k = 1, \ldots, K$, are sufficiently small, the second-order terms $\Delta_k A \cdot \Delta_k v$, $k = 1, \ldots, K$, in (3.16) can be neglected, thus, leading to the familiar first-order exact sensitivity expression (Nikolova *et al.* 2004):

$$\frac{df}{dx_k} = \frac{\partial f}{\partial x_k} + \lambda^H \cdot \left(\frac{dV_s}{dx_k} - \frac{dA}{dx_k} v \right), \quad k = 1, \ldots, K. \tag{3.20}$$

The first-order sensitivity expression (3.20) is applicable with numerical solvers utilizing unstructured grids because such grids allow for a continuous spectrum of values of the design shape parameters. This makes the arising system matrices differentiable with respect to the shape parameters. However, (3.20) is not suitable for structured-grid algorithms where allowable shape perturbations include only discrete on-grid parameter values. In this case, the second-order sensitivity expression (3.16) yields better accuracy.

3.5 IMPLEMENTATION OF OUR APPROXIMATE SENSITIVITY TECHNIQUE

We discuss in this section computational aspects of our proposed algorithm. These include the computation of the matrix variations $\Delta_k A$, the approximation to the solution

for the perturbed problems $v_k = v + \Delta_k v$, $k = 1, \ldots, K$ and the associated computational load.

3.5.1 Matrix variations

The assumed discrete perturbations are represented by a change in the constitutive parameters of the respective node links. The related system matrix coefficients change between two predefined values derived from the original and the perturbed node characteristics. This simple behavior is used to define the difference system matrices $\Delta_k A$, $k = 1, \ldots, K$.

Consider first the case where perturbations in the design parameter x_k are of volumetric type, i.e., a whole cell of size δ is being perturbed. For example, if an element of the FDTLM A-matrix corresponding to the (i, j)th cell [see Fig. 3.3(a)] in the computational domain has permittivity $\varepsilon_r = 2.32$. According to (2.2)-(2.3), this element is computed as $A(i, j; \varepsilon_r) = -\exp(-0.0628)$. If a discrete perturbation in the design parameter x_k requires a change in the permittivity of this cell to be $\varepsilon_r^p = 3$, then, the respective perturbed matrix coefficient is $A_k(i, j; \varepsilon_r^p) = -\exp(-0.0714)$ [see Fig. 3.3(b)]. Hence, the corresponding difference matrix coefficient is $\Delta_k A(i, j) = A_k(i, j; \varepsilon_r^p) - A(i, j; \varepsilon_r) \approx 0.008$.

Now, consider another example where a volumetric perturbation takes place in x_k when it relates to a perfect-conductor geometrical detail. In this case, an enlarged system of equations is considered that includes all cells which may be activated as a result of

boundary changes. The elements of the A-matrix that represent the perfect conductor are assumed to have a zero value instead of being eliminated. Accordingly, the change of the same A-element described above from an element representing a dielectric cell $A(i,j;\varepsilon_r) = -\exp(-0.0628)$ to an element representing a perfect conductor $A_k(i,j;\sigma \to \infty) = 0$ would produce a difference matrix coefficient of $\Delta_k A = -A(i,j;\varepsilon_r)$, i.e., $\Delta_k A \approx \exp(-0.0628)$. In general, the difference matrix is a sparse matrix with the nonzero elements being related to the perturbed cell(s) and the directly attached neighboring cell(s); e.g., the (i,j) th perturbed cell and its neighboring $(i+1,j)$, $(i-1,j)$ and $(i,j+1)$ th cells in Fig. 3.3.

The same concept applies when infinitesimal surface type perturbations take place. Such perturbations occur in printed and layered structures [see Fig.3.4(a)]. In this case, the A-matrix coefficients that correspond to the links normal to the surface face of the perturbed cell(s) have a reflection/transmission coefficient that changes between two values:

$$\Gamma_{1b} = \begin{cases} \Gamma_e = -1, & \text{metalization} \\ \Gamma_{21} \text{ or } \Gamma_{12}, & \text{demetalization.} \end{cases} \tag{3.21}$$

The reflection coefficients Γ_{21} and Γ_{12} in (3.21) are calculated from the intrinsic impedances of mediums 1 and 2 [see Section 2.3 and Fig. 2.2]. The elements of the difference matrix $\Delta_k A$ are computed the same way as with volumetric type of perturbations, i.e., as the difference between the original and perturbed matrices.

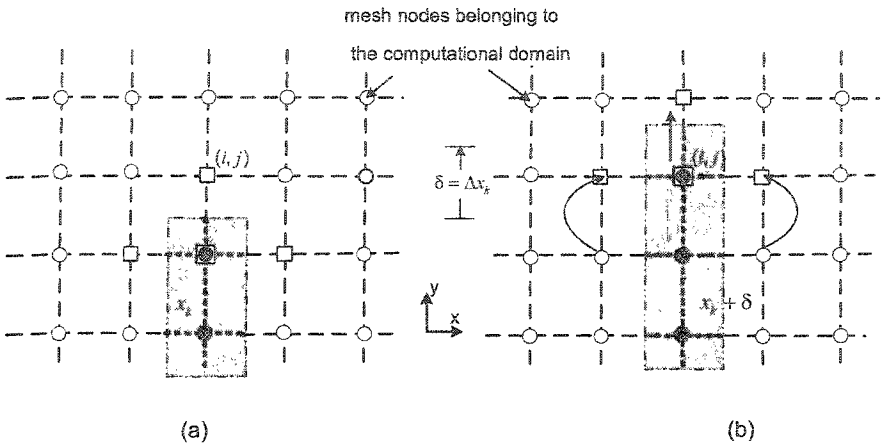

Fig. 3.3 A volumetric discrete perturbation of δ in the design parameter x_k and the corresponding mapping of the fields. The arrows denote the mapping direction: (a) the original structure with the design parameter x_k; (b) the perturbed structure with the design parameter changed to $x_k + \delta$.

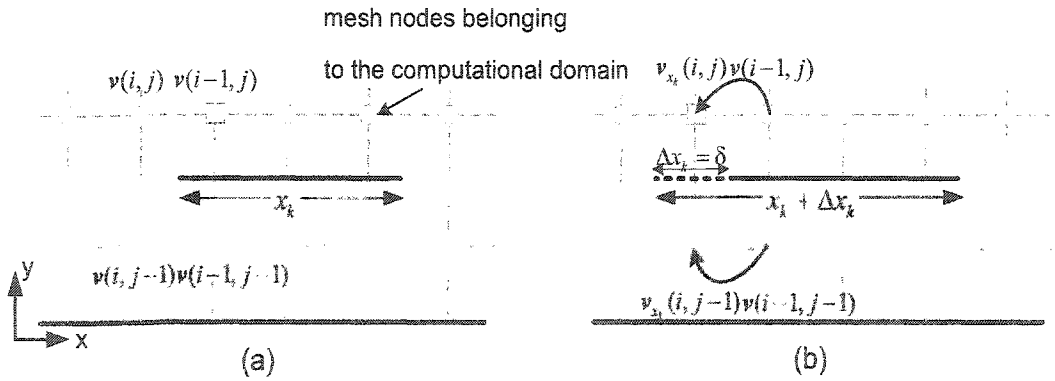

Fig. 3.4 An infinitesimal surface perturbations of size $\Delta x_k = \delta$ in the design parameter x_k and the corresponding mapping of the field. The arrows denote the mapping direction: (a) the original unperturbed structure, (b) the perturbed structure with the design parameter changed to $x_k + \delta$.

3.5.2 Approximate solutions of the perturbed problems

To preserve the computational efficiency typical for adjoint-based techniques, we avoid solving the K perturbed problems for v_k ($k = 1, \ldots, K$) by approximating the elements of $\Delta_k v$ that correspond to the nonzero elements of $\Delta_k A$. The approximation is done through a one-to-one mapping between the solution of the original and the perturbed structures in the vicinity of the local design parameter (Ali[2] *et al.* 2004),(Bakr *et al.* 2003). This approximation is based on the perturbation theory, which assumes that the EM field of the structure with a small shape or material perturbation is not much different from that of the unperturbed structure (Harrington 1961).

Table 3.1 and Fig. 3.3 illustrate this mapping approach for a volumetric type of perturbation. In this case, the solution only at the links corresponding to the nonzero elements of the difference matrix $\Delta_k A$ are mapped. These links are the ones that are directly affected by the perturbed boundary/interface. For instance, the solution of the twelve links belonging to the $(i, j-1)$ th node represented by a square node in Fig. 3.3(a) of the original problem are assigned as the solution at the respective links of the (i, j) th node in the perturbed problem also represented by squares in Fig. 3.3(b).

When conductive boundaries are perturbed, the solution at the (i, j) th node before the perturbation is $v(i, j)$. After the perturbation, the solution is approximated as

$$v_k(i, j) \simeq v(i, j-1) = 0 \tag{3.22}$$

which also follows from the vanishing field in the perfect conductor. On the other hand, when dielectric interfaces are perturbed, the field solution for the same (i, j)th node is approximated as

$$v_k(i, j) \simeq v(i, j-1). \tag{3.23}$$

Mapping is also needed at the two links normal to the perturbed boundary which are linked to the (i, j)th node, i.e., the links that belong to the neighboring $(i-1, j)$, $(i, j+1)$ and $(i+1, j)$ nodes, represented by squares in Fig. 3.3(b), of the perturbed problem. Their field solutions are assigned as that from the respective links belonging to the $(i-1, j-1)$, (i, j), and $(i+1, j-1)$ nodes in the original problem also represented by squares in Fig. 3.2(a), respectively [note the arrows in Fig. 3.3(b)].

TABLE 3.1
ILLUSTRATION OF THE MAPPING BETWEEN THE SOLUTION OF THE ORIGINAL AND PERTURBED PROBLEMS FOR A PERTURBATION IN THE DESIGN PARAMETER x_k [SEE FIG. 3.3].

cell	$(i-1, j)$	(i, j)	$(i+1, j)$	$(i, j+1)$
x_k is a dielectric object				
before perturbation	$v(i-1, j)$	$v(i, j)$	$v(i+1, j)$	$v(i, j+1)$
after perturbation	$v(i-1, j-1)$	$v(i, j-1)$	$v(i+1, j-1)$	$v(i, j)$
x_k is a metallic object				
before perturbation	$v(i-1, j)$	$v(i, j)$	$v(i+1, j)$	$v(i, j+1)$
after perturbation	$v(i-1, j-1)$	0	$v(i+1, j-1)$	$v(i, j)$

x_k : the kth ($k = 1, \ldots, K$) design parameter

v : incident voltage set at a corresponding cell, $v \in \mathbb{C}^{1\times 12}$.

The same concept is applied when approximating the perturbed problem solution due to an infinitesimal surface type perturbation. In this case, only the solutions corresponding to the two links normal to the perturbed boundary are mapped from the original to the perturbed structures. For example, Fig. 3.4(a) is the original unperturbed problem of a printed structure where x_k is the design parameter. The perturbed solution v_k due to an infinitesimal surface perturbation of $\Delta x_k = \delta$ in x_k is approximated by mapping the solution at the two normal links from the $(i-1, j)$th node in the air and $(i-1, j-1)$th nodes in the dielectric represented by squares in the original problem [see Fig. 3.4(a) and Table 3.2] to the (i, j) and $(i, j-1)$ nodes represented by squares in the perturbed problem [see Fig. 3.4(b) and Table 3.2], respectively.

The mapping approach produces very little error as long as the grid discretization is fine enough. This follows directly from the perturbation theory (Harrington 1961). The effect of the grid size on the accuracy of the estimated derivatives is discussed in more detail through examples in subsequent sections.

TABLE 3.2
ILLUSTRATION OF THE MAPPING BETWEEN THE SOLUTION OF THE ORIGINAL AND PERTURBED PROBLEMS FOR A SURFACE TYPE PERTURBATION IN THE DESIGN PARAMETER x_k [SEE FIG. 3.4].

cell	(i, j)	$(i, j-1)$
before perturbation	$v(i, j)$	$v(i, j-1)$
after perturbation	$v(i-1, j)$	$v(i-1, j-1)$

x_k : the kth ($k = 1, \ldots, K$) design parameter

v : incident voltage set at the corresponding normal links, $v \in \mathbb{C}^{1\times 2}$.

The computational overhead associated with our technique lies in the computation of the adjoint excitation $\nabla_v f$, the conjugate transposition of the system matrix $\left(A^*\right)^T$ and the approximation of the field components v_k, $k=1, ..., K$. Note that this overhead is much less than the computational requirements of a full-wave simulation. The memory requirements are also minor.

3.6 NUMERICAL EXAMPLES

We present in this section a variety of examples where we compute sensitivity estimates using our DAVM-I (3.16). The examples cover both volumetric and surface type perturbations.

3.6.1 Lossless cavity

We first illustrate the implementation of the DAVM-I for sensitivity analysis with volumetric type perturbations through a 1-D cavity example where analytical derivatives, exact-AVM, and the DAVM-I techniques can be applied, verified, and compared. The response is the input impedance of the cavity. The cavity is shorted at both ends. Its input impedance is thus purely reactive. We are interested in the sensitivity with respect to the cavity's length L, i.e., $\partial X_{in}/\partial L$. The vector of design parameters is thus $x=[L]$.

In this example, the system of equations (2.4) is not large. It is solved using LU-decomposition and the LU-factors are reused when solving the adjoint problem (3.17). Fig. 3.4 shows the sensitivities of the input reactance of the cavity with respect to its length L at $f_0=3$ GHz. The adjoint derivatives are computed as (i) exact sensitivities

using (3.20), and (ii) as approximate sensitivities using our DAVM-I (3.16). Both results are compared with the analytical derivatives [see Appendix D] calculated from the well known formula for a shorted transmission line (Pozar 1993). For the exact sensitivity, the analytical matrix derivative $\partial A/\partial L$ is computed assuming uniform shrinking/stretching of the TLM cells throughout the length of the cavity. In the case of our DAVM-I technique, the assumed perturbation of the cavity length is a one-cell metallization of the last cell at end of the line. Both AVM results show very good mutual agreement and an excellent match with the reference analytical derivative as shown in Fig. 3.5.

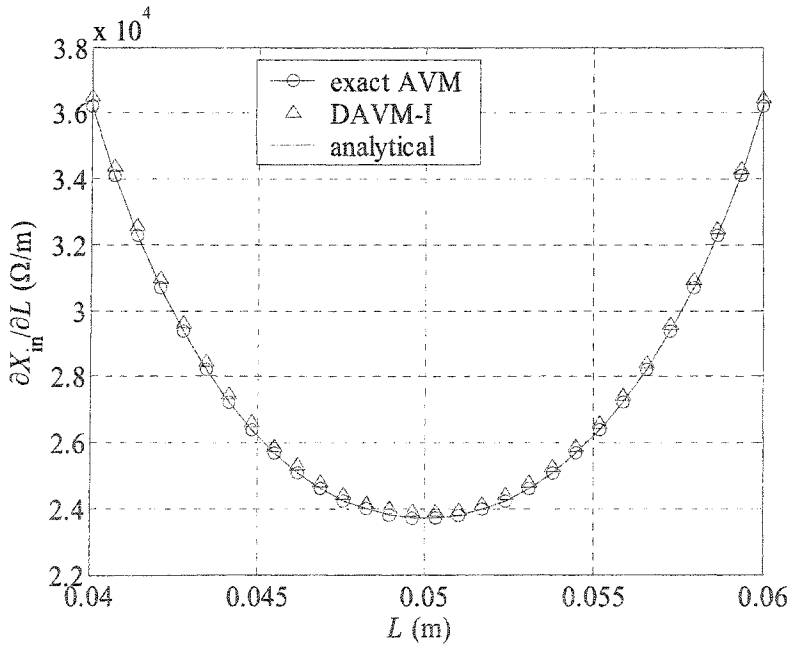

Fig. 3.5 Input impedance sensitivity of the cavity with respect to its length.

3.6.2 Exact AVM vs. approximate DAVM with on-grid perturbations: Cavity

With this example, we demonstrate that the original AVM formula (3.20) produces unreliable results when used with coarse stepwise on-grid perturbations. We show that the second-order term in our proposed DAVM-I formula (3.16) compensates for the effect of the large change in the elements of the system matrix A due to the discrete perturbations. Therefore, results produced with our discrete formula (3.16) are better.

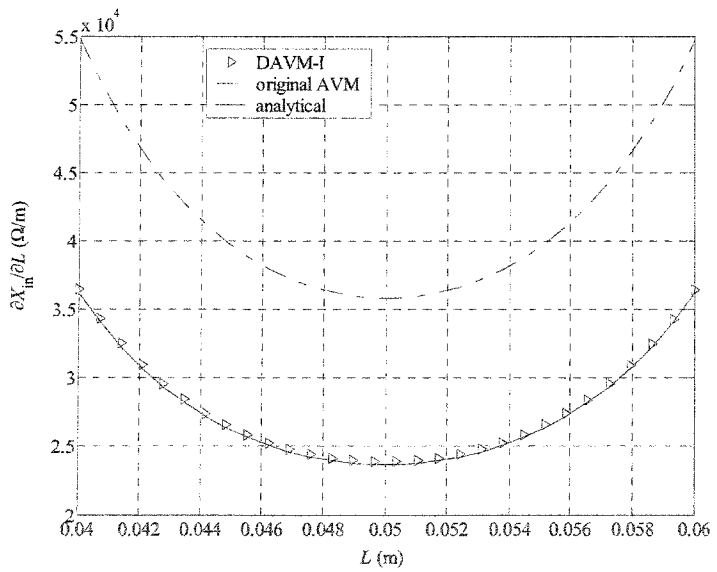

Fig. 3.6 Sensitivities of the cavity with respect to discrete perturbations in its length using the original AVM, the approximate DAVM and analytical results.

The importance of the second-order term in our sensitivity expression is shown by neglecting it in the 1-D cavity example with assumed on-grid perturbations. This means that we use the original problem solution v instead of the approximated perturbed solution v_1 (where $x_1 = L$) in (3.16). Fig. 3.6 shows a comparison between the sensitivity with the original AVM formula (no second-order term) and the sensitivity with our DAVM-I with the second-order term. Both are compared with the sensitivities calculated analytically. It is clear from the figure that the accuracy of the original AVM result with stepwise perturbations is not acceptable. This example shows that the traditional sensitivity formula performs worse than our second-order formula when coarse stepwise perturbations are implied.

3.6.3 Convergence investigation of the DAVM-I technique: Cavity

For both the exact sensitivity results computed with (3.20) and the approximate sensitivity results computed with (3.16), we assess the error as a function of the TLM grid size δ. The error is measured against the analytically calculated derivatives given in Appendix D by repeating the analysis for a number of increasingly finer grids.

Fig. 3.7 shows these errors versus the step size. As expected, the error in the exact AVM sensitivities (with analytical matrix derivatives) is smaller and affected less by the step size. The accuracy improves slowly as the step size is reduced by increasing the number of nodes N discretizing the cavity length from $N = 25$ to $N = 300$. The computational load of the full-wave simulation increases as N increases.

At first, the error in the approximate sensitivities is affected strongly by the grid

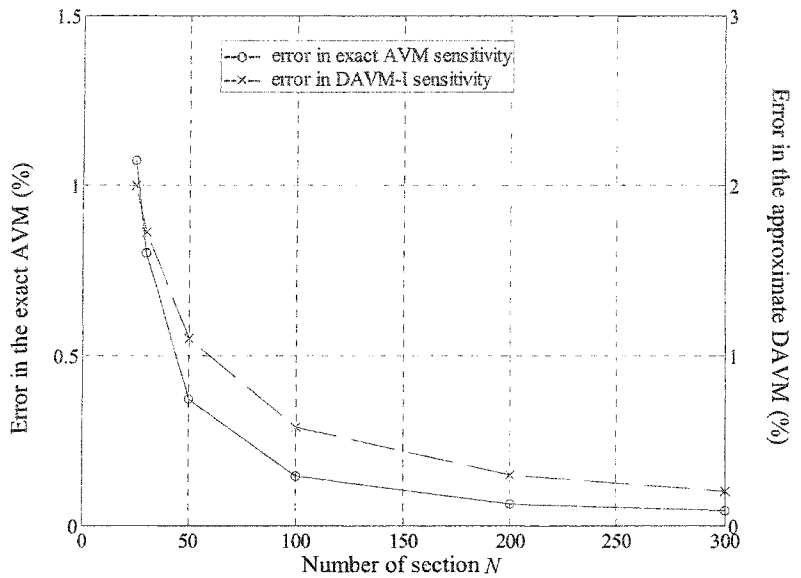

Fig. 3.7 The error against analytical results as a function of the number of cells along the length of the cavity ($x_1 = L = 0.05$ m) for the exact AVM and the DAVM-I results.

size δ. The improvement is noticeable even when a slightly finer grid is used. For example, the accuracy is almost doubled when the step size is reduced in half by doubling the number of nodes from $N = 25$ to $N = 50$. This indicates that the discretization mesh is coarse. A further, but smaller, improvement in the accuracy is achieved when the step size is reduced by a factor of two again (N goes from 50 to 100), which indicates that the solution starts to converge. The figure shows that the improvement in the accuracy is insignificant for $N > 250$. This result is also confirmed in Fig. 3.8 where the computed sensitivities converge as the step size decreases.

The choice of the discretization step size is different from one simulator to another. For a user - defined acceptable sensitivity accuracy, we recommend a

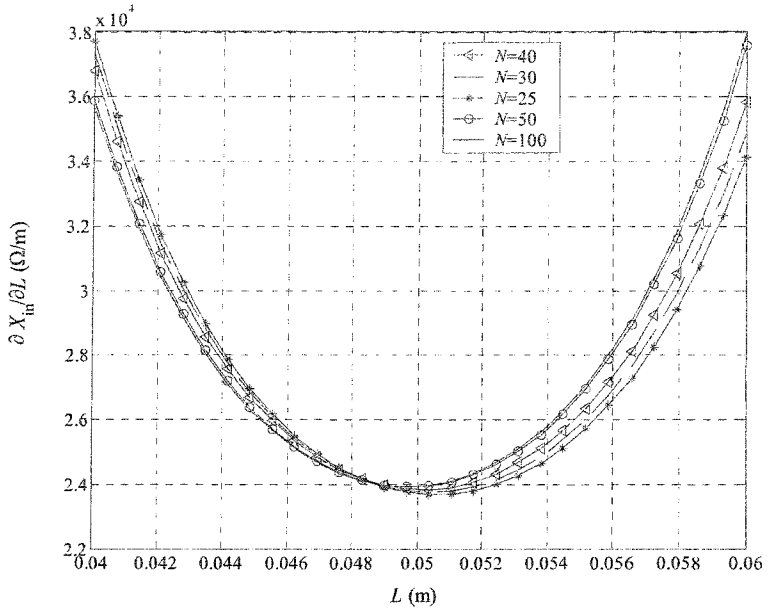

Fig. 3.8 Convergence of sensitivity results as the TLM grid becomes finer (N is the number of cells discretizing the cavity length) the DAVM-I results.

convergence test.

In general, the accuracy of our proposed technique is comparable to that of a response-level finite difference technique of the same order for a given discretization step size, i.e., if the accuracy of response-level approximations are acceptable, then, the accuracy of our discrete technique is acceptable too.

3.6.4 Hollow waveguide

We consider another example where perturbations are of volumetric type, a waveguide operating at $f_0 = 2.252$ GHz. A cubic cell of size $\delta = 2$ mm is used. Here, the solution of (2.4) is found using an iterative method. Therefore, a complete additional system analysis is needed to solve the adjoint problem (3.17).

We compute the sensitivities of the dominant mode wave impedance Z_{wg} with respect to changes in the width of the waveguide, i.e., $x_k = a$, k=1. Since changes in a happen by stretching the whole computational volume along the respective axis, $\partial A/\partial a$ is analytically available and the computation of the exact sensitivities $\nabla_a Z_{wg}$ using (3.20) is possible. The exact and discrete AVM sensitivities are compared with the analytical derivatives [see Appendix D] using the well-known formula for Z_{wg} as a function of the waveguide cross-section dimensions and frequency. In Fig. 3.9, we show the three sensitivity curves for a sweep in a. The agreement is very good.

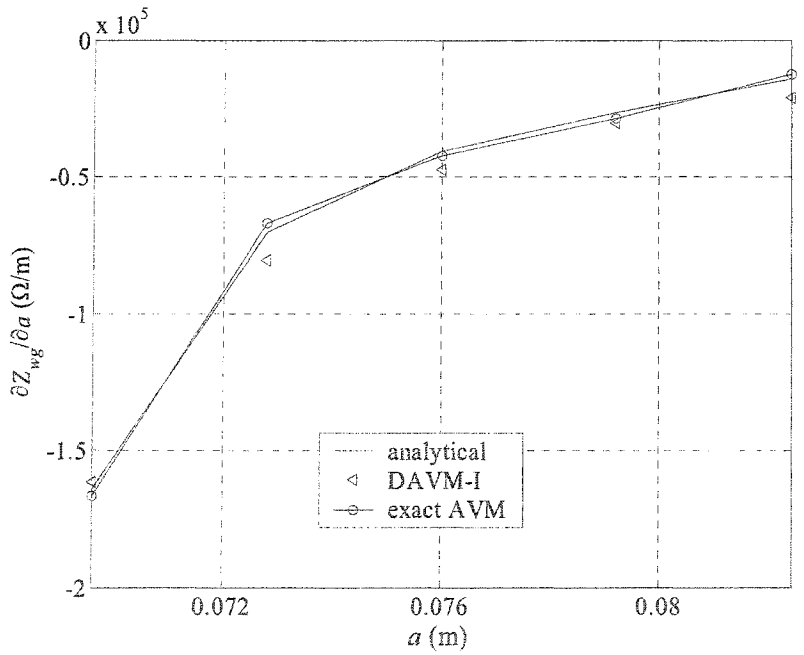

Fig. 3.9 Response derivative for the waveguide using exact and discrete adjoint techniques compared to the analytical derivative.

3.6.5 Double-resonator filter (DRF)

Using DAVM-I, we compute response sensitivities for the double-resonator filter shown in Fig. 2.6 for a range of frequencies. The filter is analyzed for its dominant mode and thus the problem reduces to two dimensions.

The response function is defined as $f = |S_{21}|$ and is shown in Fig. 2.9. The vector of design parameters is $x = [L_1 \;\; L_2 \;\; W]^T$. For comparison, the sensitivities are also computed using FFD directly at the level of the response in Figs. 3.10, 3.11, and 3.12.

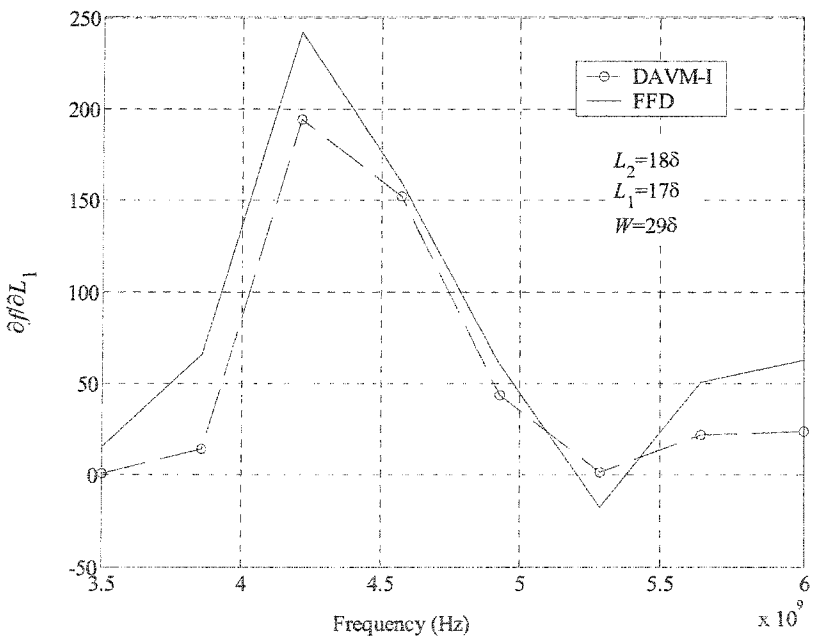

Fig. 3.10 Response sensitivity for the DRF with respect to changes in L_1 for a range of frequencies.

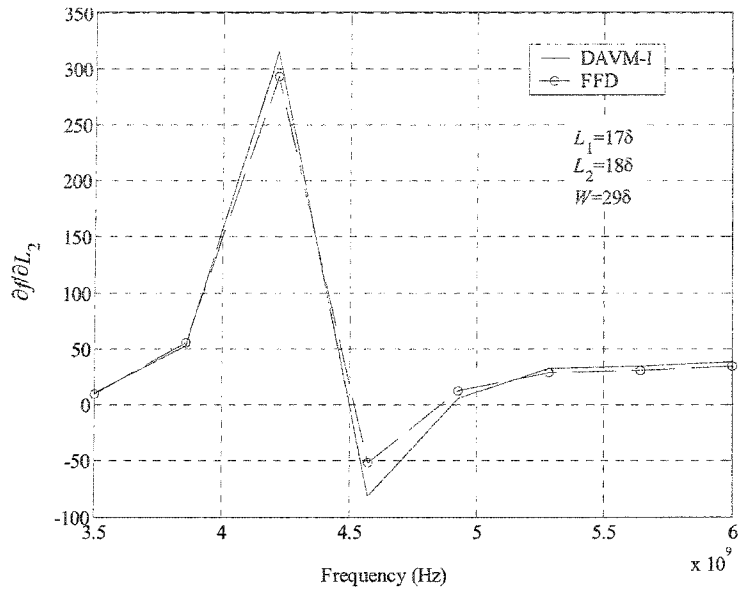

Fig. 3.11 Response sensitivity for the DRF with respect to changes in L_2 for a range of frequencies.

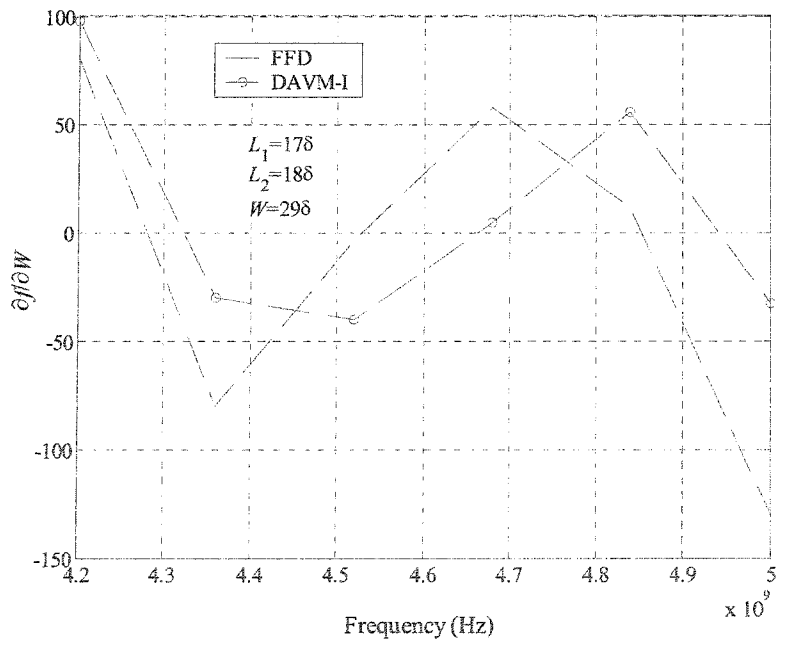

Fig. 3.12 Response sensitivity for the DRF with respect to W for a range of frequencies.

This is an example where only our discrete approach – and hence our DAVM-I formula for sensitivity estimates – can be applied to accommodate a perturbation in the design parameters. This is due to the fact that the geometrical perturbations in each of the design parameters should be independent of the other design parameters, as well as the excitation, the distance to the matching boundaries, and other unrelated geometrical and material features of the structure.

3.6.6 Microstrip line

The proposed technique is also tested with infinitesimally-thin surface type perturbations. The sensitivity of the characteristic impedance Z_c of the microstrip line shown in Fig. 3.13 is computed at 3 GHz. The substrate permittivity is $\varepsilon_r = 2.32$. Its height is $h = 2$ mm. The symmetry of the structure is used and, thus, only half of it is simulated. The design parameter is the width of the line, i.e., $x_k = W$, $k = 1$.

The derivative $\nabla_W Z_c$ is computed in two different ways: as a CFD approximation and with our discrete adjoint technique. The sensitivity of Z_c is evaluated in the range from $W = 4\delta$ to $W = 10\delta$, where $\delta = 1$ mm is the TLM grid size.

In our discrete adjoint sensitivity estimation, the derivative of the excitation with respect to the width of the microstrip line is computed with finite differences [see Fig. 3.14]:

$$\frac{\Delta V_s}{\Delta W} \simeq \frac{V_s(W + \Delta W) - V_s(W)}{\delta}. \tag{3.24}$$

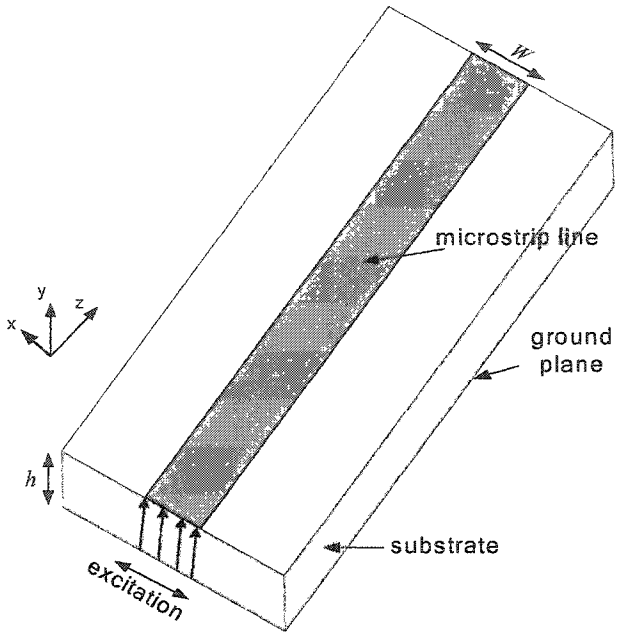

Fig. 3.13 Microstrip line.

The discrete sensitivities are compared with the CFD derivatives as shown in Fig. 3.15. A good agreement is achieved, which shows that the accuracy of our estimates is comparable to that of the CFD estimates. Our technique, however, is much more efficient.

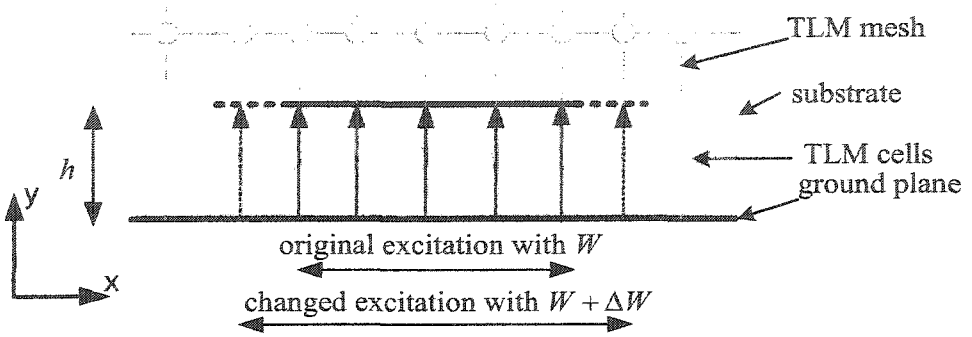

Fig. 3.14 Perturbation of the strip width and the associated change in the excitation vector V_s. Notice that the excitation voltage is now being added to the cells beneath the "metalized" faces (dash line).

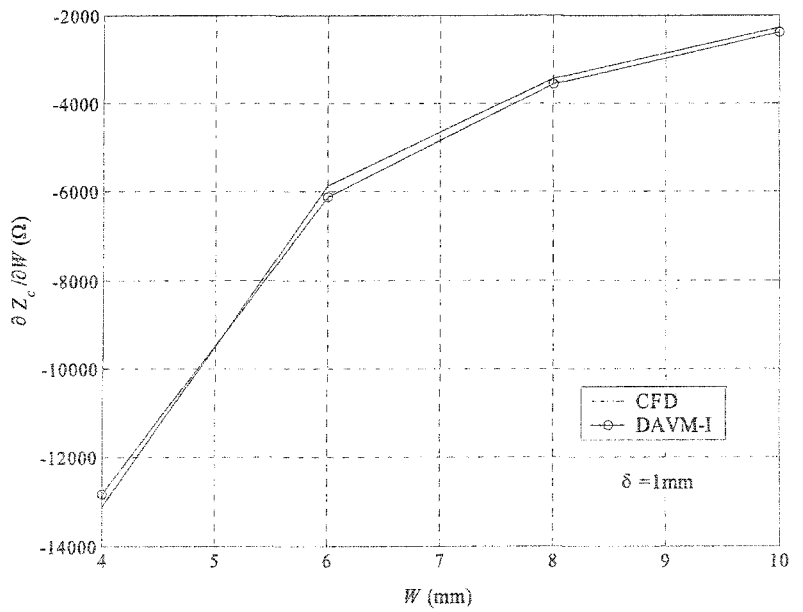

Fig. 3.15 Response sensitivity of the microstrip line for different values of W.

3.6.7 Probe-fed patch antenna

Our last example tests the proposed technique in evaluating the sensitivities of the real part of the input impedance R_{in} of a printed patch antenna [see Fig. 2.10] at 4.4 GHz. The patch is probe-fed at $W/2$ and $L/4$, where W and L are the physical width and length, respectively. The thickness of the substrate supporting the patch is $h = 1.524$ mm with permittivity $\varepsilon_r = 2.2$. The computational domain is discretized with a uniform TLM mesh of $\delta = 1.524$ mm. The domain size is $N = 35 \times 8 \times 29$ nodes.

The sensitivity of R_{in} is computed with respect to the physical length and width of the patch, i.e., $\nabla_x R_{in} = \left[\partial R_{in}/\partial L \quad \partial R_{in}/\partial W\right]$. These sensitivities are computed (i) as a FDA at the level of the response, and (ii) using our DAVM-I technique.

Figs. 3.16 and 3.17 show a comparison between the sensitivities computed with FDA and with our discrete sensitivity estimation for a sweep of the parameter L. The sensitivities for a sweep in the parameter W are shown in Figs. 3.18 and 3.19, respectively. A good match is obtained in all cases.

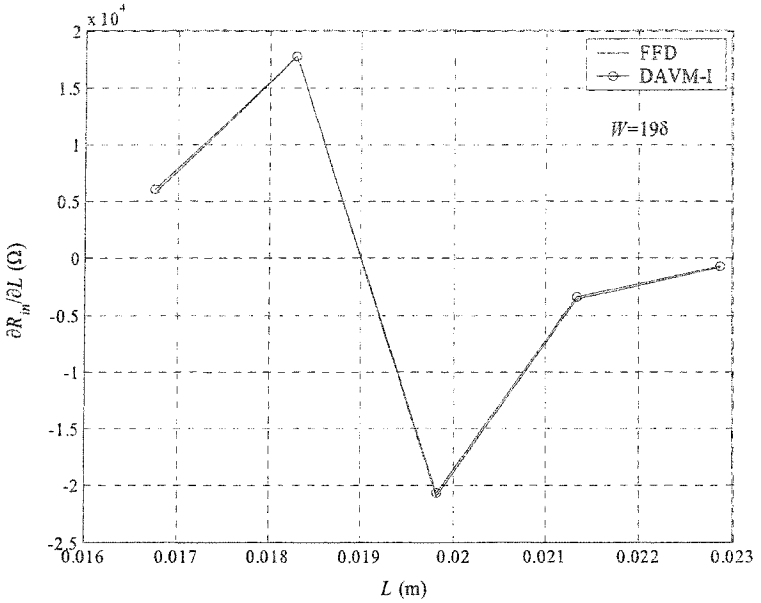

Fig. 3.16 Sensitivities of the patch antenna at $W = 19\delta$ for different values of L.

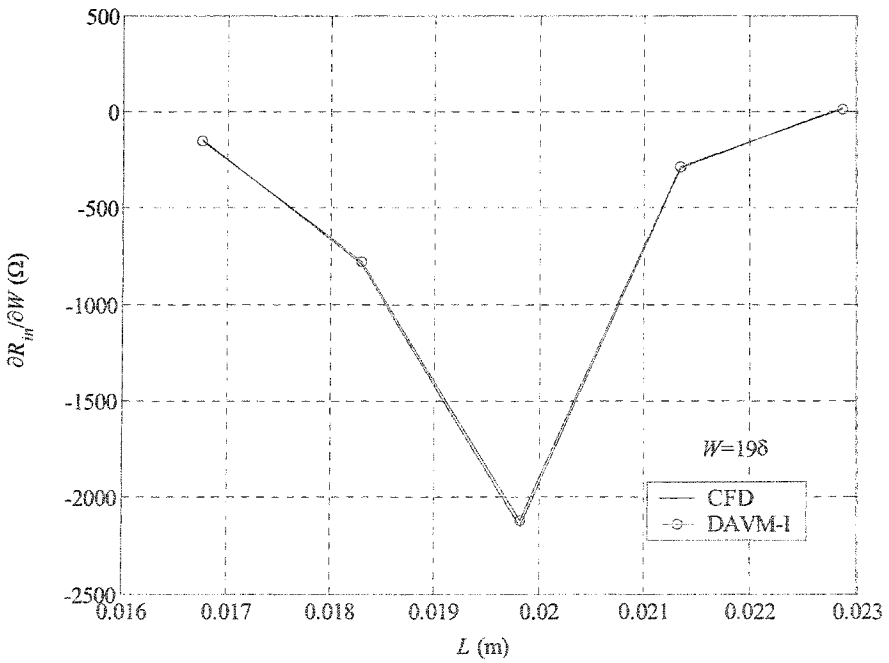

Fig. 3.17 Sensitivities of the patch antenna at $W = 19\delta$ for different values of L.

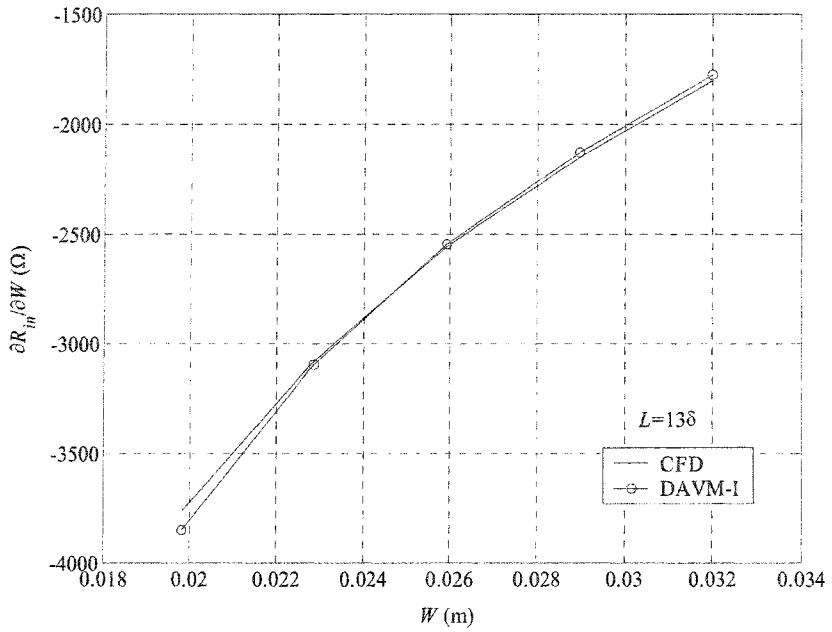

Fig. 3.18 Sensitivities of the patch antenna at $L = 13\delta$ for different values of W.

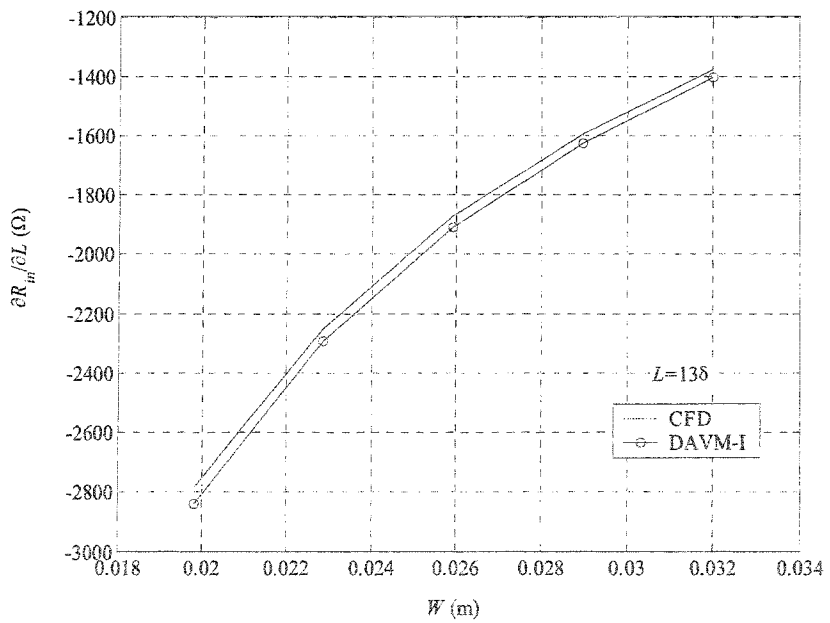

Fig. 3.19 Sensitivities of the patch antenna at $L = 13\delta$ for different values of W.

3.7 SUMMARY

We presented in this chapter a variety of techniques for sensitivity analysis with full-wave EM solvers. We first introduced simple finite-difference techniques for sensitivity analysis at the response-level. They invoke the EM simulator to run a full-wave analysis for each perturbation in each of the design parameters, i.e., if the design problem has K design parameters, the simulator runs at least K+1 full-wave simulations to compute the response and its first-order gradient.

A more computationally efficient technique, the exact AVM, was also introduced. With this technique, at most, two full-wave simulations are required for the computation of the response and its gradient regardless of K. The implementation of the AVM with the FDTLM solver was briefly discussed. The limitations encountered with such an exact approach with EM solvers based on structured grids are emphasized. These are mainly related to the computation of the derivatives of the system matrix with respect to perturbations in geometrical design parameters.

As a first step towards the successful implementation of the AVM with structured-grid solvers, we presented here our first approximate discrete AVM (DAVM-I) technique. Since our discrete technique is adjoint-based, it still requires only two system analyses to estimate the response and its gradient. Analytical derivatives of the system matrix are not required. The implementation of the technique is simple as it does not require major changes in the existing EM code. The accuracy of the estimated derivatives is good when compared to analytically calculated derivatives, finite-difference estimates and exact AVM estimates.

BIBLIOGRAPHY

Ali[1], S.M., N.K. Nikolova, and M.H. Bakr, accepted 2005. A discrete adjoint variable method for printed circuit board CAD. *INFORMS Journal on Computing.*

Ali[2], S.M., N.K. Nikolova, and M.H. Bakr, May 2004. Sensitivity analysis with full-wave EM solvers based on structured grids. *IEEE Trans. Magnetics*, vol. 40, no. 3, pp. 1521-1529.

Akel, H. and J.P. Webb, July 2000. Design sensitivities for scattering-matrix calculation with tetrahedral edge elements. *IEEE Trans. on Magnetics*, vol. 36, no. 4, pp. 1043-1046.

Bakr, M.H. and N.K. Georgieva, Sep. 2003. An adjoint variable method for frequency domain TLM problems with conducting boundaries. *IEEE Microwave and Wireless Components Lett.*, pp. 408-410.

Chung, Y., C. Cheon, and S. Hahn, Dec. 2000. Optimal shape design of microwave device using FDTD and design sensitivity analysis. *IEEE Trans. Microwave Theory Tech.*, vol. 48, pp. 2289-2296.

Chung, Y.S., C.C. Cheon, I.H. Park, and S.Y. Hahn, Sep. 2001. Optimal design method for microwave device using time domain method and design sensitivity analysis – part II: FDTD case. *IEEE Trans. Magnetics*, vol. 37, no. 5, pp. 3255-3259.

Director, S.W. and R.A. Roher, Aug. 1969. The generalized adjoint network and network sensitivities. *IEEE Trans. Circuit Theory*, vol. CT-16, pp. 318-323.

Georgieva, N.K., S.G. Glavic, M.H. Bakr and J.W. Bandler, June 2002. Feasible adjoint sensitivity technique for em design optimization. *IEEE MTT-S Int. Microwave Symp. Dig.* (Seattle, WA), pp. 971-974.

Haug, E.J., K.K. Choi and V. Komkov, 1986. *Design Sensitivity Analysis of Structural Systems.* Orlando, Florida: Academic Press, Inc.

Harrington, R.F., 1961. *Time-harmonic electromagnetic fields.* New York: McGraw-Hill book company, Inc.

Pozar, D.M., 1993. *Microwave Engineering.* New York: Addison-Wesley Publishing Company, Inc.

Nikolova, N.K., J.W. Bandler, and M.H. Bakr, Jan. 2004. Adjoint techniques for sensitivity analysis in high-frequency structures CAD. *IEEE Trans. Microwave Theory Tech.*, vol. 52, no. 1, pp. 403-419.

Nikolova, N.K., S.M. Ali, M.H. Bakr, E.A. Soliman, and J.W. Bandler, April 2004. Response sensitivity analysis with frequency-domain full-wave electromagnetic solvers. *20th Annual Review of Progress in Applied Computational Electromagnetics* (Syracuse, NY), CD ROM.

Lee, H.B., H.K. Jung, and S.Y. Hahn, May 1995. Shape optimization of H-plane waveguide Tee junction using edge finite element method. *IEEE Trans. Magnetics*, vol. 31, no. 3, pp. 1928-1931.

Lions, L.J., 1971. *Optimal Control of Systems Governed by Partial Differential Equations.* Berlin: Springer Verlag.

Webb, J.P., Sep. 2001. Design sensitivity using high-order tetrahedral vector elements. *IEEE Trans. Magnetics*, vol. 37, no. 5, pp. 3600-3603.

Webb, J.P., March 2002. Design sensitivity of frequency response in 3-D finite-element analysis of microwave devices. *IEEE Trans. Magnetics*, vol. 35, no. 2, pp. 1109-1112.

Chapter 4

IMPROVED DISCRETE SENSITIVITY ANALYSIS WITH CENTRAL DIFFERENCES AT THE SYSTEM LEVEL

In Chapter 3, we presented a novel discrete adjoint technique (DAVM-I) for sensitivity analysis with structured-grid solvers and its applications with the FDTLM. The proposed technique has superior computational efficiency over finite difference approximation (FDA) techniques which are computed at the level of the response. The proposed technique is also advantageous over the original exact AVM technique which requires analytical derivatives of the system matrix. It (i) computes the response and its gradient in the design parameter space with at most two system analyses, (ii) requires no analytical derivatives of the system matrix, (iii) is easy to implement in already existing EM codes, and (iv) has proven to provide good accuracy.

In this chapter, we propose an improvement to the discrete adjoint-based technique for sensitivity analysis with structured-grid solvers. The accuracy of the estimated derivatives with the newly proposed technique is significantly improved while

preserving the computational advantages of our original DAVM-I. Since the new technique is based on the DAVM-I, it has equivalent pre-processing and computational requirements: no analytical pre-processing of the system matrix derivatives is required, and at most two system analyses are sufficient to estimate the response and its gradient.

4.1 INTRODUCTION

Our original discrete adjoint technique DAVM-I gives results of good accuracy since it utilizes a novel sensitivity expression, which preserves the second-order term. However, as shown in Section 3.4.4 (Ali[2] *et al.* 2004), the accuracy of the computed derivatives deteriorates with a coarser grid and a highly nonlinear response function. This is because, to some extent, the advantage of the second-order term in the sensitivity formula – which compensates for the assumed coarse stepwise perturbations –are offset by the forward nature of these perturbations. The accuracy improves with a finer grid. Yet, the improvement may not be sufficient depending on the nonlinearity of the response function.

Here, we propose a second-order central sensitivity formula (CAVM-I) for approximate adjoint sensitivities with structured grid solvers (Ali[3] *et al.* 2004). It is based on the DAVM-I technique with one substantial difference: the virtual perturbations are utilized in both directions, forward and backward, for each design parameter. This preserves the advantages of the second-order term, and hence, the accuracy of the estimated sensitivities is significantly improved. The backward analysis is based on an assumed change in the material constants of the on-grid perturbed cell(s) resulting from a backward perturbation, i.e., a decrease of the design parameter.

As with all adjoint-based techniques, regardless of the number of design parameters, our new enhanced central technique CAVM-I requires the solution of only two full-wave problems in order to estimate the response and its sensitivities; i.e., it does not increase the computational effort. However, the accuracy of the estimated

sensitivities is significantly improved.

4.2 THE CENTRAL DISCRETE AVM (CAVM-I)

So far, the on-grid perturbations in the shape design parameters have been realized by the assumption of a metallization (Ali[1] *et al.* 2005),(Ali[2] *et al.* 2004), (Bakr *et al.* 2003), (Nikolova *et al.* 2004) or by a dielectric change (Ali[2] *et al.* 2004) of a cell or a cell face in the forward[1] direction (an increase of the design parameter by a cell size δ). Here, we consider another equally valid possibility, which is the demetallization or dielectric change of a cell or a cell face in the backward direction; i.e., perturbations in the design parameter x_k are of the form $x_k^p = (n-1)\delta$ [see Fig. 4.1c]. The perturbed system is defined similarly to (3.7) but with $\boldsymbol{e}_k \triangleq [0, ..., -\Delta x_k, 0, ...]^T$. We refer to this problem as the "backward problem", and its terms are marked with a $-$ sign. The backward adjoint sensitivity formula is analogous to (3.16).

The adjoint solution λ is the same in the forward and backward sensitivity formulas. $\partial f / \partial x_k$ and $\partial V_s / \partial x_k$ are usually analytically available, or are estimated with finite differences. $\Delta_k \boldsymbol{A}^{\pm}$ and $\boldsymbol{v}_k^{\pm}$ are direction dependent, and thus differ in the two formulas. The forward difference matrix $\Delta_k \boldsymbol{A}^{+}$ is found as described in Section 3.5.1, i.e., the nonzero elements of $\Delta_k \boldsymbol{A}^{+}$ are computed as the difference between two known matrices of the original and the forward perturbed matrix as:

$$\Delta_k \boldsymbol{A}^{+} = \boldsymbol{A}_k^{+} - \boldsymbol{A}, \qquad k = 1, ..., K. \tag{4.1}$$

[1] Hereafter, terms related to the forward perturbed problem are marked with a + sign.

Likewise, the backward difference matrix $\Delta_k A^-$ is computed as

$$\Delta_k A^- = A - A_k^-, \quad k = 1, \ldots, K. \tag{4.2}$$

We avoid solving the $2K$ forward and backward perturbed problems for $v_k^{\pm}$ ($k = 1, \ldots, K$) by approximating their solutions via the perturbational approach described in Section 3.5.2 (Ali[1] *et al.* 2005),(Ali[2] *et al.* 2004),(Bakr *et al.* 2003). Note that we need only incident-voltage values that correspond to the nonzero elements of the matrices $\Delta_k A^{\pm}$. The locations, at which these values are recorded for both forward and backward problems, are illustrated by the arrowed links in Fig. 4.1. The incident voltages at the arrowed links in Fig. 4.1(b) for the forward problem (open-head arrows) and those of Fig. 4.1(c) for the backward problem (bold-head arrows) are approximated by the corresponding incident voltages at the open/bold-head arrowed links of the unperturbed problem in Fig. 4.1(a), respectively. Thus, the solution at the $(i-1, j)$th node in the forward problem $v_k^+(i-1, j)$ is approximated as $v_k^+(i-1, j) = v(i, j)$ [see Figs. 4.1(a) and 4.1(b)]. In the backward problem, the solution at the (i, j)th node $v_k^-(i, j)$ is approximated as $v_k^-(i, j) = v(i-1, j)$ [see Figs. 4.1(a) and 4.1(c)].

The same mapping approach described above is used for forward and backward infinitesimally thin surface perturbations. Fig. 4.1 can be adapted to such perturbations by collapsing the plane $a'b'$ onto the ab plane or *vice versa.*

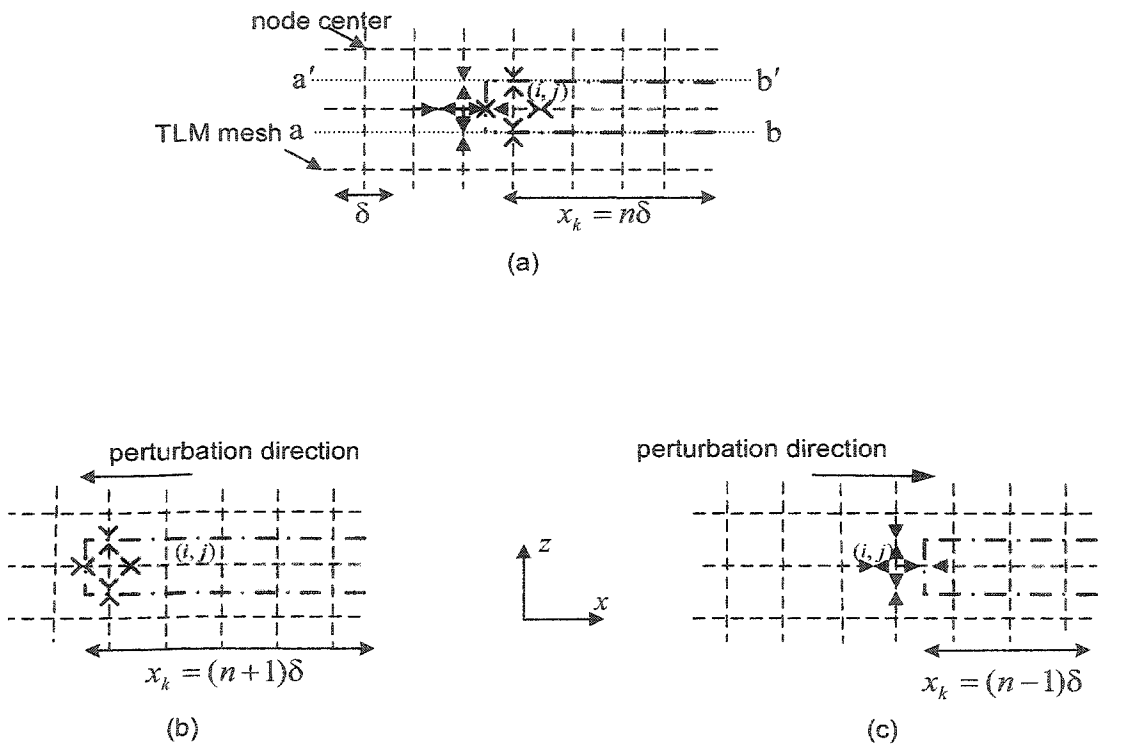

Fig. 4.1 Illustration of a one cell perturbation of a geometric detail (shaded cells): (a) the original problem, (b) the forward problem, and (c) the backward problem. The arrowed links in (b) and (c) are approximated by their corresponding ones from (a).

We write (3.16) for the forward adjoint sensitivity formula FAVM-I

$$\left(\frac{df}{dx_k}\right)_{FAVM\text{-}I} \simeq \frac{\partial f}{\partial x_k} + \lambda^H \cdot \left\{ \frac{V_{k,s}^+ - V_s}{\Delta x_k} - \frac{A_k^+ - A}{\Delta x_k} v_k^+ \right\}, \quad k = 1, \ldots, K \tag{4.3}$$

and for the backward sensitivity formula BAVM-I

$$\left(\frac{df}{dx_k}\right)_{BAVM\text{-}I} \simeq \frac{\partial f}{\partial x_k} + \lambda^H \cdot \left\{ \frac{V_s - V_{k,s}^-}{\Delta x_k} - \frac{A - A_k^-}{\Delta x_k} v_k^- \right\}, \quad k = 1, \ldots, K. \tag{4.4}$$

The central adjoint sensitivity formula (CAVM-I) is found by simplifying their average:

$$\left(\frac{df}{dx_k}\right)_{CAVM\text{-}I} \simeq \frac{\partial f}{\partial x_k} + \lambda^H \cdot \left\{ \frac{\Delta_k V_s^+ + \Delta_k V_s^-}{2\Delta x_k} - \frac{\Delta_k A^+ v_k^+ + \Delta_k A^- v_k^-}{2\Delta x_k} \right\}, \tag{4.5}$$

$k = 1, \ldots, K.$

Notice that the central formula (4.5) still requires only two full-wave simulations – of the original and the adjoint problems – to estimate the gradient with respect to all K design parameters, provided that we use our mapping technique to find the needed elements of v_k^+ and v_k^-.

4.3 NUMERICAL EXAMPLES

In this section, we show sensitivity results computed with our central adjoint technique through a variety of different structures. The structures are chosen such that: (i) different types of perturbations are possible, i.e., volumetric perturbations, as in waveguide structures, as well as metallic surface perturbations in printed structures; and (ii) the

selected response is a highly nonlinear function of its design parameters.

4.3.1 Probe-fed patch antenna

We first illustrate the central approach CAVM-I with the probe-fed patch antenna shown in Fig. 2.10 at 4.4 GHz.

The sensitivities of the input impedance $Z_{in} = R_{in} + jX_{in}$ with respect to $x = [W \quad L]^T$ for a sweep in L are computed with our CAVM-I, as well as with response-level FFD, BFD, and CFD. It is clear from the results in Figs. 4.2, 4.3 and 4.4 that the accuracy in the sensitivities computed with our approach is comparable to that of the second-order CFD. However, our approach requires only two system analyses compared to five with the CFD to compute Z_{in} and $\nabla_x Z_{in}$. Thus, for an equivalent order of accuracy, our approach reduces the number of required full-wave simulations by $(2K-1)$ at each design iteration. The efficiency of our adjoint technique is thus more pronounced in large problems with many design parameters.

This structure has a highly nonlinear response function where a small change in the design parameter results in a large change in the response. For example, at $L = 0.017$ m, 7% change in L would result in roughly 70% change in Z_{in}; while at $L = 0.02$ m, 8% change in L results in 220% change in Z_{in}. The latter point is close to resonance where the input impedance of the antenna is a highly sensitive function of L. The effect of the response nonlinearity is clearly visible in the differences between the derivative estimates obtained by the response-level FFD, BFD, and CFD. Similar differences exist among the adjoint sensitivities, as seen from the adjoint curves plotted in Figs. 4.2 and 4.3. Notice

that the central response-level and adjoint estimates agree well even at the resonance region of high response sensitivity. The difference between the derivative estimates is less pronounced for W [see Fig. 4.4]. This is due to the smoother dependence of Z_{in} on W. We also notice in this case that the adjoint techniques [see CAVM-I and FAVM-I curves in Fig. 4.4] exhibit much better mutual agreement than the finite-difference estimates at the response level. This indicates that our adjoint techniques feature better convergence for a given grid size.

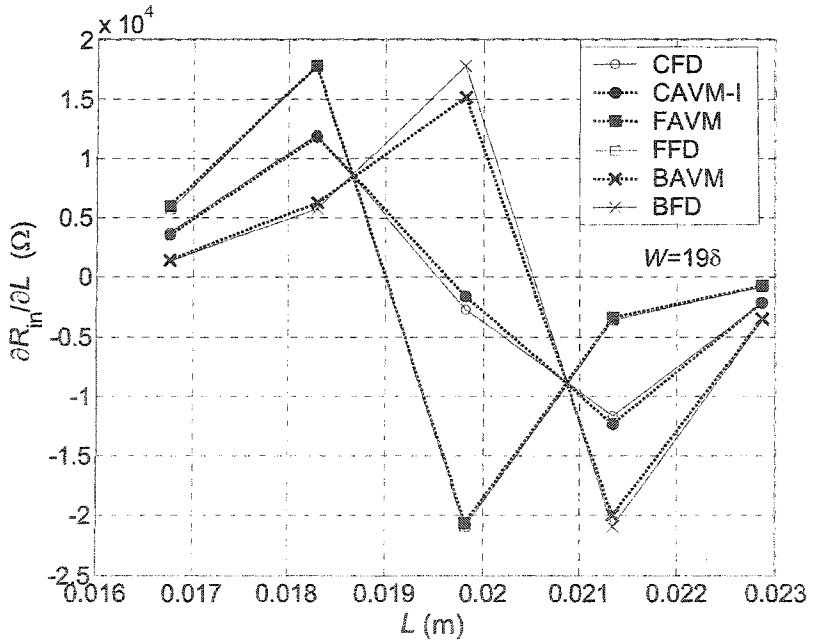

Fig. 4.2 Sensitivity of the input resistance of the patch antenna with respect to its length, $W = 19\delta$.

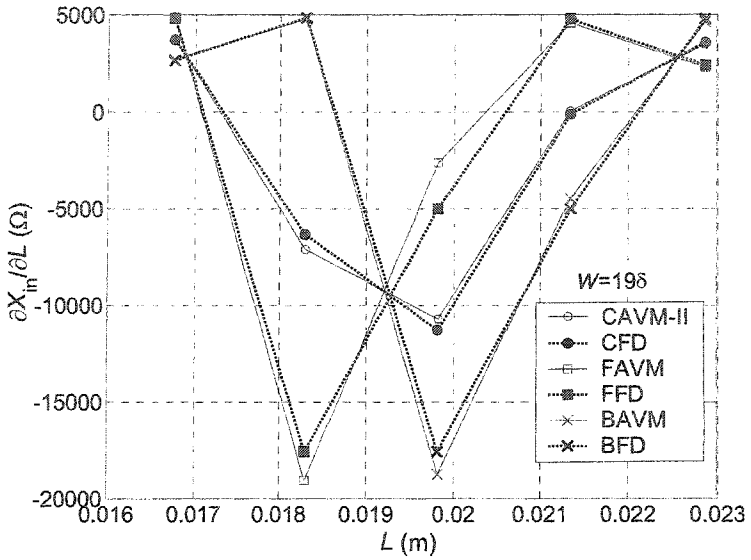

Fig. 4.3 Sensitivity of the input reactance of the patch antenna with respect to its length, $W = 19\delta$.

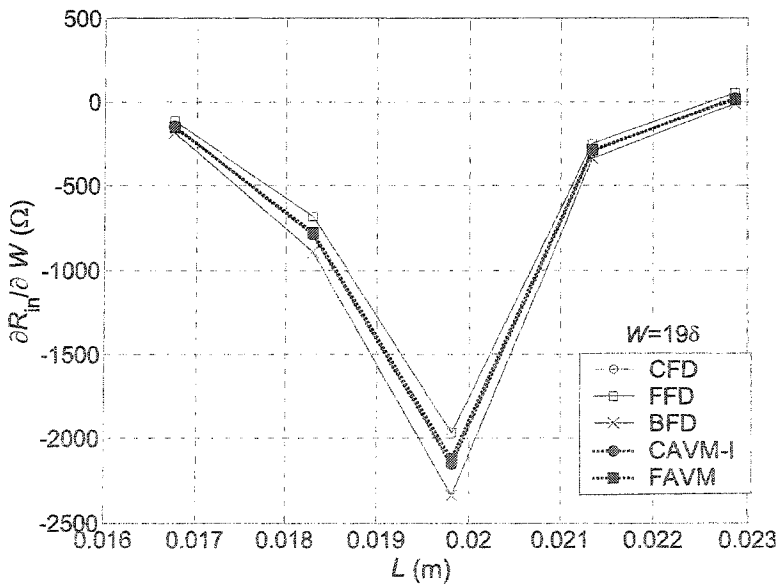

Fig. 4.4 Sensitivity of the input resistance of the patch antenna with respect to its width for a sweep in its length, $W = 19\delta$.

4.3.2 Impedance matching transformer

Next, we consider the impedance matching transformer shown in Fig. 4.5. The sensitivity of $|V|^2$, where V is the output voltage, is estimated at 7.3 GHz. The derivative is found with respect to the length of the middle section L_2 whose optimal value is $\lambda/4 = 9\delta$, where λ is the wavelength. The sensitivities are computed using our CAVM-I and are compared with response-level CFD results in Fig. 4.6. The improvement in the accuracy is obvious especially at the optimum where the response is most nonlinear.

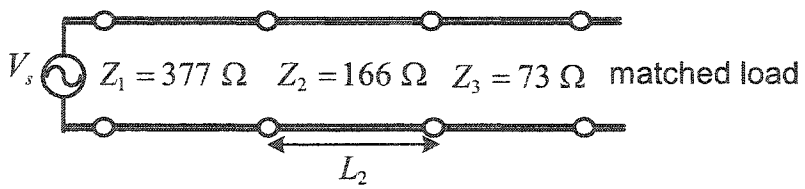

Fig. 4.5 Impedance matching transformer.

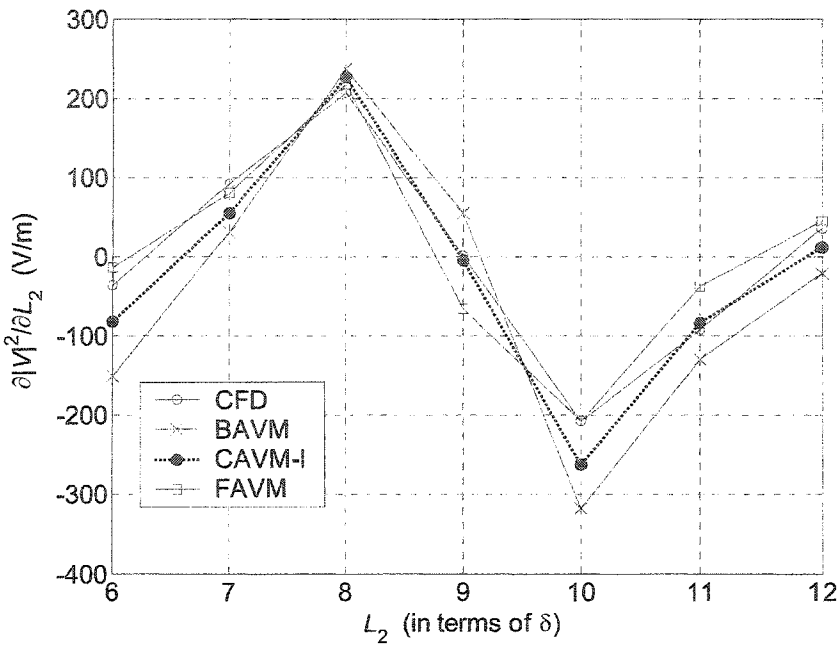

Fig. 4.6 Sensitivity of the transmitted voltage for the impedance transformer with respect to the length of the matching section.

4.4 SUMMARY

We presented in this chapter an improved discrete adjoint-based technique CAVM-I for sensitivity analysis with structured grid solvers. The presented technique offers significant improvement in the accuracy of the computed derivatives while preserving the same computational effort as our first proposed discrete adjoint approach introduced in Chapter 3, DAVM-I.

The improvement comes from preserving the advantages of the second-order term in the discrete sensitivity formula, which compensates for the stepwise on-grid perturbations in the design parameters and their effects on the system matrix. The second-

order accuracy is maintained by applying a central approach to the computation of the system matrix variations, as oppose to the forward approach in the DAVM-I. The improved accuracy is pronounced mainly with responses that are highly nonlinear functions of the design parameters and/or when coarse grid discretization of the simulator is used.

The presented technique was tested and investigated through sensitivity estimates and comparisons with response-level finite-difference approximations. The achieved accuracy in the sensitivity estimates is comparable to that of the second-order response-level central finite difference (CFD) while the computational effort is comparable to that of our original DAVM-I.

BIBLIOGRAPHY

Ali[1], S.M., N.K. Nikolova, and M.H. Bakr, accepted 2005. A discrete adjoint variable method for printed circuit board CAD. *INFORMS Journal on Computing.*

Ali[2], S.M., N.K. Nikolova, and M.H. Bakr, May 2004. Sensitivity analysis with full-wave EM solvers based on structured grids. *IEEE Trans. Magnetics*, vol. 40, no. 3, pp. 1521-1529.

Ali[3], S.M., N.K. Nikolova, and M.H. Bakr, July 2004. Central adjoint variable method for sensitivity analysis with structured grid electromagnetic solvers. *IEEE Trans. Magnetics*, vol.40, no. 4, pp. 1969-1971.

Bakr, M.H. and N.K. Georgieva, Sep. 2003. An adjoint variable method for frequency domain TLM problems with conducting boundaries. *IEEE Microwave and Wireless Components Lett.*, pp. 408-410.

Nikolova, N.K., H.W. Tam, and M.H. Bakr, April 2004. Sensitivity analysis with the FDTD method on structured grids. *IEEE Trans. Microwave Theory Tech.*, vol. 52, no. 4, pp. 1207-1216.

Chapter 5

IMPROVED DISCRETE SENSITIVITY ANALYSIS WITH ADJOINT SYSTEM PERTURBATIONS

Chapter 4 introduced a technique which improves the accuracy of the estimated derivatives with stepwise on-grid perturbations. The technique is based on our original DAVM-I approach presented in Chapter 3. It is, however, superior since it utilizes a central approach in the derivation of the system matrix derivatives. It targets responses that are highly nonlinear functions of their design parameters and the cases where the TLM grid is not discretized fine enough.

In this chapter, we introduce two other adjoint-based techniques for discrete sensitivity analysis which further improve the accuracy of the estimated derivatives. The first technique, the discrete adjoint-perturbed approach (DAVM-II), reflects the idea that the assumed discrete perturbations can take place in the adjoint problem rather than the original one as is the case with both DAVM-I of Chapter 3 and CAVM-I of Chapter 4. The second technique presented here, the discrete central adjoint-perturbed (CAVM-II)

technique, is a combination of the first technique DAVM-II and the central approach CAVM-I of Chapter 4.

5.1 INTRODUCTION

Further reduction of the computational error in the adjoint sensitivity formula is achieved with a modified sensitivity expression leading to the discrete adjoint-perturbed technique (DAVM-II) (Ali[4] *et al.* 2004), (Ali[5] *et al.* 2004). With the DAVM-II technique, the assumed perturbations in the design parameter space are stepwise on-grid perturbations that take place in the adjoint problem rather than the original one as is the case with the DAVM-I technique. This approach reduces the compound computational error arising from the computation of the sensitivity of the state variables from their own approximations. Minimizing this error leads to a reduction in the overall error of the computed sensitivities.

Using the perturbed-adjoint problem approach and the central approximate approach, a new central adjoint-perturbed formula (CAVM-II) is developed (Ali[5] *et al.* 2004). Through a convergence analysis test, we show that the CAVM-II formula provides the best accuracy of the estimated derivatives with discrete on-grid perturbations and structured-grid solvers for a given grid size of the solver.

The two techniques presented in this chapter enjoy the same computational savings as our original discrete technique DAVM-I that was introduced in Chapter 3.

5.2 THE DISCRETE SENSITIVITY FORMULA – II (DAVM-II)

Up to this point, both our discrete AVM techniques, DAVM-I and CAVM-I, assume that the virtual perturbations in the design parameters occur in the original problem, i.e., in the system described by (2.4) [see also (3.7)]. Accordingly, the variations in the state

variables $\Delta_k v^+$ ($k = 1,...,K$) are computed as in (3.9). These variations are needed later in the computation of the approximate sensitivity expression (3.15).

Alternatively, we can solve (3.7) for $\Delta_k v^+$ as

$$\Delta_k v^+ = \left(A + \Delta_k A^+\right)^{-1} \cdot \left[\Delta_k V_s^+ - \Delta_k A^+ \cdot v\right]. \tag{5.1}$$

Dividing by the perturbation Δx_k and substituting into (3.15), we arrive at

$$\left(\frac{df}{dx_k}\right) \simeq \frac{\partial f}{\partial x_k} + \nabla_v f \cdot \left(A + \Delta_k A^+\right)^{-1} \left[\frac{\Delta_k V_s^+}{\Delta x_k} - \frac{\Delta_k A^+}{\Delta x_k} v\right], \quad k = 1,...,K. \tag{5.2}$$

From (5.2), we define a new adjoint problem in the *k*th parameter as:

$$\left(A + \Delta_k A^+\right)^H \cdot \lambda_k^+ = \left[\nabla_v f\right]^H, \quad k = 1,...,K \tag{5.3}$$

which now relates to the perturbed geometry. Further, substituting the new perturbed adjoint solution

$$\lambda_k^+ = \lambda + \Delta_k \lambda^+, \quad k = 1, ..., K \tag{5.4}$$

into (5.2) results our new discrete adjoint-perturbed sensitivity formula (DAVM-II) in the *k*th parameter as

$$\left(\frac{df}{dx_k}\right)_{DAVM\text{-}II} \approx \frac{\partial f}{\partial x_k} + \lambda_k^{H+} \cdot \left(\frac{\Delta_k V_s^+}{\Delta x_k} - \frac{\Delta_k A^+}{\Delta x_k} \cdot v\right), \quad k = 1,\ldots,K. \tag{5.5}$$

Note that neglecting the second-order term in (5.1), in this case, too, reduces (5.5) to the first-order sensitivity formula (3.20).

The two second-order sensitivity expressions (3.16) and (5.5), although

theoretically equivalent, exhibit some differences when implemented in practical algorithms. This is mainly due to the self-dependence of the variations in the state variable term in (3.9), i.e., $\Delta_k v$ appears in both sides of (3.9) and hence is computed from its own approximation. As a result, the computational error in this term is expected to increase especially with highly nonlinear responses. Notice that this is not the case in (5.1) (Ali[3] *et al.* 2004), (Ali[5] *et al.* 2004).

It should be noted that neither (3.7)-(3.16) nor (5.3)-(5.5) are actually solved for a perturbation in each of the K parameters. Instead, the values of v_k and λ_k ($k=1,\ldots,K$) are approximated via a mapping approach based on the perturbational theory (Harrington 1961). The approach was discussed in detail in Section 3.5.2 and in Ali[2] (2004). It is applied here to the perturbed adjoint-problem solutions in exactly the same manner.

5.3 THE CENTRAL DISCRETE SENSITIVITY FORMULA – II (CAVM-II)

To reduce the computational error with DAVM-II (5.5) to a minimum, we consider here the same forward/backward procedure described in Section 4.2 and derive a central formula for DAVM-II (CAVM-II) as well. The CAVM-II formula is developed the same way as CAVM-I but using the forward and backward adjoint-perturbed problems instead of the forward and backward original perturbed problems. Simplifying the average of the forward/backward adjoint-perturbed formulas, we obtain

$$\left(\frac{df}{dx_k}\right)_{CAVM\text{-}II} \simeq \frac{\partial f}{\partial x_k} + \frac{\lambda_k^{H+}\Delta_k V_s^{+} + \lambda_k^{H-}\Delta_k V_s^{-}}{2\Delta x_k} - \frac{\lambda_k^{H+}\Delta_k A^{+} + \lambda_k^{H-}\Delta_k A^{-}}{2\Delta x_k}\cdot v, \qquad (5.6)$$

$k=1,\ldots,K.$

The improvement in the accuracy due to the central formulas (4.3) and (5.6) is, in some cases, very significant over the sensitivity results produced by formulas (3.16) and (5.5). Note however, that the computational load is the same for all four approaches.

5.4 NUMERICAL EXAMPLES

A number of examples that illustrate the two new proposed techniques are presented here. At the end of this section, a comparison of the accuracy of all four techniques is given to facilitate a conclusion as to which of them produces sensitivity results of best accuracy for a given TLM grid size.

5.4.1 Results produced with DAVM-II: Double-resonator filter

For the double-resonator filter illustrated in Fig. 2.6, we compute sensitivity of the response $f = |S_{21}|$ with respect to W using the DAVM-II technique (5.5). The results are compared with those produced by (i) DAVM-I from Section 3.4.5 and (ii) first-order response-level FFD, as shown in Fig. 5.1.

For a better accuracy comparison between the computed sensitivity results produced with DAVM-I and II, we compute a reference curve using the second-order CFD at the level of the response. Notice that this is a highly nonlinear response function. Even with a relatively fine grid, the FFD and CFD sensitivities disagree. Results computed with DAVM-II show acceptable accuracy compared to the reference CFD and a noticeable improvement over those computed using DAVM-I.

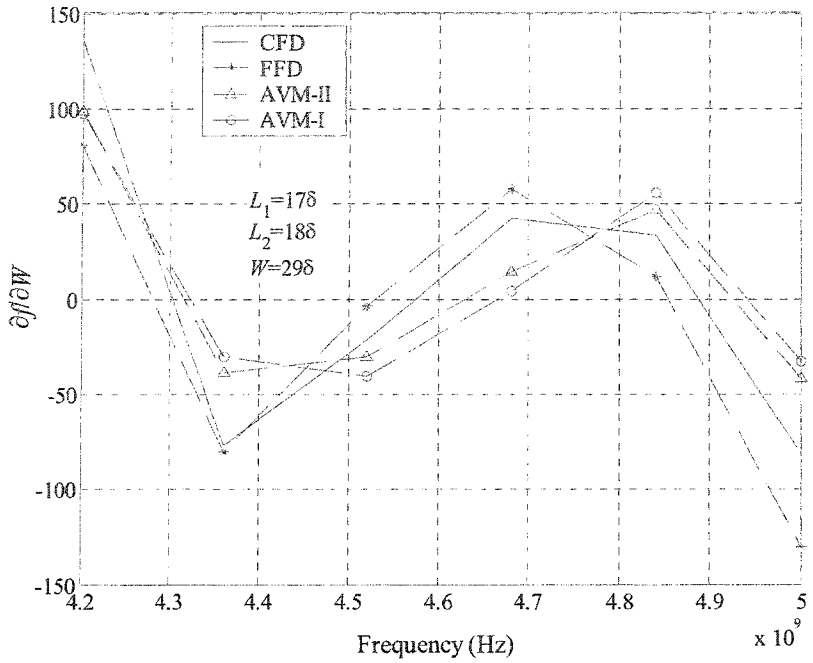

Fig. 5.1 Comparison between response level sensitivities and adjoint-based sensitivities.

5.4.2 Results produced with DAVM-II: Microstrip low-pass filter

Here, we compute response-sensitivity for the printed low-pass filter shown in Fig. 2.14. The response function is the squared modulus of the transmission coefficient of the filter, i.e., $f = |S_{21}|^2$. The sensitivities are computed with respect to changes in the vector of design parameters $x = [L \;\; W]^T$ using both DAVM-I and II. The computed results are compared with first- and second-order finite difference estimates at the level of the response as shown in Figs. 5.2 and 5.3.

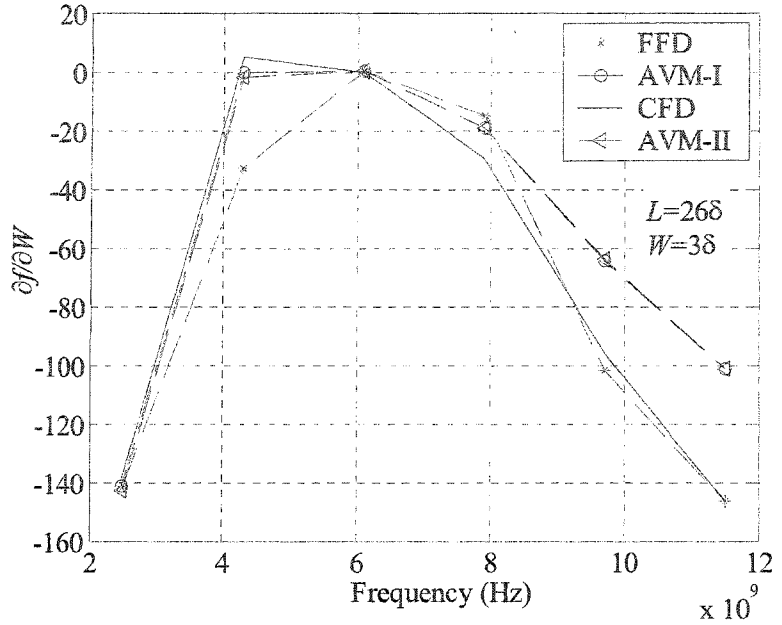

Fig. 5.2 Derivative of f with respect to W for the printed filter.

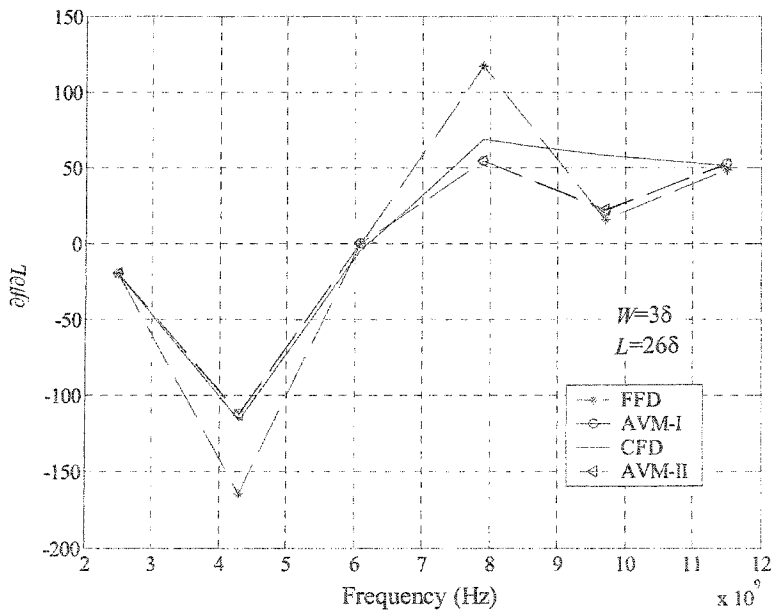

Fig. 5.3 Derivative of f with respect to L for the printed filter.

As seen from this example, the difference between the discrete adjoint-based sensitivities is not visible. This is also true for the results from the previous example when the sensitivities are computed with respect to changes in L_1 and L_2 [see Fig. 2.6]. It is thus difficult to conclude with certainty as to which approach provides better accuracy. Therefore, more detailed comparisons based on convergence analysis are needed.

5.4.3 Convergence analysis: Hollow waveguide

We test the accuracy of our adjoint approaches presented in Sections 3.3, 4.2, 5.2 and 5.3 through a convergence analysis. We compute the derivative of a response function using each of our four approaches at a given design point and compare their accuracy as the grid size δ becomes smaller. For this test to be accurate, we choose a response function that has an analytical form, and therefore, its derivative can be calculated analytically. We consider the wave impedance ($f = Z_{wg}$) of a hollow rectangular waveguide shown in Fig. 2.3. The computed adjoint derivatives are compared to the analytical derivative of this response function [see Appendix D].

The response is calculated analytically using the well-known formula for Z_{wg} as a function of the waveguide cross-section dimensions and the frequency (Pozar 1993). The response function is also computed using our FDTLM simulator. Both responses are given in Fig. 5.4.

The convergence analysis test is executed at a given design point in the highly nonlinear region of the response function. We consider the TE_{01} wave impedance of a waveguide of width $a = 5$ cm at 3.05 GHz. We calculate the analytical derivative

$\partial Z_{wg}/\partial a$ [see Appendix D]. The approximate derivatives $\Delta Z_{wg}/\Delta a$ are computed using the four discrete adjoint-based formulas and are evaluated at different discretization sizes of the TLM grid, i.e., at $\delta = \lambda/10$ to $\delta = \lambda/80$. The derivatives for a very fine grid, i.e., at $\delta \to 0$, are estimated using Matlab's (MathWorks, Inc. 2000) extrapolating functions. The results are tabulated in Table 5.1.

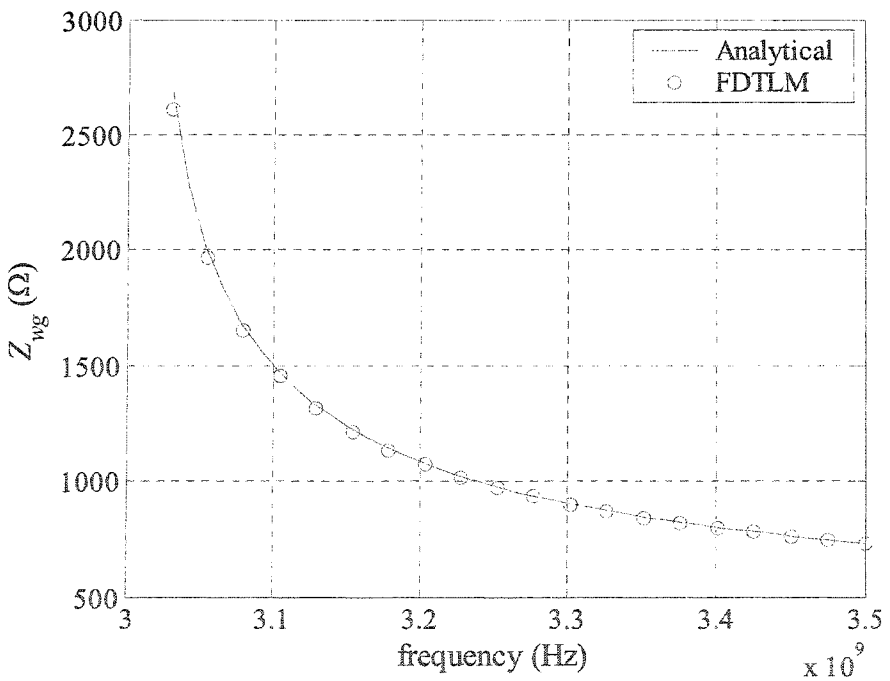

Fig. 5.4 The wave impedance of the waveguide vs. frequency at $a = 5$ cm.

TABLE 5.1
COMPARISON BETWEEN THE ANALYTICAL DERIVATIVE AND THE DERIVATIVES COMPUTED FROM THE DISCRETE-ADJOINT TECHNIQUES FROM THE CONVERGENCE ANALYSIS TEST.

δ	$\rightarrow 0$	$\lambda/80$	$\lambda/20$	$\lambda/10$
• $\partial Z_{wg}/\partial a$		-1.244		
• $\Delta Z_{wg}/\Delta a$				
AVM-I	-1.2471	-1.2481	-1.2530	-1.2550
CAVM-I	-1.2470	-1.2480	-1.2510	-1.2520
AVM-II	-1.2459	-1.2471	-1.2500	-1.2513
CAVM-II	-1.2455	-1.2460	-1.2481	-1.2501

λ : wavelength at the frequency of interest
δ : TLM mesh discretization size
Z_{wg} : waveguide wave impedance
a : waveguide width.

The table shows that all four approaches tend to converge to the analytical value of the derivative as the grid size δ becomes finer. This is due to the dependence of the field approximation in the perturbed problems – as was discussed in Section 3.4.3 – (Ali[2] *et al.* 2004) on δ. It is also due to the improved accuracy of the numerical field solution. We observe that the results produced with CAVM-II give the best outcome for any grid size compared to the other results. The CAVM-II results also show a smoother convergence than the results of the other approaches. Our interpretation to this outcome is: (i) the numerical error produced by the sensitivity expression DAVM-II (5.5), which CAVM-II is based on, is less than that of sensitivity expression DAVM-I (3.16); and (ii) the central-adjoint approach (CAVM), in general, preserves the advantages of the second-

order term $\Delta_k A \cdot \Delta_k v$ since it takes into account both forward and backward perturbations in the design parameter. With the CAVM-II, we merge the above advantages and obtain the best results.

The results also show that the difference between the DAVM-I and CAVM-I derivatives at finer grid sizes is small. However, we would like to point out that larger differences are expected for structures whose electromagnetic field is singular at the locations of the perturbed boundaries (Ali[4] *et al.* 2004). For example, sensitivity results of the response with respect to changes in the length of the patch example in Section 4.5.1 using formulas DAVM-I and CAVM-I are noticeably different. This is due to the field singularities at the edge of the patch. There are no field singularities in our waveguide example as the field smoothly decays to zero at the edge of the electric conducting walls of the waveguide. Therefore, the field variations between the approximated perturbed solution and that of the unperturbed problem are not very different. Hence, the difference in the corresponding derivatives is not so pronounced.

5.5 SUMMARY

In this chapter, we presented two new discrete adjoint-based techniques, the discrete adjoint-perturbed technique (DAVM-II) and the discrete central adjoint-perturbed technique (CAVM-II). They add improvement to the accuracy of the computed derivatives over our original DAVM-I technique. The techniques still enjoy the same computational requirements as the original DAVM-I technique.

In the first technique, the discrete perturbations in the forward direction are realized by stepwise perturbations that take place in the adjoint problem. This reduces the computational error introduced due to the evaluation of the solution of the original perturbed problems from their own approximations.

The second technique presented in this chapter integrates the above technique (DAVM-II) with the central technique introduced in Chapter 4 to result in the central adjoint-perturbed CAVM-II technique. The convergence analysis test given at the end of this chapter shows that the CAVM-II approach results in sensitivity estimates with the best accuracy among all four techniques for a given grid size.

BIBLIOGRAPHY

Ali[4], S.M., N.K. Nikolova, and M.H. Bakr, June 2004. Sensitivity analysis and optimization utilizing an approximate auxiliary problem. *IEEE/URSI Int. Symposium on Antennas and Propagation*, (Monterey, CA), vol.1, pp. 1118-1121.

Ali[5], S.M., N.K. Nikolova, and M.H. Bakr, Dec. 2004. Recent advances in sensitivity analysis with frequency-domain full-wave EM solvers. *Applied Computational Electromagnetics Society Journal.*

Pozar, D.M., 1993. *Microwave Engineering.* New York: Addison-Wesley Publishing Company, Inc.

MathWorks, Inc., MATLAB (2000) Version 6.0, 3 Apple Hill Drive, Natick MA 01760-2098.

Chapter 6

GRADIENT-BASED OPTIMIZATION USING DISCRETE ADJOINT SENSITIVITY INFORMATION

In the preceding chapters, we proposed a family of discrete adjoint-based techniques for efficient sensitivity analysis with structured-grid solvers. The techniques feature computational efficiency, accuracy and simplicity over classical FDA techniques and over the original exact AVM. We have showed through a variety of examples that the proposed discrete techniques are robust and reliable even when sensitivities of highly nonlinear responses are of interest or when a coarse-grid discretization of the TLM solver is utilized.

In this chapter, we put to the test our proposed techniques with gradient-based optimization. The optimizer is integrated with the FDTLM simulator which supplies it with the response function. The derivatives provided to the optimizer are computed using our discrete adjoint techniques.

The chapter introduces a number of practical design problems through a variety of structures such as waveguide filters, antennas and arrays.

6.1 INTRODUCTION

A general microwave design problem can be formulated as

$$x^* = \arg\left\{\min_x \quad F\left(x, f(x)\right)\right\} \tag{6.1}$$

where F is the objective function – also called the cost function – to be minimized; as defined before, x is the vector of design parameters, f is the response function; and x^* is the vector of optimum design parameters that we would like to obtain.

In gradient-based optimization, sensitivity information of the objective function F to variations in the elements of x is crucial in determining the next design iteration. It is defined as the gradient of F in the design parameter space [see (3.2)]:

$$\nabla_x F = \left[\frac{\partial F}{\partial x_1} \quad \frac{\partial F}{\partial x_2} \quad \cdots \quad \frac{\partial F}{\partial x_K}\right]. \tag{6.2}$$

Commercial EM solvers provide responses but not their sensitivities. Therefore, the integration of these solvers in an optimization design loop would typically mean that the solution to (6.1)-(6.2) is found via response-level FDA techniques. In which case, repeated analyses of the objective function (response) for each independently perturbed design parameter are needed. Such an approach can be prohibitively expensive for large problems with many design parameters.

The integration of our discrete adjoint-based techniques, on the other hand, for sensitivity evaluation with gradient-based optimizers offer significant computational savings in comparison to the previous case, i.e., when simple response-level FDA

techniques are used for gradient evaluation. The savings in each design iteration is a factor of K to $2K$. For instance, if the optimal design is reached by the optimizer in P design iterations, where $P \in \mathbb{Z}$, then, the complete design process would require $2P$ full-wave analyses to compute the responses and their sensitivities using any of our discrete adjoint-based techniques. This is in comparison to at least $(K+1)P$ full-wave analyses when the optimizer is supplied with the responses and their first-order response-level FDA derivatives. Obviously, our techniques – which are independent of the number of design parameters K – are far more efficient computationally for a comparable optimal design.

6.2 INTEGRATION OF OUR DISCRETE TECHNIQUES IN AN OPTIMIZATION DESIGN LOOP

The FDTLM simulator is linked automatically to the optimizer. The designer specifies the objective function F and initializes the vector of design parameters $\boldsymbol{x}^0 = \boldsymbol{x}^{(1)}$. The new vector of design parameters at the next iteration $\boldsymbol{x}^{(p+1)}$ recommended by the optimizer is automatically fed back into the simulator. At which point, the corresponding new response and its sensitivities are computed (Ali[6] *et al.* 2003).

Fig. 6.1 shows the general flowchart at the pth design iteration of the automated design when the required sensitivities are computed with any of our proposed discrete techniques. Since our discrete techniques assume only virtual local perturbations in the design parameters [see Fig. 3.2], the initial TLM mesh is preserved during the optimization. This simplifies the implementation into the automated design loop. The

optimization iterations are repeated P times until a certain stopping criterion specified by the designer is satisfied. The stopping criterion must reflect a successful achievement of an optimum design x^*. Usually, a well defined stopping criterion also takes into account a scenario where the optimum design cannot be achieved, and a new initial design is recommended.

The pth design iteration of the automated design when FDA techniques are utilized for response gradient evaluation is shown in Fig. 6.2. The main computational differences per design iteration involved in the gradient computation between the two techniques, i.e., FDA and adjoint-based techniques, are summarized in Table 6.1.

TABLE 6.1
COMPARISON OF COMPUTATIONAL ASPECTS BETWEEN FDA AND THE AVM FOR GRADIENT EVALUATION (PER DESIGN ITERATION)

Computational aspects	FDA techniques		AVM techniques	
	FFD/BFD	CFD	exact	DAVM
• Matrix fills	K+1	2K+1	K+1	1
• LU-factorization	K+1	2K+1	1	1
• Iterative solutions	K+1	2K+1	2	2
• Mesh generation	K+1	2K+1	1	1
• Mesh regeneration at each optimization loop	yes	yes	yes	no

K: number of design parameters.

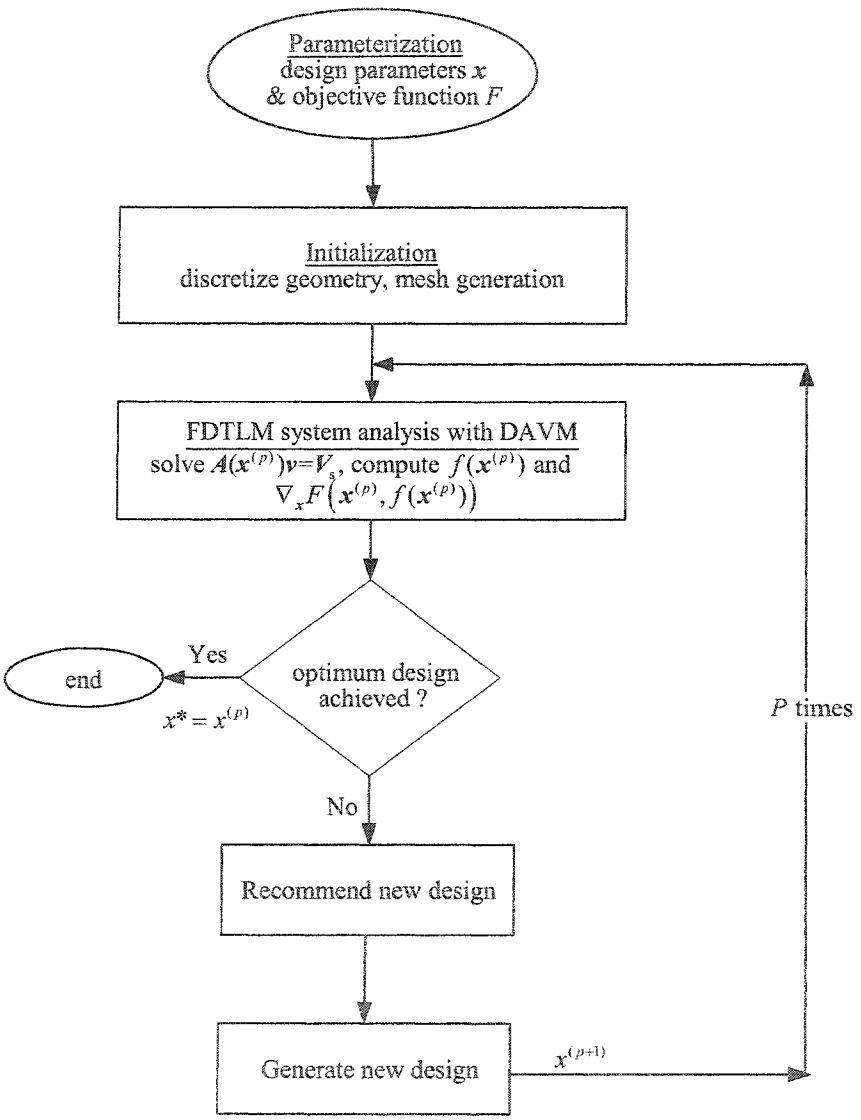

Fig. 6.1 Automated optimization at the pth design iteration utilizing DAVM sensitivities.

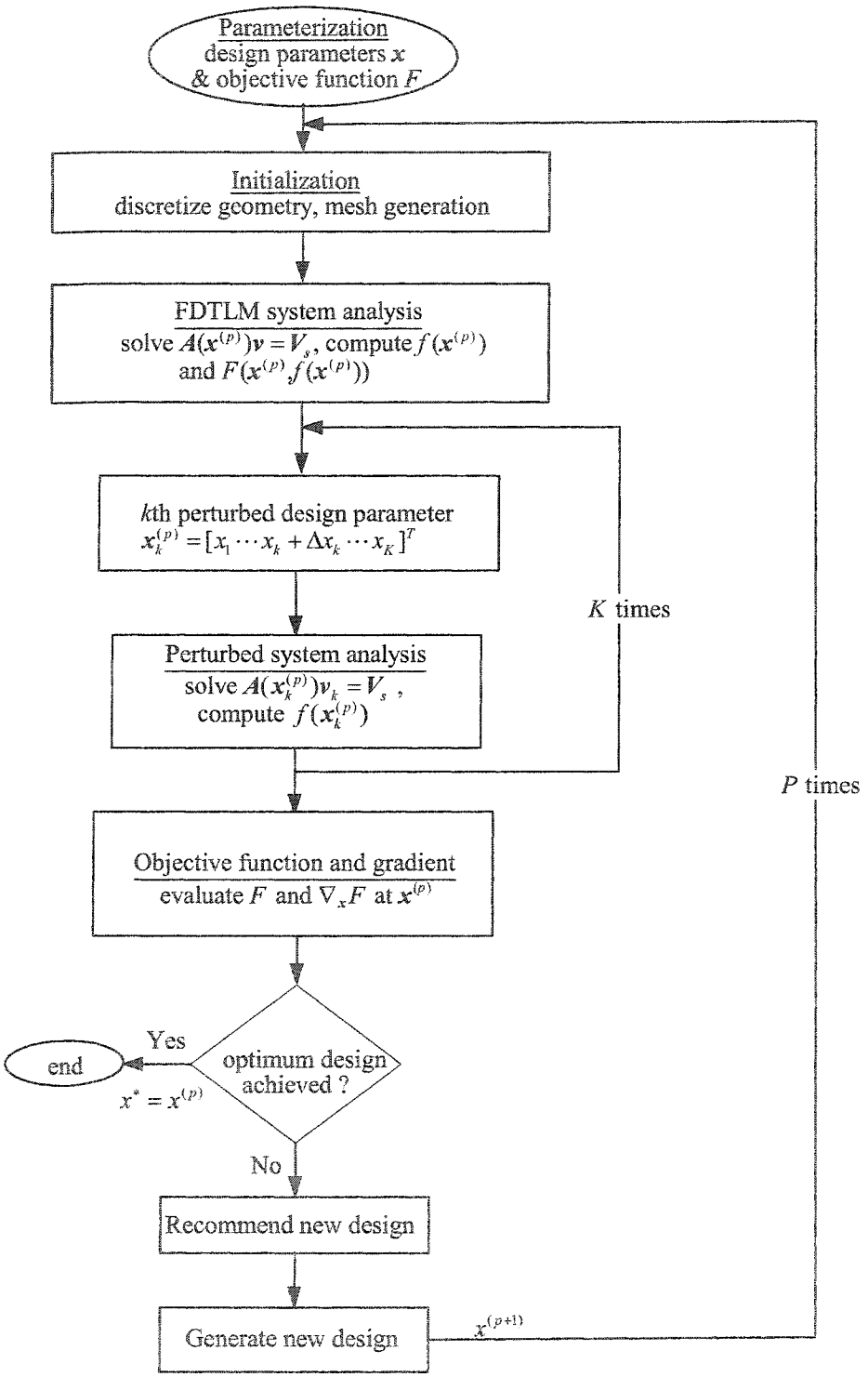

Fig. 6.2 Automated optimization at the pth design iteration utilizing FDA sensitivities.

6.3 GRADIENT-BASED OPTIMIZATION USING DISCRETE ADJOINT SENSITIVITIES.

We illustrate in this section a number of design problems which are optimized using our DAVM sensitivities integrated with the optimizer.

A number of points should be taken into consideration when integrating a full-wave simulator based on structured grids in a design optimization loop. These are important for the new design suggested by the optimizer which is to be fed back into the simulator at the next design iteration:

(i) The geometrical design parameters should always conform to the initial grid of the simulator – the design parameters are always integer multiples of the cell size in the respective direction. This is achieved by snapping the new geometry to the TLM grid.

(ii) Settings related to the general structure should remain satisfied after the new design is implemented. As an example, consider the probe-fed patch antenna shown in Fig. 2.10. It is desired that the location of the probe is always at $W/2$, where W is the patch width. If the width of the patch W is one of the design parameters, then the new design suggested by the optimizer should always fulfill this requirement. In our case where the probe is modeled with one cell located at $(W/2)+1$, and to keep the distance unchanged from the numerical absorber, W is always snapped into an odd integer number of cells.

(iii) Assumed perturbations of individual design parameters are independent of the

other design parameters, and should not affect other geometrical details or settings of the structure. For instance, consider the same patch example [see Fig. 2.10]. Perturbations in the width W should be made such that symmetry of the feed excitation with respect to the patch is preserved, i.e., perturbations in W should be made simultaneously at both the left and right sides of the patch.

The above recommendations are taken into account with all examples throughout this section.

6.3.1 Optimum length of a lossless cavity

In our first example, the objective is to minimize the magnitude squared of the input impedance for a 1-D cavity by changing its length at frequency 3 GHz. The problem is defined as

$$L^* = \arg\left\{\min_{L} \; |Z_{in}|^2\right\} \tag{6.3}$$

where L is the design parameter representing the length of the cavity; $Z_{in} = jX_{in}$ is the cavity input impedance, which in this case is purely reactive; and L^* is the optimal cavity length at the operating frequency. We use a gradient-based optimization routine *fmincon* of MATLAB® (MathWorks 2000). The routine finds the minimum of a scalar function starting at an initial estimate L^0.

The optimizer is supplied with discrete sensitivity information computed using DAVM-I (3.19). The achieved optimum cavity length by the optimizer is 0.5 m. Note that this length corresponds to a half-wavelength at frequency 3 GHz. Fig. 6.3 shows the

objective function at each design iteration. The changes in the design parameter L with each design iteration are tabulated in Table 6.2.

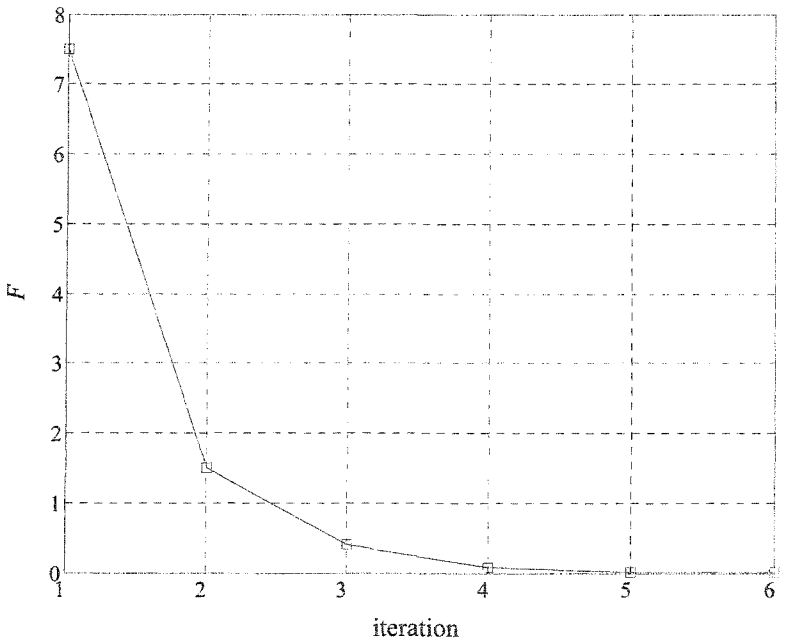

Fig. 6.3 The objective function vs. the design iterations for the cavity example.

TABLE 6.2
DESIGN PARAMETER VALUES OF THE CAVITY AT EACH DESIGN ITERATION

	$L^{(1)}$	$L^{(2)}$	$L^{(3)}$	$L^{(4)}$	$L^{(5)}$	$L^{(*)}$
L (m)	0.035	0.0575	0.0544	0.0516	0.0502	0.05

6.3.2 Optimum transmission for a bandpass filter

We optimize the DRF previously introduced in Section 2.4.2 [see Fig.2.6] to achieve a desired (target) response. The objective function consists of the differences between the computed and the target data of the scattering parameters. The design problem is defined as

$$x^* = \arg\left\{ \min_x \sum_i \left| S_{21}(\omega_i, x_k) - S_{21}(\omega_i, x_k^t) \right|^2 \right\}. \tag{6.4}$$

In (6.4), ω_i are specified frequencies in the desired band. The vector of design parameters is $x = [x_1 \;\; x_2]^T$, where $x_1 = L_1$ and $x_2 = L_2$. The target response $S_{21}(\omega_i, x_k^t)$ is a known response, which should be achieved at $x^t = [18.0 \;\; 19.0]^T$ mm. We start with an initial guess of $x^0 = [14.0 \;\; 20.0]^T$ mm and let the optimizer drive the solver toward the correct solution using derivatives computed (i) with the DAVM-I (3.19) technique, and (ii) with derivatives computed as FFD (3.4) at the level of the response. The optimum (target) response is achieved in eight design iterations at $x^* = [18.2 \;\; 19.4]^T$ mm. The design iterations are tabulated in Table 6.3. The initial response $f(x^0)$ and the optimum response $f(x^*)$ are shown in Fig. 6.4, where $f = |S_{21}|$.

Here, we utilized the MATLAB© (MathWorks 2000) function *lsqnonlin*. The function solves nonlinear least-squares problems given an initial point x^0, and finds a minimum to the sum of squares of the functions described in (6.4).

The design time required to achieve the optimal design using a PC with a Pentium

IV 3.0 GHz processor is about 1.9 hours when response-level derivatives are used and about 1.21 hours when discrete adjoint sensitivities are used. Notice that the optimal design suggested by the optimizer is the same using either technique to compute the derivatives. Hence, we achieve computational savings with our approach over the FDA technique of about a factor of 1.6 times for $K = 2$.

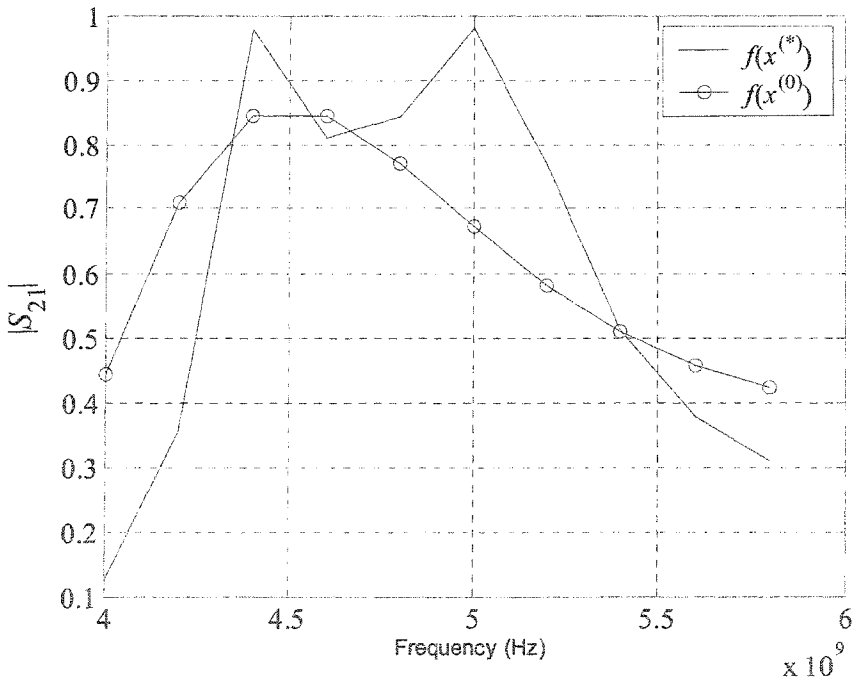

Fig. 6.4 The initial and optimum response of the double-resonator filter.

TABLE 6.3
DESIGN PARAMETER VALUES OF THE FILTER AT EACH DESIGN ITERATION

	$x^{(1)}$	$x^{(2)}$	$x^{(3)}$	$x^{(4)}$	$x^{(5)}$	$x^{(6)}$	$x^{(7)}$	x^*
L_1 (mm)	14.0	14.2	13.6	14.7	16.2	17.3	18.7	18.2
L_2 (mm)	20.0	22.3	22.8	20.1	20.4	19.1	19.6	19.4

6.3.3 Optimization of a probe-fed patch antenna

We optimize next the patch antenna described in Section 2.4.3 [see Fig. 2.10] for minimum reflection at frequency 4.4 GHz. The design problem is defined as

$$\boldsymbol{x}^* = \arg\left\{\min_{\boldsymbol{x}} \left|\Gamma(\omega_i, \boldsymbol{x})\right|^2\right\}. \tag{6.5}$$

Here, $\Gamma = |S_{11}|$ is the reflection coefficient, and $\boldsymbol{x} = [x_1 \;\; x_2]^T$, where $x_1 = L$ and $x_2 = W$. The optimizer is provided with the initial design vector $\boldsymbol{x}^0 = [18.288 \;\; 32.004]^T$ mm. The derivatives are computed at each design iteration (i) using our DAVM-II (5.5) approach, and (ii) using FFD (3.4) response-level derivatives. The optimal solution $\boldsymbol{x}^* = [19.812 \;\; 28.956]^T$ mm is obtained in five design iterations. The optimization iterations are given in Table 6.4. The initial and optimal responses $f(\boldsymbol{x}^0)$ and $f(\boldsymbol{x}^*)$ are shown in Fig. 6.5, where $f = |\Gamma|$.

TABLE 6.4
DESIGN PARAMETER VALUES OF THE PATCH ANTENNA AT EACH DESIGN ITERATION

	$x^{(1)}$	$x^{(2)}$	$x^{(3)}$	$x^{(4)}$	x^{*}
L (mm)	18.288	18.288	18.121	18.301	19.812
W (mm)	32.004	22.861	27.255	30.480	28.956

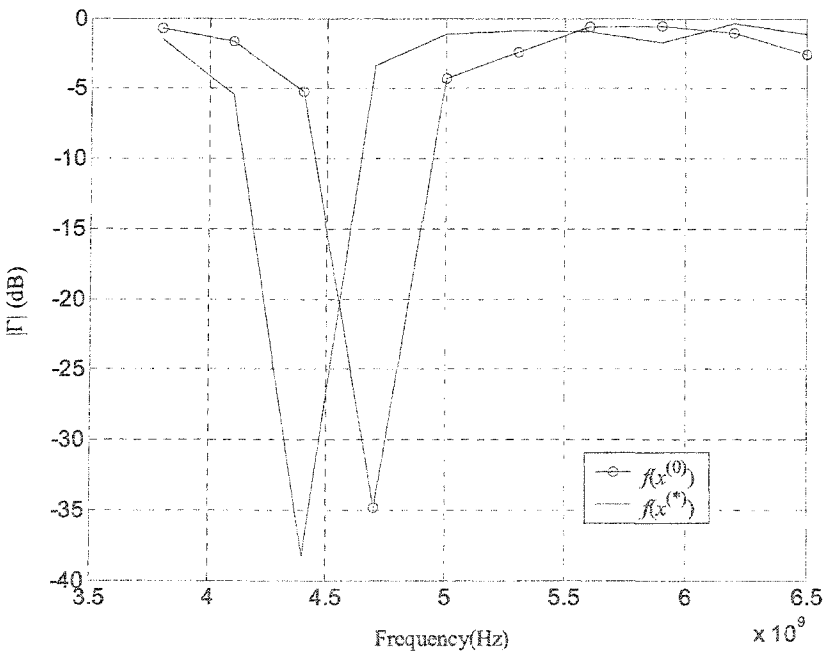

Fig. 6.5 The initial and optimum response for the patch antenna.

The design process time using a PC with a Pentium IV 3.0 GHz processor is about 1.6 hours when response-level FFD derivatives are used. This is in comparison to 1.05 hours when our discrete derivatives are used. Notice that the optimal design achieved is the same using any of the two approaches. Hence, we achieve computational savings using our derivatives by a factor of about 1.5 per design iteration for $K = 2$.

6.3.4 Optimization of an electromagnetically coupled printed Yagi antenna array

In our final design problem, we optimize the electromagnetically coupled Yagi antenna array described in (Zheng *et al.* 2003), also shown in Fig. 6.6. The optimization is carried out using a *minimax* optimizer (Madsen 2002) integrated with the FDTLM simulator. The optimizer is supplied with the Jacobian matrix computed (i) with our discrete adjoint technique CAVM-II (5.6), and (ii) with FFD at the level of the response.

The printed Yagi array consists of a driven element, a reflector, and two directors. The driven element is electromagnetically coupled to a feeding quarter-wavelength line which is in turn coupled to a feeding microstrip line. The array, its elements and the ground plate are assumed to be made of perfect conductors. The used substrate has permittivity $\varepsilon_r = 10.2$.

Our design specification is

$$|S_{11}| < -10 \text{ dB} \quad \text{for} \quad 9.7 \text{ GHz} < f_0 < 11.6 \text{ GHz} \tag{6.6}$$

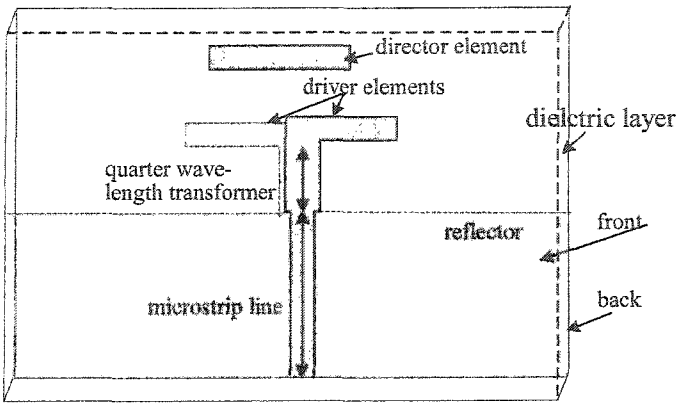

(a)

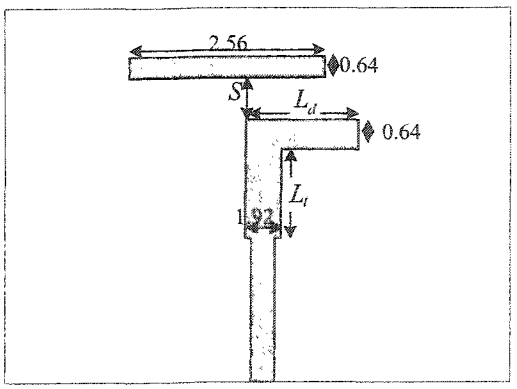

(b)

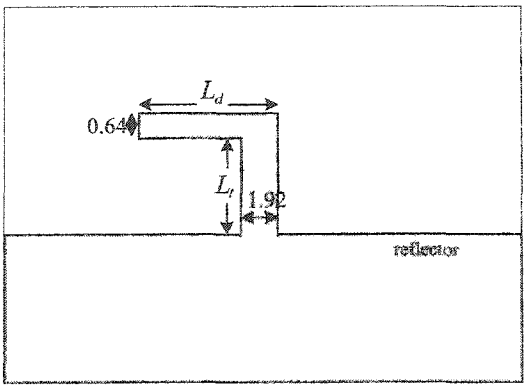

(c)

Fig. 6.6 Electromagnetically coupled Yagi antenna array (all units are in mm); (a) 3D geometry, (b) top layer, (c) bottom layer.

where $|S_{11}|$ is the return loss of the antenna, which we would like to minimize within the specified frequency range. The vector of design parameters is $x=[x_1 \ x_2 \ x_3]^T$, where $x_1 = L_t$, $x_2 = S$ and $x_3 = L_d$. Its parameters have initial values $x^0 = [5.76 \ \ 1.28 \ \ 4.48]^T$ mm. The design specification is met in 14 iterations with optimal design parameters $x^* = [7.71 \ \ 2.60 \ \ 3.22]^T$ mm. The cost of the complete design with derivatives computed using our discrete technique is about 4.3 hours while that with FFD derivatives required 8.19 hours. The savings in the computation time for the same design outcome is obvious. The initial $f(x^{(0)})$ response, where $f = |S_{11}|$, and the optimal responses $f(x^{(*)})$ are given in Fig. 6.7. The values of the design parameters per design iteration are given in Table 6.5.

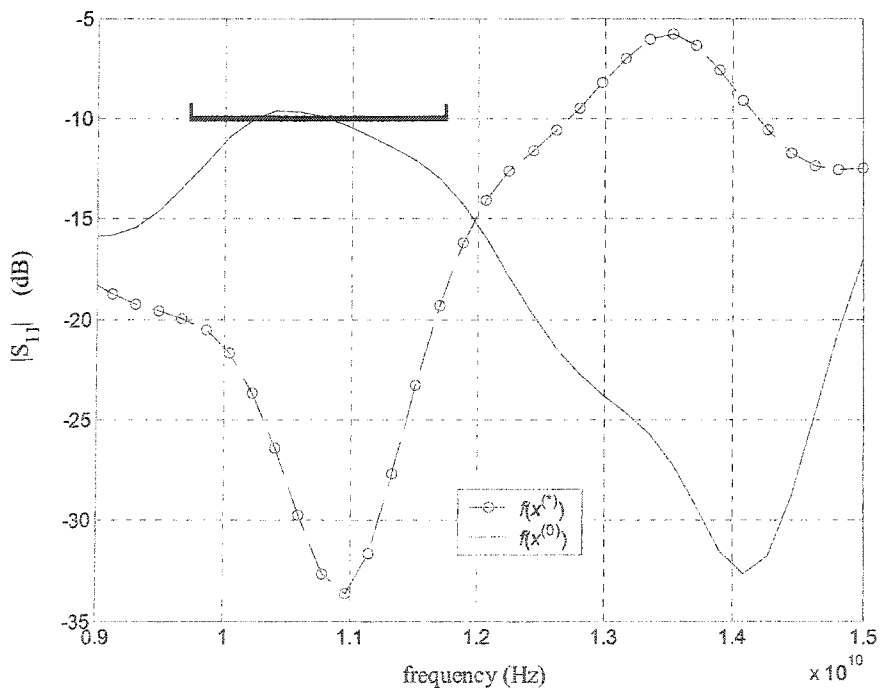

Fig. 6.7 The initial and optimal responses of the Yagi antenna array.

TABLE 6.5
DESIGN PARAMETER VALUES OF THE YAGI ANTENNA ARRAY AT EACH DESIGN ITERATION

(p)	L_t	S	L_d
1	5.76	1.28	4.48
2	5.13	1.21	5.22
3	4.46	1.22	5.65
4	5.70	0.73	5.31
5	5.72	1.32	4.72
6	6.41	1.95	3.87
7	6.45	2.66	3.85
8	8.33	1.87	2.66
9	6.42	2.71	2.73
10	8.41	3.21	4.49
11	7.05	2.76	3.81
12	7.15	3.20	3.01
13	7.69	3.41	3.21
14	7.71	2.60	3.22
all dimensions are in mm			

6.4 SUMMARY

This chapter presents gradient-based optimization where efficient and accurate sensitivity information is required. We show that with the integration of our discrete adjoint-based techniques in an optimization loop: (i) reliable designs that satisfy the design requirements can be achieved, (ii) significant time savings per design iteration are gained, and (iii) the simplicity of implementation allows reliable integration with existing optimizers such as those of MATLAB optimization toolbox.

A number of practical optimization examples where considered here such as waveguide filters, antennas and arrays. For each design problem, real-time measurements were made. These included the computational time required for a complete design when any of our proposed discrete techniques were used. For comparison, the time requirements when the design is conducted using response-level gradients where also given. The comparisons where made with respect to the first-order FFD.

BIBLIOGRAPHY

Ali[6], S.M., N.K. Nikolova, and M.H. Bakr, May 2003. Design sensitivity analysis for optimization with the frequency domain-TLM. *IEEE CCECE03 Digest*, (Montre'al, Canada), vol. 1, pp. 1971-1974.

MathWorks, Inc., MATLAB (2000) Version 6.0, 3 Apple Hill Drive, Natick MA 01760-2098.

Madsen, K., H.B. Nielsen and J. Søndergaard, Jan. 2002. *Robust Subroutines for Non-linear Optimization.* Report IMM-REP-2002-02, Informatics and Mathematical Modeling, Technical University of Denmark, DK-2800 Kongens Lyngby, Denmark.

Zheng, G., Ahmed A. Kishk, Alexander B. Yakovlev, and Allen W. Glisson, April 2004. Simplified feeding for a printed Yagi antenna. *Electronics Letters* , vol. 40 , no. 15, pp. 464-465.

Chapter 7

CONCLUSIONS AND FUTURE WORK

This thesis presents recent advances in discrete adjoint-based (DAVM) techniques for efficient sensitivity analysis of high-frequency structures, their theory and implementation in efficient electromagnetic (EM) optimization.

The analysis tool used for the simulation of the structures is based on the frequency-domain transmission line method (FDTLM). The method discretizes the structure into rectangular cells and models it as a system of linear equations[1]. This resultant system is either solved via LU decomposition or via iterative solvers, the latter being the usual choice due to the large size and sparse nature of the system of equations. The solution of the system is the distributed response of the structure – also known as the state variables – in the form of complex incident voltages. Other important performance parameters (responses) of the EM structure are functions of the state variables and the design parameters. Chapter 2 introduces a number of simulated problems with the FDTLM solver. It discusses important computational issues related to the implementation

[1] Also referred to as the original system or problem.

of the FDTLM. Throughout the chapter, comparisons are made with the corresponding numerical results from other solvers or with ones computed analytically.

Our first discrete adjoint technique (DAVM-I) is described in detail in Chapter 3. The technique has several advantages. First, its simplicity is comparable to that of response-level finite difference approximation (FDA) techniques as it requires no analytical derivatives of the system matrix. Therefore, complex and often case specific preprocessing is avoided. Second, its computational efficiency is comparable to that of the original "exact" adjoint variable method (AVM) as it requires at most two system analyses to compute the response and its sensitivities regardless of the number of design parameters. Third, its versatility matches that of the simulator itself – it allows implementation to geometrical as well as material-related design parameters regardless of the complexity and size of the structure. The chapter also introduces a number of examples where sensitivities using our proposed DAVM-I expression are computed. The results of each example are verified and compared with analytical derivatives or response-level FDA if the analytical derivative does not exist. Good agreement is achieved in all cases.

Research into improving the accuracy of the proposed technique starts in Chapter 4, where our first enhanced technique, the central discrete adjoint technique (CAVM-I), is developed. It significantly improves the accuracy of the estimated derivatives especially when highly nonlinear response functions are of interest. This is achieved by a central approach to the definition of the sensitivity expression. We define a forward problem, which describes the on-grid perturbation in the forward direction, and a

backward problem, which describes the perturbation in the backward direction. A new central sensitivity formula is derived from the formulas for the forward and the backward approaches. This formula is tested through the sensitivities of a number of structures. Comparisons are given with the response-level FDA estimates of these derivatives.

Chapter 5 introduces two other discrete adjoint-based approaches for sensitivity analysis with structured grid solvers. These offer further improvement in the accuracy of the estimated derivatives. The first, the discrete adjoint-perturbed (DAVM-II) approach, is based on the idea of minimizing the compound computational error. This error is introduced by estimating the solutions of the original perturbed problems from their own approximations. We avoid this approximation by realizing the perturbations in the adjoint problem instead of the original one. The solutions of the perturbed adjoint problems are obtained by the same mapping concept used when the perturbed original problem solutions are approximated in DAVM-I. The improvement in the accuracy is observed mostly in problems where computational error is likely to occur, for instance, with problems that are computationally large.

The second approach, the central adjoint-perturbed (CAVM-II) approach, which is also introduced in Chapter 5, is a combination of the DAVM-II approach and that of the central approach. We prove with a convergence analysis test that, for a given TLM grid size, the best accuracy is achieved using this approach.

Gradient-based optimization is one of many applications where efficient and accurate sensitivity information is crucial. We put to the test our discrete adjoint-based techniques for sensitivity evaluation by integrating them with an optimizer in Chapter 6.

The chapter introduces a number of practical design examples for a variety of structures such as waveguide filters, antennas and arrays. In all examples, real-time measurements are given. These comparisons are between the time required for the design when the sensitivities are supplied by any of our techniques in comparison to the required time if response-level FDA estimates are used.

7.1 CONTRIBUTIONS TO THE SCIENTIFIC LITERATURE

The work presented in this thesis has been published or accepted for publication in a number of refereed journals. In addition, the work has also been presented in a number of refereed conferences. They are listed as follows

7.1.1 Journal papers

Ali[1], S.M., N.K. Nikolova, and M.H. Bakr, accepted 2005. A discrete adjoint variable method for printed circuit board CAD. *INFORMS Journal on Computing.*

Ali[2], S.M., N.K. Nikolova, and M.H. Bakr, May 2004. Sensitivity analysis with full-wave EM solvers based on structured grids. *IEEE Trans. Magnetics*, vol. 40, no. 3, pp. 1521-1529.

Ali[3], S.M., N.K. Nikolova, and M.H. Bakr, July 2004. Central adjoint variable method for sensitivity analysis with structured grid electromagnetic solvers. *IEEE Trans. Magnetics.*, vol. 40, no. 4, pp. 1969-1971.

Ali[5], S.M., N.K. Nikolova, and M.H. Bakr, Dec. 2004. Recent advances in sensitivity analysis with frequency-domain full-wave EM solvers. *Applied Computational Electromagnetics Society Journal.*

7.1.2 Conference contributions

Ali[4], S.M., N.K. Nikolova, and M.H. Bakr, June 2004. Sensitivity analysis and optimization utilizing an approximate auxiliary problem. *IEEE/URSI Int. Symposium on Antennas and Propagation*, (Monterey, CA), vol. 1, pp. 1118-1121.

Ali[6], S.M., N.K. Nikolova, and M.H. Bakr, May 2003. Design sensitivity analysis for optimization with the frequency domain-TLM. *IEEE CCECE03*, (Montréal, Québec), vol. 1, pp. 1971-1974.

N.K. Nikolova, S.M. Ali, M.H. Bakr, E.A. Soliman and J.W. Bandler, April 2004. Response sensitivity analysis with frequency-domain full-wave Electromagnetic solvers. *20th Annual Review of Progress in Applied Computational Electromagnetics ACES*, (Syracuse, NY), CD ROM.

7.2 FUTURE WORK

We believe that efficient sensitivity analysis based on the adjoint variable method is a challenging and interesting field of research. Its applications with structured-grid solvers makes it even more interesting. We suggest further research as follows:

(i) The possibility of reducing the computational requirement for the sensitivity estimates to only the original analysis when network-parameters are the response functions of interest. This work – with *S*-parameters as the response function – has been implemented with an unstructured grid solver based on the finite element method (FEM). We foresee that its application with

structured grid solvers such as the FDTLM is possible and may offer further computational savings.

(ii) Through the course of this work, our proposed techniques have been implemented with the assumption that the medium is lossless. It would be interesting to investigate its implementation in lossy problems. Lossy materials introduce more computationally challenging problems and limitations.

(iii) Optimization using our adjoint sensitivities can be accelerated further. This is suggested to be done with the use of iterative solvers instead of direct solvers when defining the solution at the next iteration. With such solvers, the solution at the previous iteration is used as the initial guess. This is expected to reduce the number of iterations needed to find the solution with the minimum residual error. Hence, reduce both time and required storage. In fact, we have some interesting preliminary results that show the possibility of such an approach.

(iv) The AVM for sensitivity analysis is a known efficient method. We believe that it can be useful in other fields such as inverse problems. In such case, the problem may be described as a least squared data fitting problem that can be solved by gradient-based optimization. The required gradient is efficiently computed using our discrete adjoint-based techniques.

Appendix A

NON-UNIFORM DISCRETIZATION AND LOSSY MATERIAL MODELING WITH THE FDTLM ALGORITHM

Here, we generalize our discussion in Chapter 2 to include modeling of lossy materials and/or nonuniform discretization of EM problems with the FDTLM simulator.

A.1 NON-UNIFORM TLM GRID DISCRETIZATION

The TLM algorithm is based on transmission line theory, where space is modeled by a 3-D network of transmission lines.

The links of the symmetrical condensed node [see Fig. 2.1] are composed of transmission lines that convey currents (magnetic field) and voltages (electric field). The polarization and strength of these currents/voltages can be determined using electric parameters such as capacitors C, inductors L, resistors R and admittance G that the transmission line is composed of. If the electric parameters of each line are indicated by three subscripts specifying the unit length, direction and the polarization, then, the capacitor C per unit length d on a y-directed line polarized in the x-direction is denoted

as C_{dyx}. Using this convention, the propagation constant for line yx (i.e., lines 1 and 12 of Fig. 2.1) is (Johns *et al.* 1994)

$$\gamma_{yx} = \sqrt{j\omega L_{dyx}\left(G_{dyx} + j\omega C_{dyx}\right)} \tag{A.1}$$

where L, G and C represent the series inductance and shunt admittance and capacitance of the lines, respectively. Similarly, the characteristic impedance is

$$Z_{yx} = \sqrt{\frac{j\omega L_{dyx}}{G_{dyx} + j\omega C_{dyx}}}. \tag{A.2}$$

The medium intrinsic impedance Z is

$$Z = \sqrt{\frac{j\omega\mu}{\sigma + j\omega\varepsilon}}, \tag{A.3}$$

where σ is the medium conductivity. A condition is imposed that for all lines the characteristic impedances are the same, and equal to the impedance of the medium Z. Using this condition, by means of (A.2) and (A.1), along with some mathematical manipulation, we arrive at the general form of the propagation constants:

$$\begin{aligned}
\gamma_{xy} = \gamma_{xz} &= \frac{\gamma}{2\Delta x}\left(S_y + S_z - S_x\right) \\
\gamma_{yx} = \gamma_{yz} &= \frac{\gamma}{2\Delta y}\left(S_x + S_z - S_y\right) \\
\gamma_{zy} = \gamma_{zx} &= \frac{\gamma}{2\Delta z}\left(S_x + S_y - S_z\right)
\end{aligned} \tag{A.4}$$

where

$$\gamma = j\omega\sqrt{\mu\varepsilon}\left(1+\frac{\sigma}{j\omega\varepsilon}\right)^{1/2} \tag{A.5}$$

is the medium propagation constant, and

$$\begin{aligned} S_x &= \frac{\Delta y \Delta z}{\Delta x} \\ S_y &= \frac{\Delta x \Delta z}{\Delta y} \\ S_z &= \frac{\Delta y \Delta x}{\Delta z}. \end{aligned} \tag{A.6}$$

The propagation constants in (A.4) are used in (2.2) with the appropriate cell size which may be different in the three orthogonal direction of the grid. Caution should be taken when computing the electric and magnetic fields using (2.5) where the appropriate cell size should be used.

Notice that, in (A.6)-(A.4), if $\Delta x = \Delta y = \Delta z = \delta$, then $S_x = S_y = S_z = \delta$ and $\gamma_{xy} = \gamma_{yx} = \gamma_{zy} = \gamma$. For a lossless medium where $\sigma = 0$, then $\gamma = j\beta$ [see (2.3)].

A.2 LOSSY DIELECTRICS

Modeling with the FDTLM can be extended to include lossy materials by using the effective permittivity ε_{eff} instead of ε in the mathematical steps of Section A.1, which result in (Johns 1993):

$$\gamma_{xy} = \gamma_{xz} = \frac{\gamma_{eff}}{2\Delta x}\left(S_y + S_z - S_x\right)$$
$$\gamma_{yx} = \gamma_{yz} = \frac{\gamma_{eff}}{2\Delta y}\left(S_x + S_z - S_y\right) \qquad \text{(A.7)}$$
$$\gamma_{zy} = \gamma_{zx} = \frac{\gamma_{eff}}{2\Delta z}\left(S_x + S_y - S_z\right).$$

In (A.7), $\gamma_{eff} = j\omega\sqrt{\mu\varepsilon_{eff}}$, $\varepsilon_{eff} = \varepsilon - j\,\sigma/\omega$, and $\varepsilon = \varepsilon_o\varepsilon_r$.

Therefore, local variations in the conductivity are modeled by modifying the propagation constants of the node's transmission lines and the voltage waves, which are multiplied by a complex exponential factor of type $e^{-\gamma\delta_c}$ as per (2.2).

Appendix B

TRANSFORMATION OF A COMPLEX SYSTEM OF EQUATIONS INTO A REAL-VALUED SYSTEM

In some cases, it is convenient to work with a real system of equations instead of the complex one. Here, we give the steps of this complex-to-real system equations conversion.

Consider the complex-valued system of linear equations

$$Av = V_s . \tag{B.1}$$

The matrix A and the vectors v and V_s can be expressed as

$$\begin{aligned} A &= \Re A + j\Im A \\ v &= \Re v + j\Im v \\ V_s &= \Re V_s + j\Im V_s . \end{aligned} \tag{B.2}$$

Substituting (B.2) into (B.1)

$$\left[\Re A + j\Im A\right]\cdot\left[\Re v + j\Im v\right] = \Re V_s + j\Im V_s . \tag{B.3}$$

Equating the real and the imaginary parts of the right-hand side to those of the left-hand side results in

$$\Re A \cdot \Re v - \Im A \cdot \Im v = \Re V_s \tag{B.4}$$

and

$$\Re A \cdot \Im v + \Im A \cdot \Re v = \Im V_s . \tag{B.5}$$

Equations (B.4) and (B.5) can be expressed in a matrix form as

$$\begin{bmatrix} \Re A & -\Im A \\ \Im A & \Re A \end{bmatrix} \cdot \begin{bmatrix} \Re v \\ \Im v \end{bmatrix} = \begin{bmatrix} \Re V_s \\ \Im V_s \end{bmatrix}. \tag{B.6}$$

The real-valued system (B.6) is equivalent to the complex system (B.1). Notice however, that the system in (B.6) is twice as large as that in (B.1).

Appendix C

DISCRETE SENSITIVITY EXPRESSION FOR REAL SYSTEM OF EQUATIONS

The appendix presents the real form of the complex discrete sensitivity expression DAVM-I (3.16), i.e., the derivative of the response function f subject to the real system of equation

$$A_R(\boldsymbol{x}) \cdot v_R = V_{R,s} \tag{D.1}$$

where A_R, v_R, and $V_{R,s}$ are defined in (2.4)-(3.3).

Consider the real-valued perturbed system of linear equations that corresponds to (D.1) as a results of a perturbation Δx_k in the k th design parameter x_k

$$\begin{aligned} &\left[A_R(\boldsymbol{x}) + \Delta_k A_R\right] \cdot \left[v_R(\boldsymbol{x}) + \Delta_k v_R\right] = V_{R,s} + \Delta_k V_{R.s}, \\ &k = 1, \ldots, K. \end{aligned} \tag{D.2}$$

Here, Δ_k is the respective change in the respective matrix or vector due to Δx_k.

Simplifying and rearranging (D.2), we arrive at

$$\frac{\Delta_k v_R}{\Delta x_k} = A_R^{-1}\left[\frac{\Delta_k V_{R,s}}{\Delta x_k} - \frac{\Delta_k A_R}{\Delta x_k}(v_R + \Delta_k v_R)\right], \quad k = 1, \ldots, K \tag{D.3}$$

assuming that A_R^{-1} exists. The state variable sensitivity formula (D.3) is further substituted in the approximate derivative of f with respect to x_k

$$\frac{df}{dx_k} \simeq \frac{\partial f}{\partial x_k} + \nabla_{v_R} f \frac{\Delta_k v_R}{\Delta x_k}, \quad k = 1, \ldots, K. \tag{D.4}$$

This results in the real-valued discrete second-order sensitivity formula (Ali[2] *et al.* 2004)

$$\left(\frac{df}{dx_k}\right)_{DAVM-I} \simeq \frac{\partial f}{\partial x_k} + \lambda_R^T\left[\frac{\Delta_k V_{R,s}}{\Delta x_k} - \frac{\Delta_k A_R}{\Delta x_k}(v_R + \Delta_k v_R)\right], \quad k = 1, \ldots, K. \tag{D.5}$$

In (D.5), the adjoint solution λ_R is a real-valued vector. Its solution can be obtained using (3.6).

Appendix D

ANALYTICAL DERIVATIVES

During the course of this thesis, we compared the computed sensitivities using our discrete techniques with analytical derivatives whenever these where available. In this appendix we give the derivation of these analytical derivatives.

D.1 DERIVATIVE OF CAVITY REACTANCE WITH RESPECT TO ITS LENGTH (dZ_{in}/dL)

The input impedance of a shorted lossless 1-D cavity is purely imaginary and can be calculated analytically as (Pozar 1993)

$$Z_{in} = jZ\tan(\beta L) \tag{D.1}$$

where Z is the characteristic impedance of the medium, β is it's propagation constant, and L is the cavity length (design parameter).

The analytical derivative of Z_{in} (D.1) with respect to L is given by

$$\frac{dZ_{in}}{dL} = jZ\left(1+\tan^2(\beta L)\right)\beta. \tag{D.2}$$

D.2 WAVE IMPEDANCE DERIVATIVE OF A WAVEGUIDE WITH RESPECT TO ITS WIDTH (dZ_{wg}/da)

The wave impedance for a lossless homogenous rectangular waveguide operating in a transverse electric (TE) mode is given in (2.9) as (Pozar 1993)

$$Z_{wg} = \frac{k_w Z}{\beta} \tag{D.3}$$

where $k_w = \omega\sqrt{\mu_0 \varepsilon_0}$ is the wave number, $\beta = \sqrt{k_w^2 - k_c^2}$ is the propagation constant, $k_c = \pi/a$ is the dominant mode cut-off wave number, a is the width of the waveguide (the design parameter), and $Z = \sqrt{\mu/\varepsilon}$ is the intrinsic impedance of the material filling the waveguide.

The analytical derivative of Z_{wg} (D.3) with respect to changes in a is computed as

$$\frac{dZ_{wg}}{da} = -\frac{k_w Z \pi^2}{\left(k^2 - \frac{\pi^2}{a^2}\right)^{3/2} a^3}. \tag{D.4}$$

BIBLIOGRAPHY

Ali[1], S.M., N.K. Nikolova, and M.H. Bakr, accepted 2005. A discrete adjoint variable method for printed circuit board CAD. *INFORMS Journal on Computing.*

Ali[2], S.M., N.K. Nikolova, and M.H. Bakr, May 2004. Sensitivity analysis with full-wave EM solvers based on structured grids. *IEEE Trans. Magnetics*, vol. 40, no. 3, pp. 1521-1529.

Ali[3], S.M., N.K. Nikolova, and M.H. Bakr, July 2004. Central adjoint variable method for sensitivity analysis with structured grid electromagnetic solvers. *IEEE Trans. Magnetics*, vol. 40, no. 4, pp. 1969-1971.

Ali[4], S.M., N.K. Nikolova, and M.H. Bakr, June 2004. Sensitivity analysis and optimization utilizing an approximate auxiliary problem. *IEEE/URSI Int. Symposium on Antennas and Propagation*, (Monterey, CA), vol. 1, pp 1118-1121.

Ali[5], S.M., N.K. Nikolova, and M.H. Bakr, Dec. 2004. Recent advances in sensitivity analysis with frequency-domain full-wave EM solvers. *Applied Computational Electromagnetics Society Journal.*

Ali[6], S.M., N.K. Nikolova, and M.H. Bakr, May 2003. Design sensitivity analysis for optimization with the frequency domain-TLM. *IEEE CCECE03 Digest*, (Montre'al, Canada), vol. 1, pp. 1971-1974.

Akel, H. and J.P. Webb, July 2000. Design sensitivities for scattering-matrix calculation with tetrahedral edge elements. *IEEE Trans. on Magnetics*, vol. 36, no. 4, pp. 1043-1046.

Ansoft HFSS (2001), Version 3.0.25, Ansoft Corporation, Four Station Square, Suite 200, Pittsburgh, PA 15219.

Bakr, M.H. and N.K. Georgieva, Sep. 2003. An adjoint variable method for frequency domain TLM problems with conducting boundaries. *IEEE Microwave and Wireless Components Lett.*, pp. 408-410.

Chung, Y., C. Cheon, and S. Hahn, Dec. 2000. Optimal shape design of microwave device using FDTD and design sensitivity analysis. *IEEE Trans. Microwave Theory Tech.*, vol. 48, pp. 2289-2296.

Chung, Y.S., C.C. Cheon, I.H. Park, and S.Y. Hahn, Sep. 2001. Optimal design method for microwave device using time domain method and design sensitivity analysis – part II: FDTD case. *IEEE Trans. Magnetics*, vol. 37, no. 5, pp. 3255-3259.

Christopoulos, C., 1995. *The Transmission-line Modeling Method TLM.* IEEE Press, New York.

Director, S.W. and R.A. Roher, Aug. 1969. The generalized adjoint network and network sensitivities. *IEEE Trans. Circuit Theory*, vol. CT-16, pp. 318-323.

Georgieva, N.K., S.G. Glavic, M.H. Bakr and J.W. Bandler, June 2002. Feasible adjoint sensitivity technique for em design optimization. *IEEE MTT-S Int. Microwave Symp. Dig.* (Seattle, WA), pp. 971-974.

Haug, E.J., K.K. Choi and V. Komkov, 1986. *Design Sensitivity Analysis of Structural Systems*. Orlando, Florida: Academic Press, Inc.

Harrington, R.F., 1961. *Time-harmonic electromagnetic fields*. New York: McGraw-Hill book company, Inc.

Huygens, C., 1690. *Traite de la Lumiere*. Paris: Leiden.

Johns, D. and C. Christopoulos, 1994. New frequency-domain TLM method for numerical solution of steady-state electromagnetic problems. *IEE Proc. Sci. Means Technol.*, vol. 141, pp 310-316.

Lee, H.B., H.K. Jung, and S.Y. Hahn, May 1995. Shape optimization of H-plane waveguide Tee junction using edge finite element method. *IEEE Trans. Magnetics*, vol. 31, no. 3, pp. 1928-1931.

Lee, H.F. and Wei Chen, 1997. *Advances in Microstrip and Printed Antennas*. New York: John Wiley & sons, Inc.

Lions, L.J, 1971. *Optimal Control of Systems Governed by Partial Differential Equations*. Berlin: Springer Verlag.

MathWorks, Inc., MATLAB (2000) Version 6.0, 3 Apple Hill Drive, Natick MA 01760-2098.

Madsen, K., H.B. Nielsen and J. Søndergaard, Jan. 2002. *Robust Subroutines for Non-linear Optimization*. Report IMM-REP-2002-02, Informatics and Mathematical Modeling, Technical University of Denmark, DK-2800 Kongens Lyngby,

Denmark.

Nikolova, N.K., J.W. Bandler, and M.H. Bakr, Jan. 2004. Adjoint techniques for sensitivity analysis in high-frequency structures CAD. *IEEE Trans. Microwave Theory Tech.*, vol. 52, no. 1, pp. 403-419.

Nikolova, N.K., S.M. Ali, M.H. Bakr, E.A. Soliman, and J.W. Bandler, April 2004. Response sensitivity analysis with frequency-domain full-wave electromagnetic solvers. *20th Annual Review of Progress in Applied Computational Electromagnetics* (Syracuse, NY), CD ROM.

Nikolova, N.K., H.W. Tam, and M.H. Bakr, April 2004. Sensitivity analysis with the FDTD method on structured grids. *IEEE Trans. Microwave Theory Tech.*, vol. 52, no. 4, pp. 1207-1216.

Pasalic D., R. Vahldieck and J. Hesselbarth, 1999. The frequency-domain TLM method with absorbing boundary conditions. *IEEE MTT-S Int. Microwave Symp. Dig.*, pp. 1669-1672.

Pozar, D.M., 1993. *Microwave Engineering.* New York: Addison-Wesley Publishing Company, Inc.

Sadiku, M.N., 2001. *Numerical Techniques in Electromagnetics.* Boca Raton, FL: CRC Press LLC.

Taflove, A., 1995. *Computational Electromagnetics: The Finite-Difference Time-Domain Method*, Norwood: Artech House, Inc.

Webb, J.P., Sep. 2001. Design sensitivity using high-order tetrahedral vector elements.

IEEE Trans. Magnetics, vol. 37, no. 5, pp. 3600-3603.

Webb, J.P., March 2002. Design sensitivity of frequency response in 3-D finite-element analysis of microwave devices. *IEEE Trans. Magnetics*, vol. 35, no. 2, pp. 1109-1112.

Zheng, G., Ahmed A. Kishk, Alexander B. Yakovlev, and Allen W. Glisson, April 2004. Simplified feeding for a printed Yagi antenna. *Electronics Letters* , vol. 40 , no. 15, pp. 464-465.

AUTHOR INDEX

G

H

J

L

M

N

AUTHOR INDEX